R 672

Technical Report

TIRE–PAVEMENT FRICTION COEFFICIENTS

April 1970

Sponsored by

NAVAL FACILITIES ENGINEERING COMMAND

NAVAL CIVIL ENGINEERING LABORATORY

Port Hueneme, California

115

TIRE–PAVEMENT FRICTION COEFFICIENTS

Technical Report R-672

Y-F015-20-01-012

by

Hisao Tomita

ABSTRACT

An investigation consisting mainly of a literature review and a review of current research done outside NCEL was conducted to determine the methods needed to provide safe, skid-resistant surfaces on Navy and Marine Corps airfield pavements. Much of the information reported herein serves to update the information contained in NCEL Technical Report R-303. For example, new information is included on friction-measuring methods, correlation of the measuring methods, factors affecting friction coefficients, minimum requirements for skid resistance, and methods of improving the skid resistance of slippery pavements. However, some new topics which are of recent interest are also discussed in detail. These topics include hydroplaning, the mechanism of rubber friction, the friction associated with various operating modes of aircraft tires, the relationship of friction coefficients to pavement surface texture and to surface drainage of water, and the effects of pavement grooving on hydroplaning and on friction coefficients.

All the information from the investigation is summarized, and recommendations are given for research and development efforts needed to provide safe, skid-resistant surfaces for airfield pavements.

AD 602 830

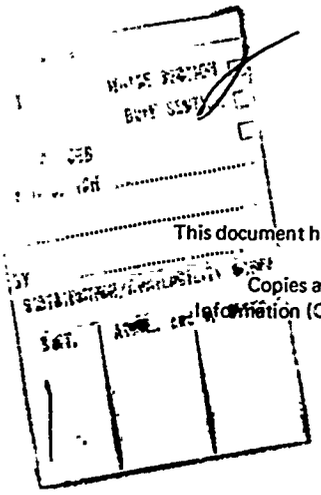

CONTENTS

INTRODUCTION

Background

The Navy has experienced a number of aircraft skidding incidents on airfield runways. Some of these incidents have been the direct result of low friction coefficients between aircraft tires and water- or slush-covered runways. As a result the Naval Civil Engineering Laboratory (NCEL) was requested to study the problem in fiscal years 1963 and 1964. The objective of the investigation was to develop a set of criteria from which a reliable and accurate field device could be designed and constructed to measure tire-pavement friction coefficients. A review of the aircraft skidding problem was made, and a thorough literature search was conducted on the subject of tire-pavement friction coefficients. Summarized landing-incident reports for a 2-year period were reviewed to determine if the magnitude of the friction coefficients was an important factor. The literature review resulted in a state-of-the-art study and covered the skid prevention research of companies and agencies involved in the design and construction of highway and airfield pavements and in the design of aircraft, vehicles, brakes, and tires. All results and findings from the investigation were reported by Tomita (1964). The report recommended against developing a field measuring device for the Navy then since the Federal Aviation Agency was involved in developing a similar device under contract.

More recent reports of skidding incidents on Navy and Marine Corps airfield runways have shown the need for better methods of providing skid-resistant surfaces to new as well as to old pavements.* For example, a newly constructed runway in Vietnam is closed to aircraft traffic during the monsoon season; lack of braking action was reported by pilots landing on fog-sealed, wet runways at two Navy airfields; and a tanker skidded over a rubber-deposited area and overran a runway at a Navy airfield. In FY-68 NCEL was assigned the task of investigating and developing methods of making new and existing airfield pavement surfaces resistant to the skidding of aircraft, whether the surfaces are wet or dry. This report is the preliminary step of that assignment.

* The examples given were related to the author during his investigations.

The end results and findings from future research and development efforts are to be incorporated into appropriate Naval Facilities Engineering Command manuals and specifications for distribution to design and field personnel.

Scope

This report covers many of the important factors involved in friction coefficients as related to pavement surfaces and aircraft tires and brakes. Most of the information was derived from a comprehensive literature review. Emphasis in this report will be placed on updating the information found in Technical Report R-303 (Tomita, 1964) by presenting new information found in recent publications. Some new topics include the phenomenon of hydroplaning, which has been receiving much consideration in recent years; the mechanism of rubber friction; the relationship of pavement surface texture and surface drainage of water to friction coefficients; and the grooving of pavements to combat hydroplaning and to increase the friction coefficient. The report also includes recommendations for research and development efforts needed by the Navy to meet the objective of providing skid-resistant runway surfaces for aircraft operations.

Since the information has been gathered from various sources, different terms relating to the friction coefficient between tires and pavements have been encountered. An effort has been made in this report to reduce the number of terms as much as possible. However, it is not possible to use a single term since the phenomenon is considered under various conditions and modes of wheel rotation. In addition, measurements are taken with various devices. The basic terms used in this report are coefficient and number (100 x coefficient). Where appropriate, various adjectives are used with the basic terms to describe the phenomenon as accurately as possible.

TIRE HYDROPLANING PHENOMENON

A considerable amount of interest has been generated in recent years on the phenomenon of tire hydroplaning on wet pavement surfaces. The phenomenon is serious because the braking coefficient during hydroplaning equals that on an icy surface, or, according to some investigators, approximately 0.05. Knowledge of hydroplaning is accumulating at a rapid rate. Three types of hydroplaning are now identified:

1. *Dynamic.* The tire is lifted off the pavement surface and is completely supported by a layer of water.

2. *Viscous.* This phenomenon occurs generally on a smooth, damp pavement surface which provides a very thin film of fluid not penetrated by the tire. It can occur at much lower velocities than those required for dynamic hydroplaning.

3. *Reverted rubber.* In this phenomenon the heat from the friction at the tireprint boils the water and softens the rubber. This forms a seal, which delays water expulsion, and the steam then prevents contact of the tire with the pavement surface.

All three types of hydroplaning can occur during one landing. However, only the dynamic hydroplaning, because it appears to be the most usual phenomenon observed, will be discussed in detail in the subsequent paragraphs.

Physical Description of Dynamic Hydroplaning

When enough water is present on a pavement surface to cover the protruding aggregates, the tire at some critical ground velocity can encounter the phenomenon of dynamic hydroplaning. This phenomenon can be explained by the fact that the water film must be ejected by the pressure of the rolling tire before contact can be made with the pavement surface. This process is time-dependent because of the effects of inertia and viscous forces of the water. With an increase in velocity, the time available for ejecting the water film decreases, and vertical hydrodynamic lift of the tire is initiated. This initiation is the beginning of hydroplaning. With continued increases in velocity, the area occupied by the water film increases with respect to the total contact area of the tire, and partial hydroplaning occurs. At some critical velocity the entire contact area is occupied by the water film. When this condition exists the entire load is supported by the hydrodynamic lift, and complete hydroplaning is attained. Under this condition the tire may stop rotating and plane along the wet surface. Thus the phenomenon is termed "hydroplaning" or "aquaplaning." The braking effectiveness and lateral stability of a vehicle or an aircraft are almost entirely lost when the tires are at the complete hydroplaning condition.

Horne and Dreher (1963) reported that the hydroplaning phenomenon was first noticed and experimentally demonstrated by the National Aeronautics and Space Administration (NASA) during a tire treadmill study by Harrin (1958). The treadmill study was prompted by an indication of the hydroplaning phenomenon during the landings of aircraft ranging from modern jet fighters with high tire pressures and high landing velocities to small executive planes with low tire pressures and low landing velocities. From experimental

investigations involving an extensive analysis of still photographs and motion picture film and from other research efforts, Horne and Leland (1963) found the following factors present during hydroplaning:

1. *Detachment of tireprint.* Photographs taken through glass plate showed that at complete hydroplaning the tire is completely detached from the glass plate and totally supported by water.

2. *Suppression of bow wave.* Photographs revealed that the spray angle of the tire bow wave from the horizontal progressively decreases with an increase in forward velocity. The bow wave completely disappears at the higher velocities.

3. *Maximum fluid drag.* Experimental results indicated that the fluid drag reaches a maximum value at a ground velocity near the complete hydroplaning velocity. A large reduction results with further increases in ground velocity.

4. *Spin-down of tire.* Photographs and motion pictures showed that freely rolling wheels in the hydroplaning condition slow their spin or completely stop spinning on water-covered runways. There are two causes of this spin-down: First, the fluid drag can approach near zero, and of course there is no other drag because the direct tire–pavement contact is eliminated by the detachment of the tire. Second, the center of pressure of the lift force moves forward of the axle and creates a spin-down moment. This moment is apparently great enough to cause the spin-down.

5. *Loss of directional stability.* Results from tests with a jet transport on a slush-covered runway in the presence of a 9-knot direct crosswind indicated that the aircraft in the hydroplaning condition drifts in the lateral direction and yaws. These results suggest that hydroplaning can cause serious problems during takeoffs and landings in the presence of crosswinds.

6. *Loss of traction.* Test results indicated that the loss of braking traction is associated with hydroplaning. Since the tire is detached from the pavement and since water cannot develop significant shear force, it is futile to apply the brakes.

Apparently these six factors apply to both aircraft and automobile tires on wet pavement surfaces.

Hydroplaning Velocity

The velocity at which a tire experiences complete dynamic hydroplaning is of great importance. For example, knowledge of the critical velocity will permit a decision by a pilot to land on a wet runway or divert to another

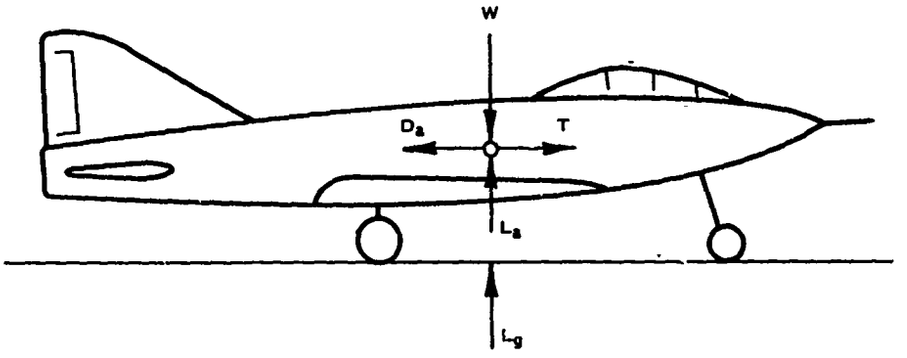

Figure 1. Forces on a landing jet aircraft under hydroplaning condition.

airfield. The dynamic hydroplaning velocity can be determined by considering the forces on an aircraft during unbraked landing rollout (Figure 1). It is assumed that the horizontal forces—residual thrust, T, and aerodynamic drag, D_a—are approximately equal and create no net moment about the nose or main wheels. In addition, no drag force is assumed to be present at the wheels. Summing the vertical forces will give

$$L_g + L_a = W^* \tag{1}$$

where L_g = sum of the vertical ground forces through all gears

L_a = aerodynamic lift

W = static weight of the aircraft

At complete hydroplaning, L_g can be considered to be the vertical component of the hydrodynamic pressure on the tires. Thus

$$L_g = \frac{1}{2} C_t \rho V^2 A_t \tag{2}$$

where C_t = lift coefficient of the tire

ρ = mass density of water

V = forward velocity

A_t = tire contact area

* The reader is referred to the nomenclature on the foldout page at the end of the report.

From aerodynamic theory, L_a can be expressed as

$$L_a = \frac{1}{2} C_a \rho_a V^2 A_a \qquad (3)$$

where C_a = lift coefficient of the aircraft

ρ_a = mass density of air

A_a = uplift area of the aircraft

Substituting Equations 2 and 3 into Equation 1 yields

$$V = V_h = \left(\frac{2W}{C_t \rho A_t + C_a \rho_a A_a} \right)^{1/2} \qquad (4)$$

where V_h is the hydroplaning velocity, or the minimum velocity at which complete hydroplaning occurs. The complete hydroplaning condition remains at velocities higher than V_h. At some velocity below V_h hydroplaning begins, and in between these velocities the tires are in a state of partial hydroplaning. The velocity at which hydroplaning begins has not been clearly defined.

It is desirable that the hydroplaning velocity, V_h, in Equation 4 be as high as possible, and if it is higher than the aircraft touchdown velocity, the problem of complete hydroplaning will not be encountered during the landing rollout. However, for a given landing, most of the terms in Equation 4 remain constant and cannot effect a change in V_h. As stated by Hurt (1960), the aircraft lift coefficient, C_a, is a function of the shape of the wing and the angle of attack and its magnitude can be varied by changing the position of the flaps and other aerodynamic control surfaces. But a change in C_a will bring about an opposite change in A_t. For example, a retraction of the flaps will decrease C_a but will increase the net vertical wheel load. This in turn increases A_t, as reported by Kummer and Meyer (1962). Thus, there is no significant net change of the denominator of Equation 4.

Moore (1966) reported that hydroplaning may occur when the tire is initially rolling or locked as in braking. The hydroplaning velocity for the rolling and locked wheel is called the hydroplaning-limit-in-rolling and hydroplaning-limit-in-sliding, respectively. The hydroplaning velocity of Equation 4 corresponds to the rolling limit, which is higher than the sliding limit by as much as 100% under certain conditions. Thus, the dangerous condition of hydroplaning can be experienced continually from velocities above the rolling limit to that of the sliding limit if the wheels are locked. For example, assume that an aircraft lands at a velocity above the rolling

limit and the brakes are applied shortly after touchdown. The wheels lock and control of the aircraft cannot be regained until a velocity below the sliding limit is reached. During the deceleration caused only by air drag, the aircraft might drift out of control and off the edge of the runway. It may be argued that wheel rotation at velocities below the rolling limit will be regained upon release of brakes. This argument is logical. However, Moore (1966) reported that once a tire stops rotating under hydroplaning at velocities above the sliding limit, rotation is not usually regained.

Horne and Dreher (1963) presented an equation similar to Equation 4, obtained by equating the vertical wheel load, F_v, to Equation 2, resulting in

$$V = V_h = \left(\frac{2 F_v}{C_t \rho A_t} \right)^{1/2} \tag{5}$$

Based on experimental studies at NASA Langley Research Center, Horne and Dreher (1963) were able to simplify Equation 5 to

$$V_h = 9\sqrt{P_t} \tag{6}$$

in which V_h is expressed in knots and the tire inflation pressure, P_t, in psi. This simplification is based on three assumptions: First, that the average tire contact pressure, F_v/A_t, in Equation 5 is approximately the same as P_t; second, that the fluid density is approximately that of water; and third that C_t is approximately 0.7. All assumptions seem logical, but Yoder (1959) indicated that the contact pressure depends on the magnitude of P_t. For high-pressure tires, the contact pressure is actually less than P_t, since the walls are in tension. For low-pressure tires, the converse is true. No quantitative values were provided by Yoder to support these statements, but it can be seen that the V_h determined on the basis of Equation 6 can be on the unsafe side if P_t is high and the contact pressure low. However, Horne and Leland (1963) reported good correlation of V_h as determined by Equation 6 and experimental results. As shown in Figure 2, there appears to be reasonable agreement between the experimental and calculated velocities for F_v ranging from 925 pounds to 22,000 pounds and for P_t ranging from 24 psi to 150 psi.

Horne and Leland (1963) investigated the susceptibility of aircraft to hydroplaning by comparing the maximum velocities at takeoff and at landing with the V_h of many aircraft. The results, as shown in Figure 3, indicate that practically all aircraft considered are susceptible to hydroplaning during ground operations.

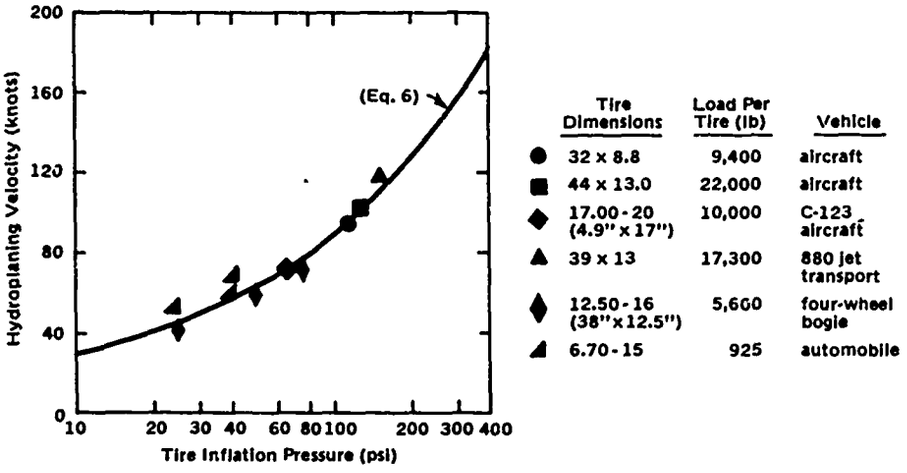

Figure 2. Experimental and calculated tire hydroplaning. (© Horne and Leland, 1963. Used by permission.)

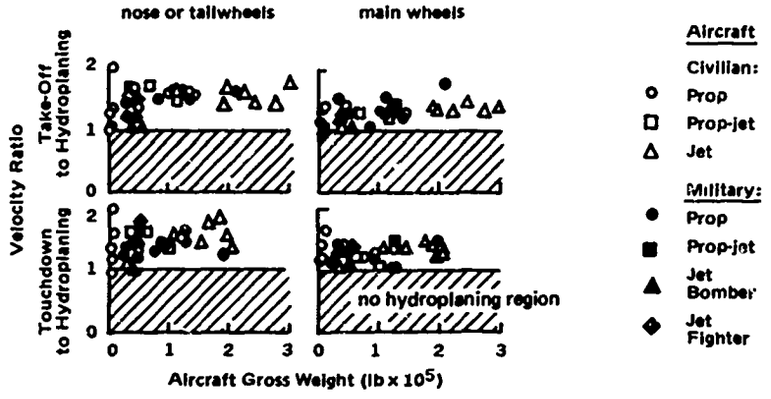

Figure 3. Susceptibility of current aircraft to hydroplaning. (© Horne and Leland, 1963. Used by permission.)

Factors Affecting Hydroplaning

The fluid depth on the pavement is assumed to be greater than the depth of the tire tread groove in Equation 4. However, the effects of some important factors contributing to the depth of water and to hydrodynamic pressure are not considered. Some of these factors affecting hydroplaning, especially those related to the pavement surface, will be discussed in this section.

Depth of Water. As previously mentioned, water on the runway surface is responsible for tire hydroplaning. The depth of water on the runway surface is dependent on many factors. These include the intensity of precipitation, the presence of transverse and longitudinal slopes, the flow coefficient, the unevenness of the pavement, resulting in puddles of water in the depressed areas, and the velocity of wind directly above the pavement surface.

The depth of water generally increases with increasing intensity of precipitation, but decreases with increasing slope of runway surface. The sloping of runway surfaces is limited because of aircraft operational requirements. A high transverse slope will cause lateral instability of aircraft during crosswind conditions, especially on wet runways with low friction coefficients. Horne and Dreher (1963) reported that a 9-knot crosswind yawed and displaced a full-scale jet transport on a slush-covered runway. The slope of the runway was not given. The Department of the Navy (1959) requires a transverse slope of 1% to 1-1/2% for Navy runways with no longitudinal slope. A minimum of 1% longitudinal slope is required if there is no transverse slope. The origin and basis of these specifications for Navy runways are not known. However, a recent series of landing incidents on a newly constructed runway in Vietnam has indicated a need for a critical review of these specifications.*

The flow coefficient (such as Manning's) for pavement surfaces can range between 0.010 and 0.020. In the theory of open channel flow this range can vary the flow by 100%. However, the actual effect of the flow coefficient on the depth of water on pavement surfaces is not simple to determine because of the difficulty in measuring the flow coefficient.

A uniform depth of surface water on a runway is not easily maintained because of pavement unevenness that results in the formation of random water puddles of various sizes. The unevenness is partly caused by lack of construction control and by differential pavement settlement under load. Resurfacing is necessary when a large number of puddles are created during normal precipitation. In recent years, however, refined electronic control systems on the newer types of paving machines have minimized the unevenness during construction to a great extent.

* Personal communication to NCEL representative.

Proper water drainage can be offset by the effects of a forceful surface wind blowing up the pavement slope. Such a wind can hold back the draining water, resulting in depths greater than normal under the same intensity of precipitation.

The interaction of the previously discussed factors makes it difficult to predict precisely the depth of water on a runway surface during precipitation. Variation in depth can be expected from one precipitation period to the next; the changes in intensity during a given precipitation period as well as the location of the runway are factors that contribute to this variation. The variation in turn has made it difficult to define accurately, from field experiments, the depth or range of depth at which hydroplaning is induced. Horne and Dreher (1963) reported that for smooth tread tires on comparatively smooth simulated pavement surfaces, hydroplaning can occur at depths as low as 0.02 to 0.09 inch. For full-scale aircraft tires, also with smooth tread and operating on a smooth concrete surface, hydroplaning can occur at depths ranging from 0.1 to 0.4 inch. Trant (1959) indicated that water depths of 0.2 to 0.3 inch are required on a concrete runway to hydroplane a rib-tread automobile tire. Horne and Dreher (1963) reported that hydroplaning can also occur at depths slightly greater than 2 inches.

Lift Pressure. The foregoing discussion indicates that a normal precipitation or a slushy condition on a runway can create a water depth great enough to result in a vertical component of hydrodynamic pressure sufficiently large to lead to hydroplaning. At the Langley landing-loads track Horne and Dreher (1963) successfully measured the hydrodynamic pressure acting on the wet surface under a tire. Their measurements were accomplished with flush diaphragm-type pressure gages, which were placed just below the surface of the runway at the centerline of the tire path. Figure 4 shows the pressure distributions at ground velocities of 30 knots and 85 knots. At $V = 30$ knots the tire is in the partial hydroplaning region, and at $V = 85$ knots in the complete hydroplaning condition. Horne and Dreher (1963) noted three points of interest suggested by the distribution in Figure 4: (1) the hydrodynamic pressure develops ahead of the initial tire contact point; (2) negligible hydrodynamic pressure is developed at the rear of the tire print; and (3) the peak hydrodynamic pressure for the 85-knot pressure distribution is much greater than the tire inflation pressure. The first two points combine to shift the center of pressure forward with increase in velocity. This shift together with the increase in pressure causes the spin-down moment of an unbraked wheel in the complete hydroplaning condition.

Basically, two factors are involved in changing the lift pressure: tire-tread design and pavement surface textures. Tires with an adequate tread design, such as circumferential grooves, provide vents or voids for water drainage and

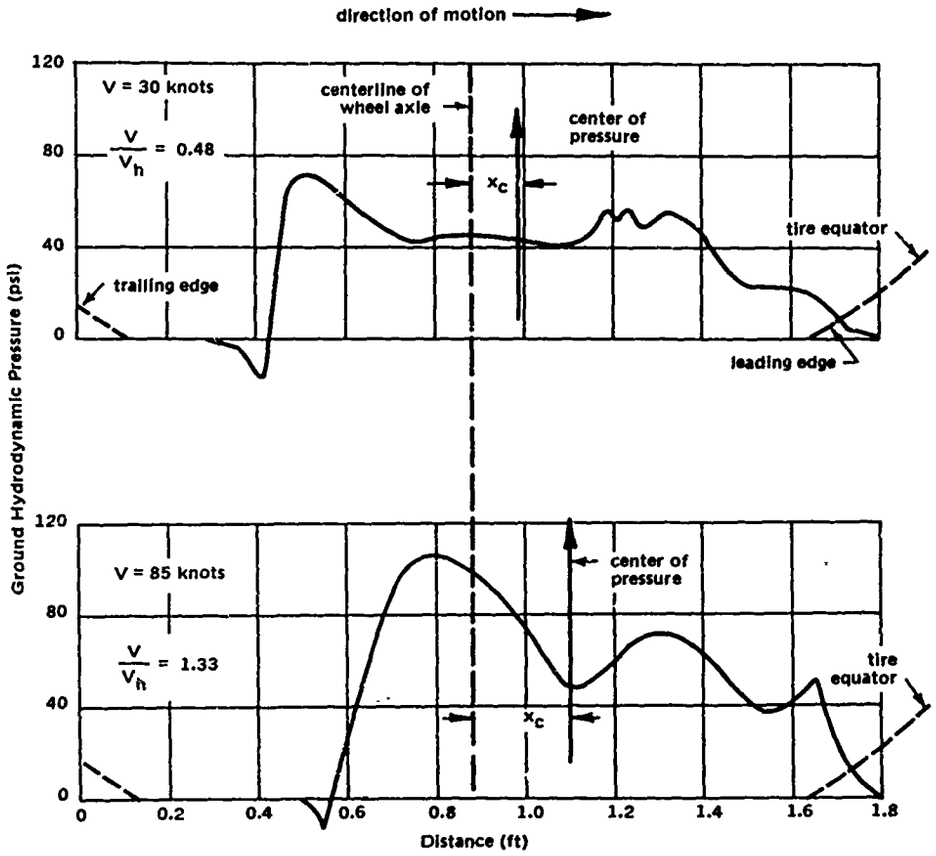

Figure 4. Tire ground pressure signatures on water-covered runway. Vertical load per tire, approximately 5,600 pounds; tire pressure, 50 psi; water depth, 0.5 inch. (© Horne and Dreher, 1963. Used by permission.)

pressure relief. Lateral edges made with molded slots and cut slits provide a wiping action over wet pavement surfaces. These tire tread features result in a higher hydroplaning velocity than do smooth tires. In addition, the grooves increase the minimum depth at which hydroplaning occurs. Horne and Dreher (1963) reported that the partial hydroplaning region is considerably less for rib-tread tires than for smooth-tread tires, even when the water depth is greater than the tire groove depth. Mainly because of shear strength requirements, the extent of treading is generally limited to circumferential grooves in high tire pressure—high speed aircraft tires used on modern jet aircraft.

By similar reasoning, a coarse or open-textured pavement surface will permit hydrodynamic pressure to be relieved more readily than a smooth or dense-graded surface. Thus, a coarse surface results in a higher hydroplaning velocity and requires a deeper minimum water depth than does a smooth surface. Moore (1966) developed a method of measuring the water drainage capabilities of various surface textures under static conditions. However, a method of measuring the water drainage or the pressure-relieving capabilities of various surface textures under hydrodynamic conditions is needed, since the water under the rolling tires of high-speed aircraft must be rapidly expelled to prevent hydroplaning. No quantitative values relating the hydrodynamic pressure and the variation in coarseness of surface textures have been uncovered during this investigation. A method of establishing such a relationship will contribute greatly to the determination of the texture required to effectively combat hydroplaning.

Transverse and longitudinal grooves have been cut in pavement surfaces on an experimental basis to reduce the possibility of hydroplaning on airfields as well as on highways. The Ministry of Aviation (1961) used transverse grooves 1/4 inch wide and 1/8 inch deep, with 1-inch pitch, on a portland cement concrete (PCC) runway. Apparently, experience has shown this groove size and pitch to be the most desirable for relieving hydrodynamic pressure.

Grooving is more recent in the United States than in Great Britain. However, Horne (1967) reported that grooving is being intensively studied in the United States by NASA, the Air Force, and the Federal Aviation Agency (FAA). The objectives of grooving are to provide a pressure-relieving mechanism, thereby reducing the opportunity for hydroplaning, and to increase the friction coefficient. Horne (1967) reported that 22 freeze–thaw cycles had no apparent effect on grooved PCC slabs. No decrease is detected in the friction coefficient with an increase in the number of freeze–thaw cycles. Horne (1967) also conducted an extensive investigation to determine the optimum groove arrangement for tire traction at the Langley landing-loads track. Preliminary results indicated that the 1/4-inch-wide, 1/4-inch-deep, 1-inch-pitch groove pattern provides the greatest increase in traction over the ungrooved PCC surface.

However, all groove arrangements improve traction. In addition, the results indicated no increase in rolling resistance nor any tire damage under yawed rolling conditions or during braking well beyond the incipient skid point.

In April 1967 the FAA grooved the instrumented runway at Washington National Airport in its entirety to improve aircraft-stopping performance when the runway is wet. A 1/8-inch-wide, 1/8-inch-deep, 1-inch-pitch transverse groove pattern was used on the 150-foot by 6,800-foot asphaltic concrete (AC) runway. The cost of the grooving operation was $0.09 per square foot. Results of pilot reports obtained by Horne (1967) indicated an improvement in stopping performance as a result of the grooving. However, the grooves have been fouled by soft rubbery material which appears to be reverted rubber from tires.

The FAA also grooved PCC and AC taxiways at Cleveland, Salt Lake City, Las Vegas, Miami, and New York City airports to determine the effects of water, snow, ice, varying ambient temperatures, and aircraft traffic loads on pavement grooves. The groove patterns varied: 1/8-inch, 1/4-inch, or 3/8-inch widths, with 1/8-inch or 1/4-inch depths, with 1-inch, 1-1/2-inch, or 2-inch pitches were used. Horne (1967) reported that the grooves in the AC taxiway at the Las Vegas Airport have started to fail through plastic flow of the asphalt. A similar trend has been observed at Miami and Salt Lake City. There are some indications that the wider grooves (1/4 inch to 3/8 inch wide and 1/4 inch deep) trap stones on runways, causing a potential housekeeping problem.

In August 1966 the Air Force grooved two PCC runways in an effort to improve landing performance during wet operations. A 1/4-inch-wide, 1/4-inch-deep, 2-inch-pitch transverse groove pattern was selected. However, only the center 37-foot width of the runway was grooved in a discontinuous pattern consisting of a series of 26-inch grooved and 26-inch ungrooved sections. Improved drainage during precipitation has been observed, and aircraft skidding incidents have been significantly reduced. Horne (1967) reported that one accident occurred on one of the grooved runways, but the aircraft was off the side of the grooved section. The Air Force plans grooving more runways.

The Air Transport Association (ATA), in the interest of aircraft safety, sponsored the grooving of selected runways at two commercial airports, Kansas City Municipal Airport and Kennedy International Airport. At Kansas City the 1/8-inch-wide, 1/4-inch-deep, 1-inch-pitch transverse grooves were sawed in May 1967. Both AC and PCC sections of a runway were grooved at a cost of approximately $0.14 per square foot. Horne (1967) reported no deterioration of the pavement sections which can be attributed to grooving after 5 months of service. Increased water drainage has been observed during precipitation. Practically no water spray from aircraft wheels has been

observed during operations on the grooved runway; in contrast a considerable amount is generally observed on ungrooved runways. In addition, since grooving, fewer aircraft are now diverted to another airfield during precipitation. This factor indicates improved landing performance as well as the pilots' confidence in landing on the grooved runway.

A PCC runway at Kennedy International Airport was grooved in its entirety in August 1967 at a cost of $0.13 per square foot. The transverse grooves were 1/8 inch deep, with a 1-3/8-inch pitch, and with the width varying from 3/8 inch at the pavement surface to 5/32 inch at the bottom of the grooves. In addition to the beneficial effects of grooving found at Kansas City, Horne (1967) reported that during precipitation most aircraft use the high-speed turnoff rather than the end taxiway turnoff.

It has recently been reported in the popular press that at least six states have grooved sections of highway pavements to combat hydroplaning: California, Texas, Washington, Oregon, Minnesota, and Georgia. New York and New Jersey are considering grooving. The grooves are generally in the longitudinal direction, 1/8 inch deep and 3/4 inch apart, with the width equal to the thickness of diamond-cutting blades. Such grooving patterns have been used in California on several freeway sections that had high accident rates during wet weather prior to the grooving. On one 900-foot section of a freeway, there were 48 wet-weather accidents per year prior to grooving. In the year following the grooving only one accident occurred. In another section of a freeway 26 accidents were experienced within a year before grooving and none after. The popular press, reporting periodically on grooving, indicates that the grooves serve to offset the tendency of hydroplaning without sacrificing the riding qualities of the pavement or the handling characteristics of automobiles.

MECHANISM OF RUBBER FRICTION

Some aspects of the basic laws of friction and the theory of skidding were reviewed during the previous investigation reported by Tomita (1964). H. W. Kummer and W. E. Meyer of Pennsylvania State University have conducted a thorough investigation on the mechanism of rubber friction (1962, 1967). The following discussions on the subject are based mainly on their work.

When a rubber tire is in contact with a pavement surface, almost all the deformation is taken up by the rubber, since the modulus of deformation of the pavement, especially that of PCC, is much greater than the modulus of deformation of the rubber. Thus the behavior of rubber is important in the frictional process even though the surface characteristics of the pavement

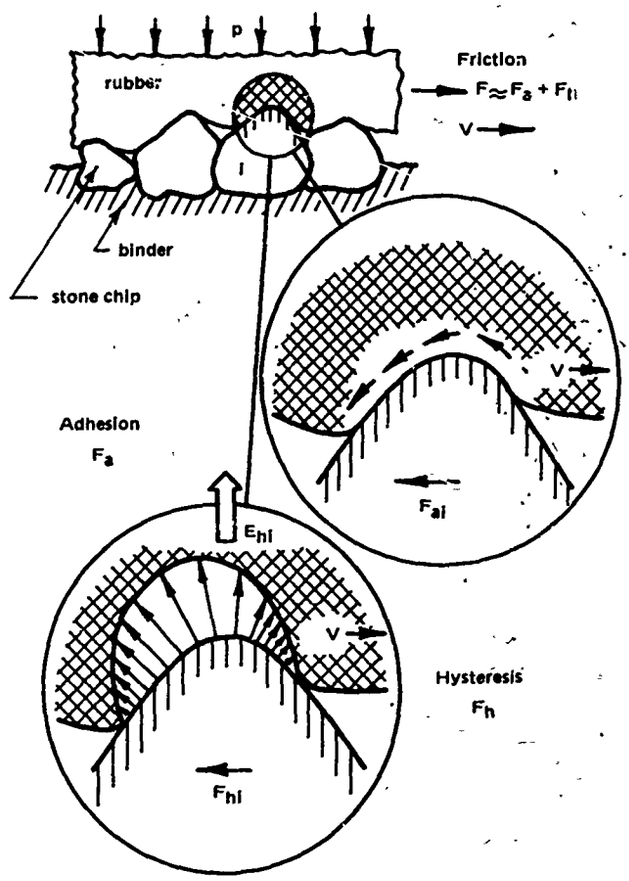

Figure 5. The two principal components of rubber friction: adhesion and hysteresis. (© Kummer and Meyer, 1967. Used by permission.)

govern to a large extent the magnitude of the available friction. The frictional process takes place on a molecular scale, with its magnitude affected by a large number of factors and combination of factors. For this reason, it is difficult to isolate and determine the controlling factors from a purely empirical or theoretical approach. Kummer and Meyer (1967) have taken a simplified theoretical approach combined with laboratory and field experiments to better understand the tire–pavement frictional process.

In the simplified theoretical approach Kummer and Meyer (1967) consider a uniformly loaded rubber block sliding over a rough-textured dry or wet pavement surface, as illustrated in Figure 5. The total friction force, F, is the sum of two major components: the adhesion force, F_a, and the hysteresis force, F_h. Thus

$$F = F_a + F_h \qquad (7)$$

The F_a for the rubber contacting a simple particle is the product of the interface shear strength, B, and actual contact area, A_i. The summation of all the individual products yields the available adhesion force:

$$F_a = B \sum_{1}^{N} A_i = BA \tag{8}$$

where A is the total area of contact for N number of aggregate particles.

The hysteresis force, F_h, is the effect of damping or reacting elastic pressure of the rubber during the deformation around the aggregate particle. The unsymmetrical deformation of the rubber is opposed by its damping, producing the pressure distribution shown in the lower enlargement of Figure 5. Integrating the pressure over the area will provide the resulting force, the horizontal component of which is F_h. The hysteresis force can also be expressed as the summation of the unit energy, E_i, dissipated for each aggregate particle during a unit sliding length, b. That is

$$F_h = \frac{1}{b} \sum_{1}^{N} E_i = \left(\frac{1}{b}\right) E \tag{9}$$

where E is the total energy dissipated within the rubber for N number of aggregate particles.

Substituting Equations 8 and 9 into Equation 7 yields

$$F = BA + \left(\frac{1}{b}\right) E \tag{10}$$

The total vertical load of the rubber block is the contact pressure, p, times the gross geometric area, A_n, of the block. Dividing Equation 10 by the load yields

$$FC = FC_a + FC_h \tag{11}$$

where $FC = F/p A_n$ = the measured friction coefficient

$FC_a = BA/p A_n$ = the adhesion coefficient

$FC_h = E/b p A_n$ = the hysteresis coefficient

or $FC_h = Q D/b p A_n$ because $E = Q D$ where Q is the volume of rubber involved in the deformation and D is the energy dissipated per unit volume of rubber caused by damping.

The equation for the measured friction coefficient is expressed as

$$FC = \left(\frac{A}{A_n}\right)\left(\frac{B}{p}\right) + \left(\frac{QD}{A_n}\right)\left(\frac{1}{bp}\right) \qquad (12)$$

A number of implications can be drawn from Equation 12. Under the dry condition a high adhesion coefficient, FC_a, can be obtained by making the ratio of the actual particle–rubber contact area to the gross geometric area of the rubber block, A/A_n, as high as physically possible. This can be accomplished by providing a very smooth surface together with a soft rubber which will readily adapt to any remaining microscopic surface roughness. Then the ratio A/A_n will for all practical purposes be equal to unity. A high ratio of shear strength to vertical pressure, B/p, will also provide a high FC_a. Removing contaminants from both surfaces for a clean contact area and reducing the pressure will provide a high B/p ratio. Contaminants consist of any dirt, debris, or lubricant which will decrease B at the contact interface. Water also acts as a lubricant, and a smooth surface traps the water film, greatly weakening the B of the bond. Improvement in B is made by increasing the surface roughness to facilitate water drainage. The increase in the FC_a provided by the water drainage more than compensates for the decrease caused by lowering the A/A_n ratio.

Equation 12 indicates that the hysteresis coefficient, FC_h, can be increased by increasing the volume of the rubber involved in the deformation, Q, and by increasing the energy dissipated by damping, D. Sharp-tipped particles with a high height-to-width ratio combined with soft rubber will provide a high Q.

Equation 12 also indicates that both FC_a and FC_h are decreased by increasing the pressure, p. However, Kummer and Meyer (1967) reported that a detailed investigation has shown the FC_h to be practically independent of pressure applied to a rubber block. If this is true, p effects only the FC_a and in turn the FC. It can then be concluded from experimental results that the decreasing effect of p on the FC is greater than the increasing effect of the A.

From Equations 11 and 12 and the previous discussions, it can be seen that for a knobby, well-polished, and lubricated surface FC will primarily represent the FC_h ($B \sim 0$ and hence $FC_a \sim 0$). The FC_a is predominant on a clean, dry, and macroscopically smooth surface (A is large, but $Q \sim 0$ and $FC_h \sim 0$). These statements can be confirmed by results of skid tests on smooth, dense-graded and coarse, open-graded asphaltic concrete surfaces under both dry and wet conditions. Some of these results have been previously summarized by Tomita (1964).

Snowdon (1963) reported that the dynamic modulus and damping properties of rubber are functions of temperature as well as frequency. The mechanical properties of high-damping rubber are more temperature-sensitive than those of low-damping rubber, such as natural rubber. Since the friction coefficient is dependent on material properties, it will obviously be sensitive to temperature and velocity. Results of laboratory and field measurements by practically all researchers in this field have shown that on wet surfaces the friction coefficient decreases as the velocity increases. The effects of temperature on the friction coefficient have been given less attention than those of velocity.

Figure 6 illustrates the relationship between the sliding velocity, pressure, and adhesion coefficient of rubber sliding on a glasslike or a macroscopically smooth surface. The following features, noted by Kummer and Meyer (1967), help to explain the relationship between these factors:

1. On a dry, macroscopically smooth (glasslike) surface the FC_a increases very rapidly and peaks at the critical sliding velocity of approximately 0.1 mph.

2. The FC_a decreases with an increase in pressure, p.

3. There is a drastic reduction in the FC_a when the surface is wet, and there is no prominent peak in the curve. This reflects the reduction in shear strength, B, at the contact interface. The remaining FC_a reflects in part the hysteresis coefficient, caused by the microscopic roughness.

4. Though not illustrated in Figure 6, the shape of the curves, especially the peaks at the critical sliding velocity, is dependent on the rubber properties previously described. There is also a corresponding shift of the curves towards higher critical velocities with an increase in the temperature of the contact interface and towards lower velocities with a decrease in temperature.

Figure 7 shows the hysteresis coefficient, FC_h, for three types of tire-tread rubber sliding on an open-textured, well-lubricated surface. The natural rubber is considered a low-damping rubber, the styrene butadiene rubber a medium-damping rubber, and the butyl rubber a high-damping rubber. The following features noted by Kummer and Meyer (1967) help to explain the characteristics of the hysteresis coefficient:

1. The FC_h is not sensitive to a change in velocity in the range where the FC_a experiences the greatest change. A significant increase in FC_h occurs at high velocities.

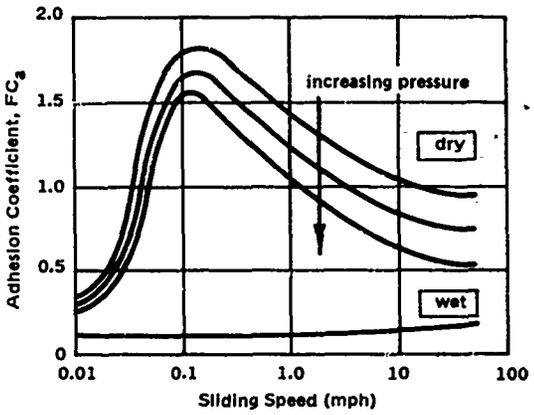

Figure 6. Typical adhesion coefficients of tire tread rubber sliding on macroscopically smooth surfaces. (© Kummer and Meyer, 1967. Used by permission.)

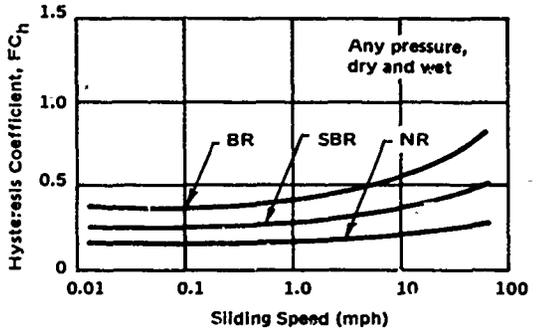

Figure 7. Typical hysteresis coefficients of tire tread rubber sliding on a pebblelike, well-lubricated surface (NR = natural rubber; SBR = styrene butadiene rubber; BR = butyl rubber). (© Kummer and Meyer, 1967. Used by permission.)

2. Though not illustrated in Figure 7, FC_h increases with an increase in the damping properties, D, of the rubber block, provided the volume of rubber deformed, Q, is not affected. The FC_h is for all practical purposes independent of pressure, p. It is not significantly affected by contamination and lubrication at the contact interface. The FC_h, like the FC_a, changes with variations in temperature. However, at any given vehicle velocity the FC_h always decreases with an increase in the temperature of the contact interface.

The preceding discussions on the effects of various factors on the FC_a and FC_h have been summarized in Table 1. Although the discussion has been for idealized conditions, namely a rubber block sliding on a smooth or

rough, wet or dry surface, it should be helpful in understanding the friction characteristics between tires and pavements. The relationship can be seen if the rubber block connected to a common base or tire carcass is regarded as tread elements in contact with the pavement.

Table 1. Change of Adhesion and Hysteresis Coefficients Due to the Increase of an Individual Variable (All Other Variables Held Constant) (© Kummer and Meyer, 1967. Used by permission.)

Variable	Adhesion Coefficient	Hysteresis Coefficient
Surface characteristics:		
Roughness (micro, macro)	decreasing	increasing
Contamination	decreasing	not affected
Lubrication	decreasing or zero	slightly decreasing
Rubber characteristics:		
Elasticity	decreasing	decreasing
Damping	increasing	increasing
Operational parameters:		
Slider load	decreasing	not affected
Sliding speed:		
Range 0-10 mph	increasing or decreasing*	not affected
10-50 mph	decreasing	slightly decreasing
50-100 mph	decreasing	increasing
Temperature	increasing or decreasing**	decreasing

* At contact area temperatures above 200°F the adhesion peak may shift to a critical sliding speed of as much as 10 mph.

** Depending on sliding speed.

OPERATING MODES OF AIRCRAFT TIRES AND ASSOCIATED FRICTION

The airfield pavement surface must provide sufficient friction forces during all operating modes of aircraft tires. Various types of aircraft are operated by the Navy and Marine Corps. However, the fighter-attack aircraft with single-wheel tricycle landing gear are in the majority and appear from experience to be critical with respect to meeting skid-resistance requirements. Transport and patrol aircraft generally have lower landing velocities and reverse thrust for deceleration. Fighter-attack aircraft can be considered to

have nose wheel steering for maneuvering on the ground and brakes on the main wheels only. One or two of the newest attack aircraft are equipped with an antiskid braking device, but many of the naval aircraft now in service are not. Antiskid brakes are being developed for automobiles and are expected to be introduced on a limited basis in the near future. The function and resulting effect of antiskid brakes on stopping capability have been previously discussed by Tomita (1964). Rudder and other aerodynamic surfaces also provide control for aircraft, but these are generally effective only at high velocities. Aircraft tires can roll and slip under normal operating conditions and skid under emergency conditions.

Free-Rolling Mode

The free-rolling mode of the aircraft occurs when no brakes are being applied to the rotating wheels. This occurs during taxiing, takeoff, and landing. Most of the friction forces caused by the differential movement of the tread elements at the contact interface are canceled under this mode. Therefore, the net free-rolling force transmitted by the tire is small on dry pavements and is of little interest in general. However, any significant amount of resistance to the free-rolling tires during takeoff can result in a longer takeoff distance, requiring a correspondingly longer runway length or a higher engine thrust than normal. Tabor (1959) concluded that this resistance can be kept low by modifying the geometry of the tire to give a long, narrow configuration of contact and by using a fine-textured pavement surface. This decrease must necessarily be limited since rolling resistance is directly related to hysteretic loss of the rubber, which in turn is directly related to frictional resistance. In addition, any amount of frictional resistance will add to the total resistance and aid in the deceleration when landing.

When a pavement is covered with a film of water or with slush there is a fluid-displacement drag of the free-rolling tire at velocities below hydroplaning. This fluid drag can be represented by a hydrodynamic equation similar to that for lift (Equation 3). In addition, the aircraft will be retarded by spray drag, which results from water spray impinging on the landing gears and the underside of the aircraft. Horne and Leland (1963) reported on the various aspects of the retarding force caused by water or slush on the pavement. Figure 8 shows the variation of slush drag with velocity for a single wheel. Note that the calculated results from the fluid drag equation are close to the average experimental results. Thus the retardation can be represented by the hydrodynamic drag equation. Figure 9 shows the variation of slush drag with velocity for a jet transport, for four slush depths. The results show that the drag increases and peaks at approximately 120 knots and decreases with a

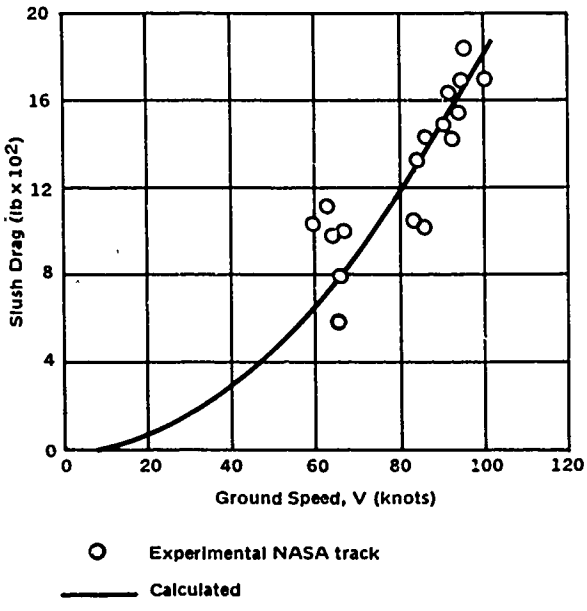

Figure 8. Slush drag on single wheel. (© Horne and Leland, 1963. Used by permission.)

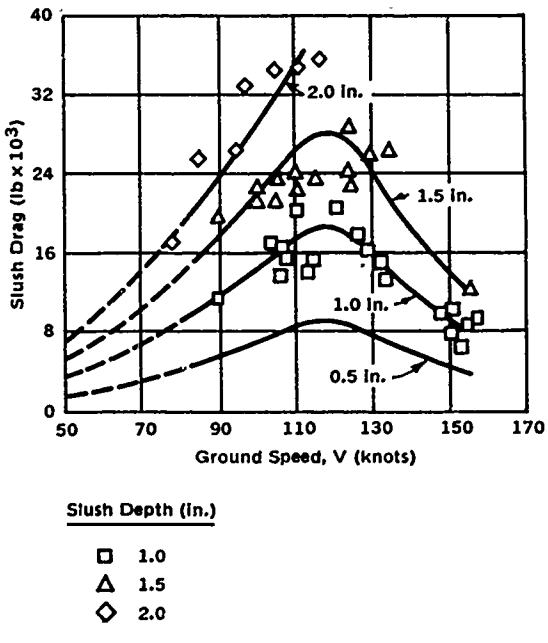

Figure 9. Slush drag on jet transport. (© Horne and Leland, 1963. Used by permission.)

further increase in velocity for three of the four slush depths. The slush drag is greater for the deeper slush at all velocities. The effect of tire pressure, P_t, on slush drag, as determined from tests at the NASA landing-loads track, is shown in Figure 10. The results show that the peak slush drag is higher for the higher P_t and that the peak for the higher P_t occurs at a higher velocity than does the peak for the lower P_t. The effect of slush depth on the takeoff performance for a jet transport is shown in Figure 11. The curves in Figure 11 correlate well with those of Figure 9. That is, the deeper slush depths cause higher drag and consequently more decrease in takeoff performance than the shallower depths.

The preceding discussion indicates that friction force is small and of little consequence for a free-rolling aircraft wheel on dry pavement. However, the presence of water film or slush on the runway can cause drag forces which can seriously tax the takeoff performance of aircraft. During a landing, however, these drag forces can be of benefit in decelerating the aircraft if the velocity is below that at which hydroplaning occurs.

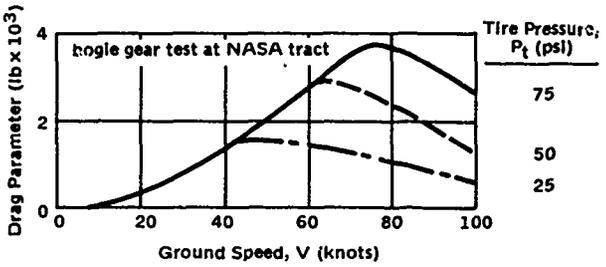

Figure 10. Effect of tire pressure on fluid drag. (© Horne and Leland, 1963. Used by permission.)

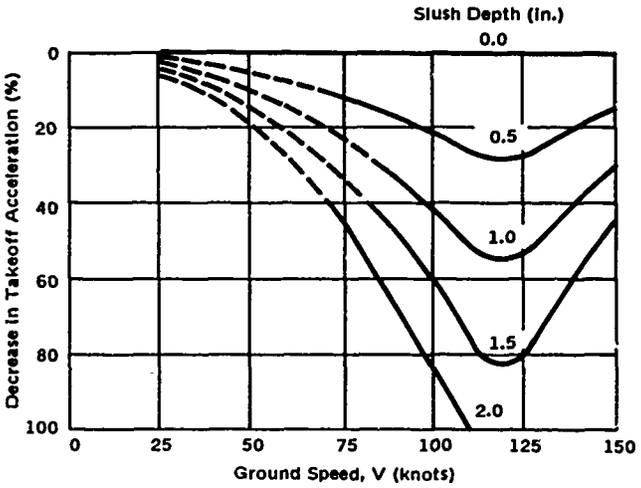

Figure 11. Loss of takeoff performance in slush. (© Horne and Leland, 1963. Used by permission.)

Slipping Mode

Tires are subject to three slipping modes: the drive slip, the brake slip, and the cornering slip. Drive slip is defined as

$$S_d = 100\left(\frac{\omega_t - \omega}{\omega}\right) \tag{13}$$

where S_d = drive slip in percent

ω_t = angular velocity of the slipping tire or torqued wheel

ω = angular velocity of the freely rolling tire corresponding to the velocity of the vehicle

In drive slip the ω_t is greater than ω, and the drive slip becomes 100% when the wheel spins twice as fast as the rolling wheel. The drive slip mode is important for ground vehicles that apply torque to the wheels for mobility. Such is not the case for aircraft operating on an airfield. Only a very small amount of S_d might be generated during takeoff because of the angular momentum of the wheels. There is also some S_d during wheel-spinup at touchdown, but only for a short period of time. Since the S_d is of lesser importance than brake or cornering slip, it will not be considered further in this investigation.

The brake slip, S_b, may be defined as

$$S_b = 100 \left(\frac{\omega - \omega_t}{\omega} \right) \tag{14}$$

For a free-rolling wheel the S_b is zero ($\omega_t = \omega$), but for a locked wheel the brake slip is 100% ($\omega_t = 0$). At this maximum brake slip the tire is in the skidding mode. The importance of the S_b has been emphasized by many researchers in skid resistance. However, it will be discussed further here because tires of aircraft as well as ground vehicles are primarily in the brake slip mode during deceleration. For the purpose of distinguishing the results obtained under the brake slip mode from others, the term brake slip coefficient (BSC) will be used. The term is defined as

$$BSC = \frac{F_b}{F_v} \tag{15}$$

where F_b = friction force under the brake slip mode

F_v = wheel load

Figure 12 shows the changes in brake slip number (BSN) with respect to slip for a tire on dry and wet surfaces (BSN is 100xBSC). Kummer and Meyer (1967) reported that initially the BSN increases approximately in proportion to the brake slip. This occurs because the tire tread elements must slide at a velocity in proportion to the increasing S_b. As shown in Figure 6, the adhesion coefficient initially increases with sliding velocities. The critical sliding velocity of most tread elements is reached at the critical brake slip point. This peak point is sometimes referred to as the incipient skid point and the coefficient as the peak coefficient. Any further increase in braking torque cannot be balanced by the resistance at the tire–pavement interface, and the wheel locks and skids. In general, there is a rapid transition from the

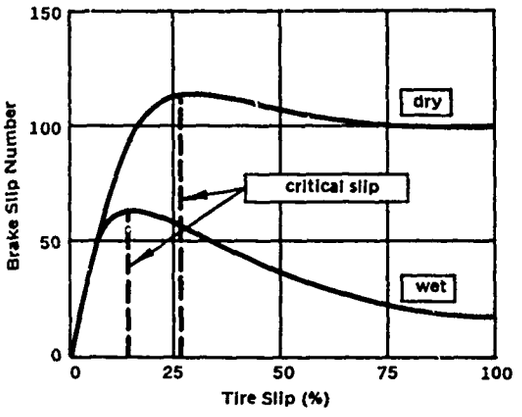

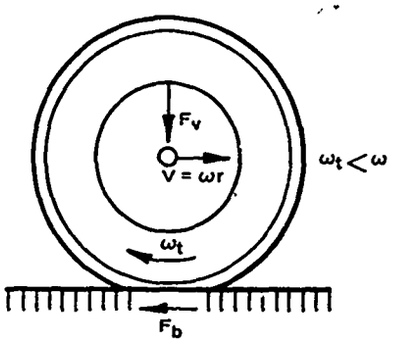

Figure 12. Frictional characteristics of tires operating in the brake slip mode. (© Kummer and Meyer, 1967. Used by permission.)

critical slip point to the full skid point or locked-wheel condition. On a dry surface a slight reduction in BSN is observed between these two points. This slight decrease is caused by the increase in temperature and velocity above the critical sliding velocity. A higher rate of reduction is observed on a wet surface because of the buildup of hydrodynamic pressure as well as some of the temperature and velocity effects.

The hysteresis coefficient peaks at high velocities and contributes to the BSN. Tomita (1964) reported that some increase in friction coefficient between aircraft tires and runways is found above a certain high velocity and that this increase is attributed to the decrease in vertical load caused by aerodynamic lift. However, the hysteresis component may be the major contributor to the increase at such a high velocity.

Another important slipping mode of a tire is the cornering slip mode. The cornering slip in percent may be defined as

$$S_c = 100 \sin \alpha \qquad (16)$$

where α is the slip angle or the angle between the direction of motion and the tire plane. An aircraft turning off a runway to a taxiway especially through a high-speed turnoff requires a high cornering force to successfully accomplish the maneuver. The cornering slip coefficient (CSC) is defined as

$$CSC = \frac{F_c}{F_v} \qquad (17)$$

where F_c is the cornering slip resistance or force. Figure 13 shows the characteristics of a tire in the cornering slip mode and the relationship of cornering slip number (CSN) with α (CSN is 100x CSC). Figure 13 shows that the CSN increases with slip angle up to the point of critical slip angle and then begins to decrease. As expected the peak CSN and critical slip angle are higher for a dry surface than for a wet surface. The explanation for this behavior is the same as that for the brake slip mode except that the tread elements have a sidewise component.

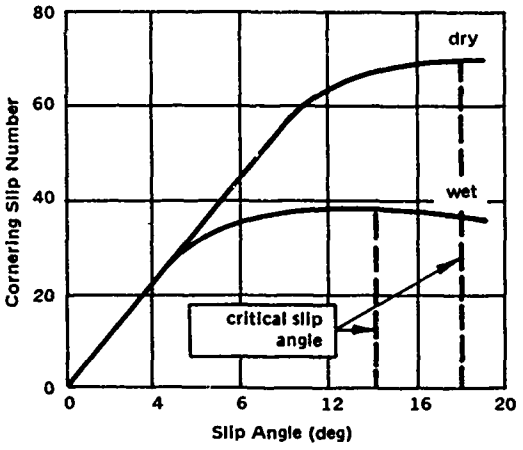

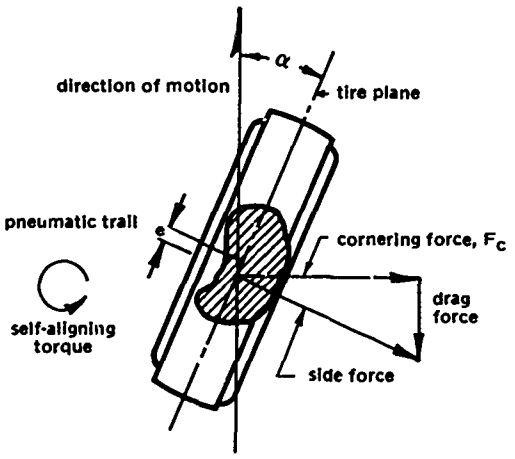

Figure 13. Frictional characteristics of tires operating in the cornering slip mode. (© Kummer and Meyer, 1967. Used by permission.)

Skidding Mode

As previously mentioned, the skidding mode of a tire occurs at the maximum slip of 100%. This mode is generally not a normal operating mode but can be considered to occur during an emergency. A driver of a vehicle sensing an oncoming accident will generally "stand" on the brakes, which causes the wheels to lock and skid on the pavement surface. This results in a stopping distance longer than that under the critical brake slip condition for the vehicle. As pointed out by Tomita (1964), the skidding of aircraft tires even for 1 second can result in excessive tire wear and sometimes in tire blowout. The skidding mode of the tire for aircraft, therefore, should be avoided as much as possible. However, the skidding mode has been used to measure and appraise the frictional characteristics of many pavements and will be considered in this investigation.

The friction coefficient under the skidding mode is designated the skid coefficient (SC) and is defined as

$$SC = \frac{F_{sk}}{F_v} \tag{18}$$

where F_{sk} is the friction force under the skidding mode, or skid resistance. Under this mode it appears that all the tread elements slide at the same velocity and in the same direction. However, the elements are subjected to different pressures. Those near the center of the contact area are subjected to higher pressures than those near the entrance or exit of the contact area. The thicker fluid film at the entrance lowers the shear strength in that area and the volume of rubber deformed at high velocities. Thus the contributions of the various tread elements to the total skid resistance differ.

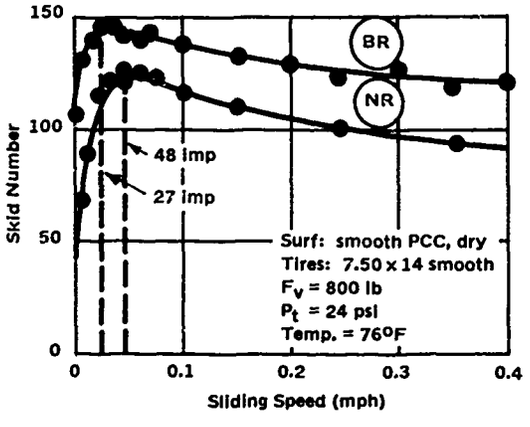

Figure 14. Frictional characteristics of natural rubber (NR) and butyl rubber (BR) tires operating in the skidding mode. (© Kummer and Meyer, 1967. Used by permission.)

Figure 14 shows the relationship of skid number (SN) with velocity for two types of rubber tires on a dry, smooth PCC surface (SN is 100xSC). As shown in Figure 14 the SN increases to a critical sliding velocity and decreases thereafter like the BSN versus slip ratio curves of Figure 12. Kummer and Meyer (1967) reported that the decrease in SN is sometimes accompanied by an audible chatter of the rubber. Under wet conditions the SN can be low at high velocities. The reasons for the low SN are the effects of high velocity, low shear resistance, low volume of deformed rubber, and high temperature.

FRICTION-MEASURING METHODS

Various types of equipment and methods for measuring tire-pavement friction coefficients have been discussed in the previous report by Tomita (1964). The types include the stopping-distance method, the deceleration

method, the skid trailer method, the bicycle wheel apparatus of the National Crushed Stone Association, and the British pendulum tester. Brief descriptions of the devices and methods were provided; results from correlation tests were compared; and the advantages and disadvantages of the devices or methods were given. The following paragraphs describe some of the improvements made to the various methods, variations in test procedures, newly developed devices, and results of correlation tests conducted since those reported by Tomita (1964).

Stopping-Distance Method

The stopping-distance method duplicates the conditions of an automobile in a panic stop better than any other method. This method is generally considered to measure the friction coefficient under the non-steady-state sliding mode. An average **SC** is measured between two points of a skidding vehicle. However, some **BSC** is included if the distance measurement is made from the point of brake application and not from the onset of the skid. Thus a higher value than the actual **SC** can be obtained with this method.

In the stopping-distance method an automobile is properly instrumented for the continuous monitoring of velocity, distance, and time. As reported by Rizenbergs and Ward (1967) combinations of these parameters can be used in appropriate work-energy equations to obtain friction coefficients. The work-energy principle applied to a stopping automobile states that

$$F(X) = \frac{1}{2}\left(\frac{W}{g}\right)\left(V_1^2 - V_2^2\right) \qquad (19)$$

where X = skidding distance

W = static weight of the vehicle

g = gravitational acceleration

V_1 = initial velocity

V_2 = final velocity

From Coulomb's law of friction

$$F = (FC)W \qquad (20)$$

Combining Equations 19 and 20 and substituting the proper factors for velocity in mph yields the stopping-distance coefficient (SDC)

$$SDC \sim FC \sim \frac{V_1^2 - V_2^2}{30X} \quad (21)$$

The skidding distance can be expressed in terms of average velocity and time by

$$X = \frac{1}{2}(V_1 + V_2)(t_2 - t_1) \quad (22)$$

where t_1 = time at the start of measurement

t_2 = time at the end of measurement

Combining Equation 22 with Equations 19 and 20 and substituting the proper factors for V in mph and 32.2 ft/sec for g yields

$$SDC = FC = \frac{0.0456(V_1 - V_2)}{t_2 - t_1} \quad (23)$$

After conducting an extensive investigation, Rizenbergs and Ward (1967) reported that the use of an automobile is extremely unsatisfactory for regular skid testing. Interference with traffic flow, time required for the test, hazards to testing personnel, number of technicians required (4) and high average cost ($25.00 per site per lane) are some of the reasons. Kummer and Meyer (1967) reported that the use of stopping-distance automobiles for routine skid tests appears to be on the decline. Csathy, Burnett, and Armstrong (1968) also reported on the declining use of the stopping-distance method.

All of the previously cited difficulties with the stopping-distance method are not applicable to testing airfield runway pavements. Tests will generally be conducted on runways when no aircraft traffic exists, so there will be no interference and fewer hazards to testing personnel. A runway also has a wider paved area on which the vehicle can veer during the skid, permitting possibly higher test velocities than can be used on highways. In addition the brakes of the test vehicle can be modified to provide diagonal braking, which ensures lateral stability. The modification consists of installing solenoid valves between the brake master cylinder and wheel cylinders so that brake pressure can be applied only to the left-front and right-rear wheels or to the right-front and left-rear wheels. A hard application of brakes will result in locking only one set of the diagonally opposite wheels. The other set of wheels receiving no brake torque rotates at a velocity corresponding to

the velocity of the decelerating vehicle. These rotating wheels, as reported by Tomita (1964), are capable of generating side force and provide lateral stability to the vehicle.

Deceleration Method

The deceleration method is generally used in conjunction with the stopping-distance method. A decelerometer is usually mounted on the floor of the automobile, and the deceleration is measured during the skid. The friction force caused by the deceleration is given by

$$F = md = \frac{Wd}{g} \tag{24}$$

where m = mass

d = deceleration

By use of Coulomb's law of friction, Equation 24 can be reduced to a simple function for the deceleration coefficient (DC):

$$DC = FC = \frac{d}{g} \tag{25}$$

During braking, the front end of the automobile tilts down, and a correction factor for this tilt is generally used. The use of an improper correction factor has been cited as the major error in this method. This error associated with the "dive" has long been recognized. It has been thoroughly discussed by Tomita (1964).

Some of the disadvantages previously cited for the stopping-distance method also apply to the deceleration method. In spite of its shortcomings, the deceleration method appears to be capable of showing the variation in friction coefficient with changes in the pavement surface conditions. Table 2 shows average decelerometer readings on asphaltic concrete surfaces before and after application of a fog seal coat. The seal coat was applied at the rate of 0.1 gal/yd^2. As expected, the readings in Table 2 are lower for the wet surface than for the dry surface. They are also lower after the seal coat has been applied.

The Air Force has developed a method of determining the ground roll distances of aircraft on runways with various surface conditions (Figure 15). The method is based on decelerometer readings, called the runway condition readings (RCR), taken with the James brake decelerometer. Aircraft ground

rollout distance measurements are taken on a dry PCC runway having an RCR of 23 or above. Ground roll distances corresponding to lower values of RCR are obtained by analysis. A chart such as shown in Figure 15 is developed for each type of aircraft and is included in the corresponding Air Force flight manual.

Table 2. Mean Decelerometer Readings (ft/sec^2) on Asphaltic Concrete Runways Before and After Seal Coat

Pavement Area	Before Seal Coat		After Seal Coat		Remarks
	Dry	Wet	Dry	Wet	
El Paso Airport					
Runway 8-26	25.9	23.2	22.3	19.6	initial speed, 20 mph
Taxiway J	–	–	25.9	22.7	initial speed, 20 mph
Taxiway L	–	–	24.2	–	initial speed, 20 mph
Taxiway D	26.2	–	–	–	initial speed, 20 mph
Taxiway C	–	–	24.5	23.5	initial speed, 20 mph
NAS, Point Mugu					
Runway 9-27	–	–	17.5	9.0	initial speed, 30 mph
Parallel taxiway	20.3	19.8	–	–	initial speed, 30 mph
Runway 3-21	–	–	17.5	11.5	initial speed, 30 mph

In the Air Force method, RCR are periodically taken on runways when the surfaces are dry, wet, slushy, snow covered, or icy. A manual is available on the installation, adjustments, and test procedures for the James brake decelerometer. The current readings are given to air traffic control personnel, who relay the applicable reading to the pilots. The pilots determine the required ground roll distances and decide to land or divert to other airfields for safe landings.

The Air Force method assumes that a safe landing can be made on a runway if the runway length is greater than the required ground roll distance. It does not relate the RCR to aircraft braking coefficients in usable form mainly because of the low test velocity (20 mph) of the vehicle used to obtain the RCR. Consequently, the Air Force method provides little information on a runway whose condition is slippery and on which an aircraft may exhibit lateral instability during ground operations. Test data for the Air Force method evaluated on various types of pavement surfaces are being analyzed and results are expected in the near future.

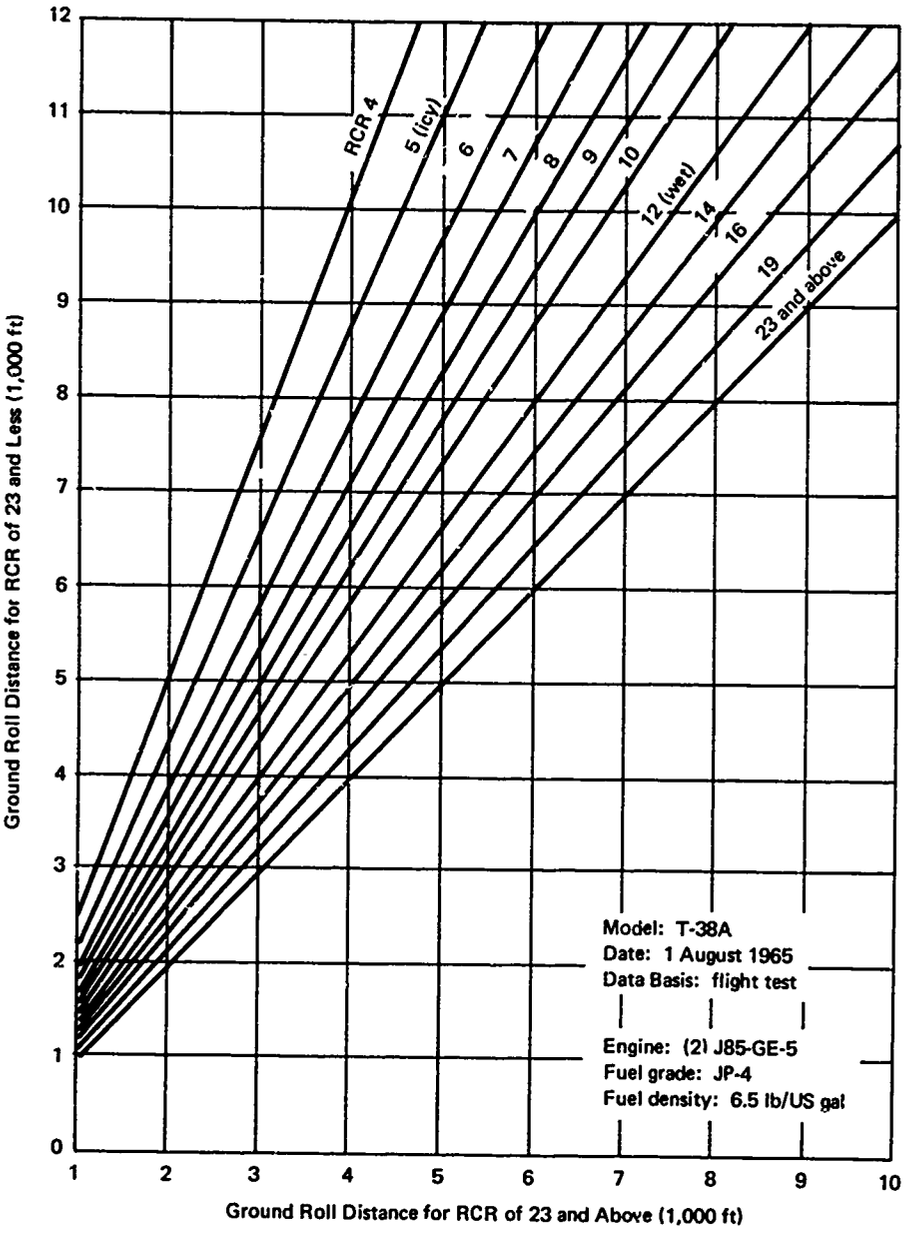

Figure 15. Effect of runway condition readings (RCR) on ground roll distance of T-38A aircraft. (From Department of the Air Force, 1967.)

Skid Trailer Method

Considerable effort has been made in recent years to improve the skid trailer method. Its quick testing capability and the fact that it does not significantly interfere with traffic may have stimulated developers to make the improvements. ASTM Committee E-17 on Skid Resistance has approved a tentative method of testing the skid resistance of pavements by using a skid trailer (ASTM E274-65T). For this trailer, the skid-resistant force at the tire-pavement contact is obtained from the measurement of wheel torque. Kummer and Meyer (1967) reported that trailers which measure the hitch forces have proven to be unsatisfactory and are no longer in use.

With the exception of the trailers used by NASA, FAA, and some European countries, all trailers measure the friction coefficient under the skidding mode. Thus, the results are presented as skid coefficients or skid numbers. Figure 16 shows the three basic variations of the trailer method currently in use. The bending moment, **M**, is measured with the trailer in the skidding mode shown in Figure 16a. As shown in Figure 16a

$$SC = FC = \frac{F_{sk}}{F_v} = \frac{\frac{M}{F_v} - k - \left[(h-r)\left(\frac{d}{g}\right) - (k-f)\right]\left(\frac{a}{a-f}\right)}{r + \left[(h-r)\left(\frac{d}{g}\right) - (k-f)\right]\left(\frac{a}{a-f}\right)\left(\frac{j}{a}\right)} \qquad (26)$$

Equation 26 shows that the **SC** is not directly related to **M** and is affected by many other factors. These factors include the location of the center of gravity, deceleration or acceleration effects, and the geometric ratio **j/a**. In general, fluctuations in velocity are unavoidable during testing and the ratio $d/g \neq 0$. The only simplification of Equation 26 which can be made is to let **h** approach **r** for the trailer.

The force F_1 is measured for the type of trailer shown in Figure 16b. The **SC** for this type is given by

$$SC = FC = \frac{\left(\frac{c}{r}\right)\left(\frac{F_1}{F_{vo}}\right)}{1 - \left(\frac{h-j}{a-f}\right)\left(\frac{d}{g}\right) - \left(\frac{j}{a}\right)f_o} \qquad (27)$$

where $f_o = F_{sk}/F_{vo}$

F_{vo} = static wheel load

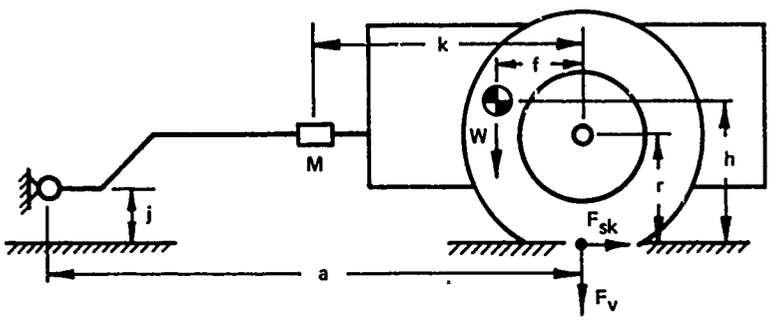

(a) General Motors original design.

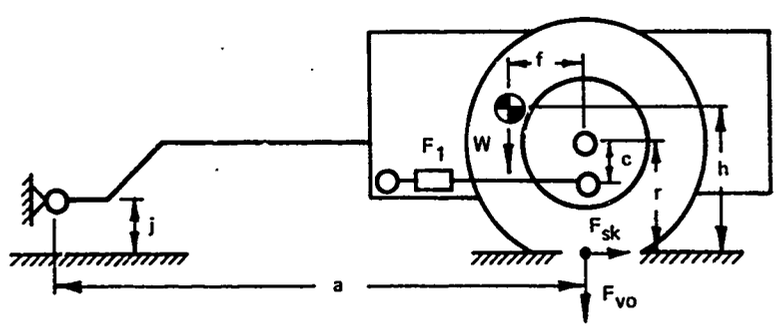

(b) Cornell Aeronautical Laboratory design.

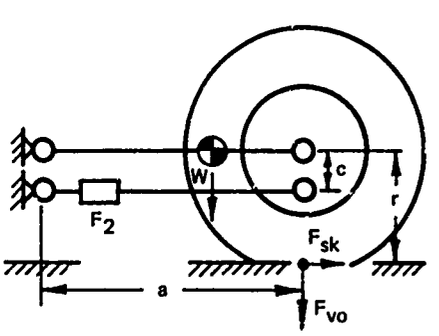

(c) Pennsylvania State parallelogram design.

Figure 16. Skid trailer types used in the United States. (© Kummer and Meyer, 1967. Used by permission.)

As was found for the preceding type of trailer, the SC is not directly proportional to the measured parameter F_1 and is affected by operational and geometric factors. Since $d/g \neq 0$ for this type of trailer either, Equation 27 can be simplified when h approaches j. In addition, if the ratio $j/a = 0$, a linear relationship is obtained between F_1 and SC. However, this ratio cannot be achieved but only approached by making j small and a large. Thus, this type of trailer is generally constructed with a low j and a long a. The h should also be low and ideally the same as j. Again, this ideal condition can only be approached but not attained in practice.

The type of trailer shown in Figure 16c represents the most simple and compact design. The SC, which is proportional to F_2, can be represented by

$$SC = FC = \left(\frac{c}{r}\right)\left(\frac{F_2}{F_{vo}}\right) \tag{28}$$

Equation 28 shows that the SC is directly proportional to the measured force F_2, and no effects of velocity fluctuations or of geometric factors are present.

Equations 26, 27, and 28 relate the three measured parameters, the bending moment M and the forces F_1 and F_2, to the SC for the three types of trailer. In the locked-wheel mode the friction force shifts the center of the tire contact area rearward with respect to the wheel axis. The effects of this tireprint relocation is neglected in the equations.

The original trailer developed by General Motors Proving Ground (GMPG) in 1957 was of the type shown in Figure 16a, but it was later converted to the type shown in Figure 16b. Goodenow, Kolhoff, and Smithson (1968) reported on the recent improvements made on the GMPG model II trailer. The improvements include the addition of the slipping mode and the elimination of the effects of inertial torque at points between free-rolling and locked wheel modes. Also considered was correcting the effects of tireprint relocation caused by the application of the brakes.

The slipping mode of the GMPG model II trailer is monitored during the regulated lockup of one of the trailer wheels. Zero to 100% slip constitutes one cycle. The time rate of this cycle can be varied up to a maximum of 10 seconds. However, no provisions are made to hold the percent slip at a fixed value or to recycle within the range of zero to 100%. In obtaining the percent slip the direct current voltages representing the unbraked wheel velocity and the braked wheel velocity are summed in a difference amplifier. Then this quantity is divided by the direct current voltage of the unbraked wheel and is presented as output on an oscillograph.

The corrected wheel torque of a braked wheel is the total wheel torque less the inertial torque, which is the product of the polar moment of inertia and angular deceleration of the braked wheel. This correction is achieved in the following manner:

1. The total wheel torque is converted to the volts per inch-pound scale.

2. The analog voltage representing the braked wheel velocity is differentiated to obtain voltage representing the angular deceleration. A potential which represents the inverse of the polar moment of inertia is divided into the deceleration voltage, and the result is scaled to the same volts per inch-pound scale as the total wheel torque.

3. A difference amplifier is used to sum the voltages representing total wheel torque and the quantity obtained in step 2, resulting in an analog voltage for the corrected wheel torque. This analog voltage is recorded on a direct-writing oscillograph.

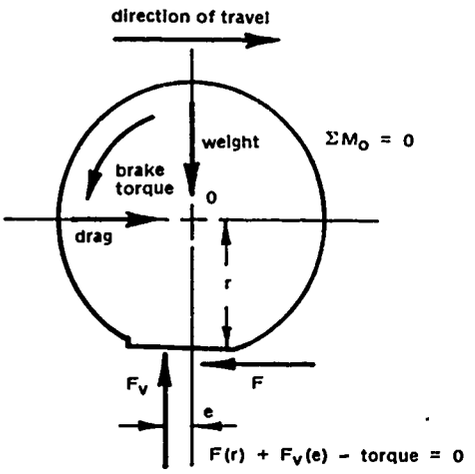

Figure 17. Free-body diagram of braked tire. (© Goodenow, Kolhoff, and Smithson, 1968. Used by permission.)

Figure 17 illustrates the relocation of the tireprint of the braked wheel. The moment created by the relocation adds to that caused by the friction force. To define the magnitude of the effects of this phenomenon, Goodenow, Kolhoff, and Smithson (1968) made static and dynamic measurements of all the components of the free-body diagram in Figure 17. Tests were performed on various types and brands of tires at room temperature and immediately after warm-up on a vehicle. A range of tire inflation pressures was also used. The test results for all tires and conditions showed a linear relationship between tireprint displacement and friction force up to an equivalent friction coefficient above 1. Thus, for any given vertical load, the effects of tireprint displacement can be expressed as a percent error, defined as

$$H = \left(\frac{T_m - F_t r}{F_t r} \right) 100 \qquad (29)$$

where H = percent error

T_m = measured torque

F_t = true friction force

r = tire radius

The test results showed that the variation in inflation pressure and temperature has considerable effect on the H. Pressure variation in some tires can change the percent error by a factor of 3, with the error decreasing with increasing pressure. Percent error ranged from 2% to 10% for the static tests at room temperature and from 3% to 9% for the warm tires. A similar range of percent error was obtained under dynamic tests. However, differences exist between corresponding static test results and between corresponding dynamic test results.

The skid trailer developed by the Cornell Aeronautical Laboratories is of the type shown in Figure 16b. Similar trailers are currently used by the Bureau of Public Roads, the New York State Department of Public Works, and the Portland Cement Association.

The type of trailer shown in Figure 16c, developed by Pennsylvania State University, is a single-wheel trailer that is currently being used by the Pennsylvania Department of Highways as well as by the University. The British Road Research Laboratory has developed a smaller trailer of similar design.

Domandl and Meyer (1968) reported on the addition of the brake slip mode to the Pennsylvania trailer. To control the locking of the wheel, the signal from the impulse generator is used to deenergize the brake system solenoid. Wheel lock can be prevented altogether or for a predetermined period of time. The following modes of operation are achieved:

1. A cycle timer actuates the brake at constant time intervals and releases it automatically.

2. The release signal can be used as an override. For this mode, the brake is actuated each time the wheel velocity increases above a certain point set on the release control. If the setting on the release control is varied, the wheel can be made to run-up to the free-rolling velocity or to some velocity below free-rolling velocity.

3. Manual braking and release are possible at any time. So that the testing capability in the skidding mode is retained, provisions are made to bypass the brake release. This permits locked-wheel tests in accordance with ASTM E274-65T.

Figure 18 shows two reproduced oscillograms illustrating the brake slip and skidding modes of the Pennsylvania trailer. The behavior of the angular wheel velocity, ω, velocity of the vehicle, V, and friction force, F, during the braking procedure is indicated by numbers 1 through 5 in the lower oscillogram and 1, 2, 4, and 5 in the upper oscillogram. At point 1 the brakes are applied and ω begins to decrease and F to increase. The critical slip point is reached at point 2, where F is maximum. At point 3 on the lower oscillogram the skidding mode begins with $\omega = 0$ and continues until point 4. Under the locked-wheel condition, F is lower than the F at critical slip. Brake release begins at point 4, and spin-up to free rolling occurs at point 5. Between these points, F again passes through the critical slip point before decreasing to zero. The lack of point 3 in the upper oscillogram indicates that the skidding mode was not reached by the wheel.

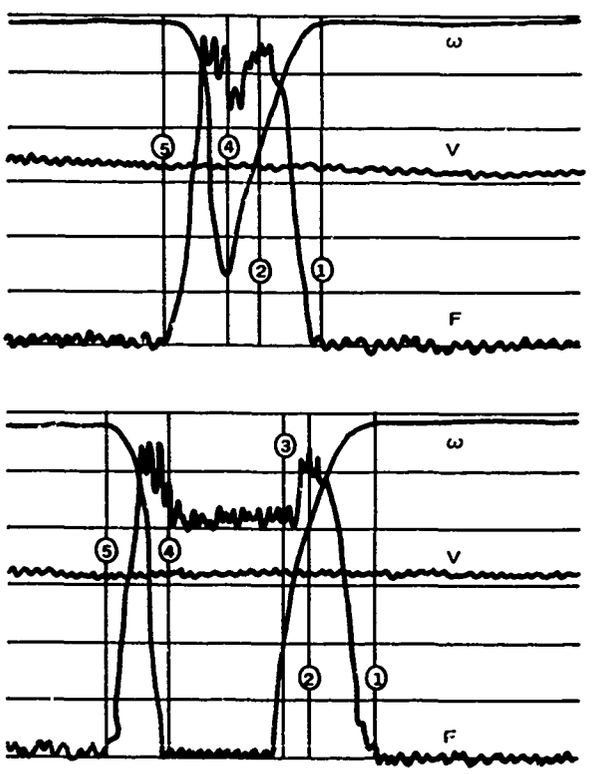

Figure 18. Replicas of typical oscillograms of brake slip and skidding modes of the Pennsylvania trailer. Numbers are explained in text.

Portable Testers

Two small portable skid testers were previously described by Tomita (1964): the bicycle-wheel apparatus of the National Crushed Stone Association and the British pendulum tester. No basic changes have been made on these testers since then. The British tester has gained some popularity recently in the United States, mainly because it is comparatively small, inexpensive, and accurate. The tester basically works on the principle that the energy lost by the pendulum during the swing is equal to the work done in overcoming the friction between the slider and the surface. A tentative method for testing and calibrating the tester is found in ASTM E303-66T. The tester may be used for field as well as for laboratory testing. It is especially suitable for laboratory testing because it requires only a small test area (3 by 5 inches).

Pennsylvania State University developed the Pennsylvania State drag tester as a supplement to the Pennsylvania State trailer. It consists of a small two-wheel cart which drags the edge of a small rubber specimen over the pavement. As the tester is "walked" along the pavement, the drag force in the skidding mode is measured by a hydraulic load cell and is displayed on a dial gage as a multiple of the friction coefficient. The operator has little difficulty in reading the dial because of the careful damping of the system. The tester is small and is simply constructed. It requires no set-up time and is suitable for spot-checking the skid resistance of pavement surfaces. The commercial version of the tester is called the Keystone Mark IV Resistance Tester. Kummer and Meyer (1967) reported that it is presently undergoing field trials by seven state highway departments.

Walsh (1966) reported on the development of the New York Thruway skid test cart. It works on the principle of twin parallelograms suspended on friction-free bearings and mounted on a wheeled chassis. A skid fitted with a section of the tire tread and attached to a pick-up device slides on the pavement surface. For testing on wet pavement, a watering system wets the pavement surface ahead of the tread. Two jets are provided for laying lines of red dye on the pavement. One jet is fixed on the cart, the other on a movable arm. As the friction coefficient increases, the arm moves away from the stationary jet, increasing the distance between the dye lines. The reverse is true with a decrease in the friction coefficient. A calibrated scale is provided to convert the distance between the dye lines to friction coefficients.

Table 3 lists the principal specifications of the three portable testers. All three are commercially available from the distributors shown. Since instrument constants, variations in sliding length, and adjustments by operators are involved in skid measurements, the resulting data are not the same. Thus, as indicated in Table 3, the number from the scale of the pendulum tester is

referred to as the British pendulum number (BPN) and from the scale of the New York drag tester as the drag test number (DTN). The skid test cart results are in friction coefficients.

Table 3. Specifications of Commercially Available Portable Pavement Friction Testers (© Kummer and Meyer, 1967. Used by permission.)

Specification	Pendulum Tester	Drag Tester	Skid Test Cart
Principle	energy balance	force measured	force measured
Mechanism	mechanical	hydraulic	mechanical
Slider form	inclined shoe	inclined shoe	curved segment
Rubber*	natural†	natural or ASTM E-249	ASTM E-249
Contact width (in.)	3	3	1-1/2
Length‡ (in.)	1/8	1/8	3/4
Area‡ (sq in.)	0.37	0.37	1
Slider load (lb)	5.9	6.0	20-25
Contact pressure‡ (psi)	16	16.2	22.5
Test weight (lb)	27	20	110
Transport weight (lb)	27	20	40
Sliding speed (mph)	6-7	3-4	3-4
Data reported as	BPN	DTN	FC
Dimensions (in.)	26 x 18 x 26	30 x 10 x 22	36 x 14 x 14
Distributor	Soiltest§	Die-A-Matic¶	Test Lab§
List price ($)	795.00	550.00	1,200.00

*Furnished by distributor.

†ASTM Method of Test E303 for use of the pendulum tester prescribes for the slider rubber the compound specified in ASTM Standard E-249 for the standard pavement test tire.

‡Typical conditions; actual values depend on state of slider wear.

§Chicago, Ill.

¶York, Pa.

CORRELATION STUDIES

Efforts made by various organizations to correlate the results of skid measurements obtained with various devices were reported by Tomita (1964). One of these earlier correlation studies was associated with the First International Skid Prevention Conference, held in August 1958. Recently, similar studies have been given increased emphasis, resulting in extensive programs at Tappahannock, Virginia, during the summer of 1962; at Dunnellon Airport, Florida, in October-November 1967; and at NASA's Wallops Station, Virginia, in the spring of 1968.

Correlation Between Friction-Measuring Devices

Dillard and Mahone (1963) reported on the correlation study at Tappahannock, Virginia. The objectives of the primary experiment were as follows:

1. To determine the relationship between devices within the three groups tested (trailers, stopping-distance cars, and portable testers).

2. To determine the relationship between the three groups of devices.

3. To determine the factors causing any discrepancies in measurements taken with devices of similar design.

4. To provide an opportunity for discussion between developers of friction-measuring devices.

In addition to the primary experiments, secondary experiments were conducted at Tappahannock. These experiments were devoted to studying the effect of water film thickness, comparing the self-watering systems of various trailers, investigating the effect of vertical load on friction coefficients, and studying the variations associated with the British pendulum tester. The primary experiments are discussed in detail, and findings from the secondary experiments are recorded, in the following paragraphs.

A total of eight skid trailers, four stopping-distance automobiles, and three types of portable testers were included in the program. The portable testers included the Pennsylvania State drag tester, the bicycle wheel appartus of the National Crushed Stone Association, and ten British pendulum testers.

The standard ASTM E-17 tire for pavement tests (ASTM E240-66) was used wherever possible. Since standard tires of the proper size were not available for some of the trailers and cars, tires were purchased with the same

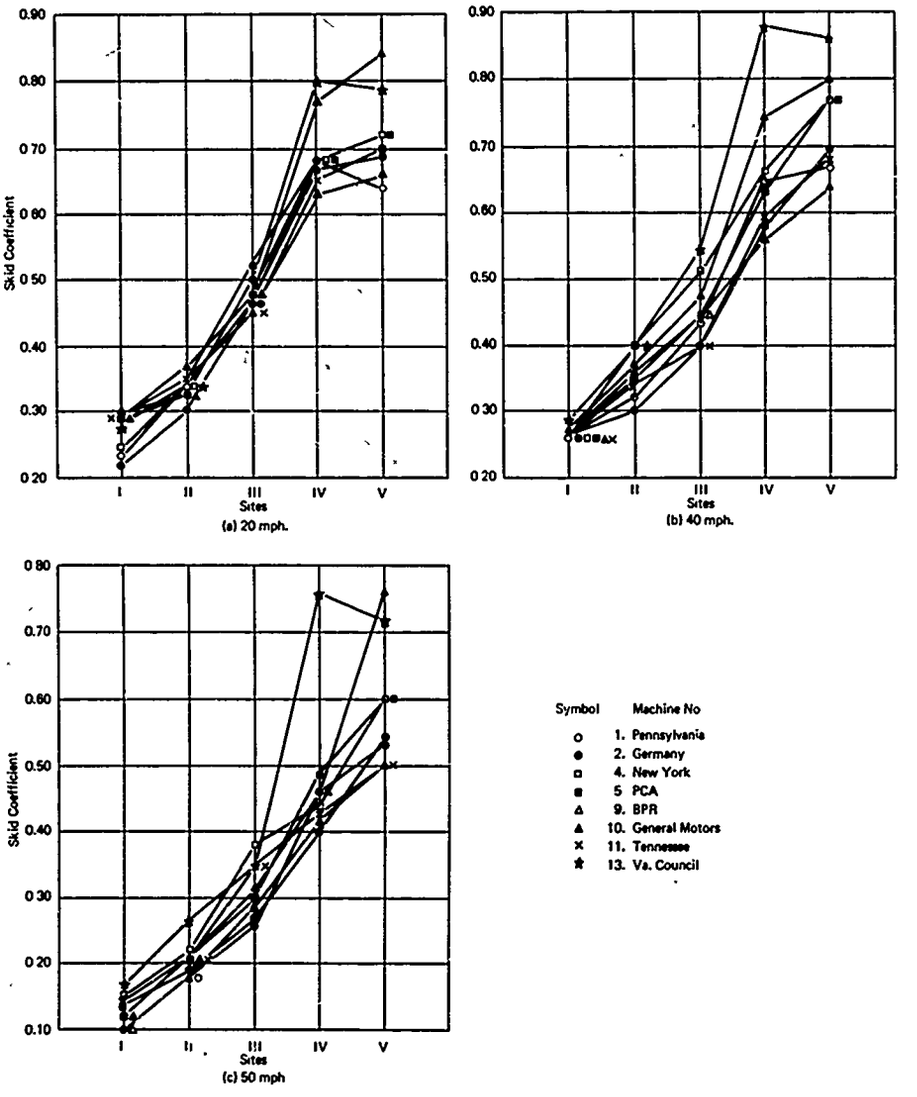

Figure 19. Summaries of trailer data. (© Dillard and Mahone, 1963. Used by permission.)

rubber compound used in the ASTM E-17 tires. The same compound was used in the sliders of five of the ten British pendulum testers, British natural rubber sliders being used in the other five testers.

Five test sites were selected on a flight strip at Tappahannock. Site I was sprayed with yellow traffic paint and polished with a steel bristle power broom. Site II was a relatively rough textured asphaltic surface sprayed with an asphalt emulsion. Site III had a fine slurry seal made with the same emulsion as Site II mixed with 6 to 8 lb/gal of fine sand. Site IV was a fine-textured sand mix similar to the one used by the Virginia Department of Highways. Site V was a section of the existing strip which had a siliceous sand-gravel surface in good condition.

The skid coefficients for the trailers on all five sites at 20 mph, 40 mph, and 50 mph are shown in Figure 19. Each data point represents an average of four measurements. All trailers show the same general trend of skid coefficient with respect to the test sites. However, there is some spread at each test site for every test velocity. The spread is greatest in Sites IV and V, with trailer numbers 10 and 13 providing appreciably higher skid coefficients than others.

Three types of stopping-distance measurements were made: (1) the "chalk-to-gun" method, (2) the stopmeter connected to a fifth wheel (both previously described by Tomita, 1964), and (3) the observed stopping distance, which is the distance from the beginning of the skid mark to the back wheels of the stopped vehicle. An observer is necessary to note the beginning of the skid for the last measurement.

Table 4 shows the stopping-distance coefficients obtained from the three types of measurements for 20 mph, 30 mph, and 40 mph. The stopping-distance coefficients obtained with the stopmeter are lower than those for the other two methods. However, the results from the chalk-to-gun and observed stopping distance measurements agree closely. Both the differences and agreements in the results can be easily explained. A fast-responding micro-switch activated the stopmeter shortly after braking but before the wheels locked. Thus the stopmeter included the locked-wheel distance plus some distance traveled during wheel retardation. In effect, the stopmeter measured the total distance covered from the time of brake application to the point where the vehicle came to rest. On the other hand, the observed stopping distance was measured between the wheel-lock point and the vehicle resting point. Apparently the delay in the chalk gun upon braking marked the pavement near the point of wheel lock. Therefore, close agreement between the results obtained from these last two methods is to be expected.

Since the test velocity is constant for the British pendulum testers, the slide lengths were varied in the investigation. These were 4.6 inches, 4.8 inches, and 5.0 inches. Prior to any testing, the instrument constants of the British pendulum testers were determined. This involved measuring the pendulum weights, the moment of the bearing housing, the center of gravity,

Table 4. Comparison of Stopping-Distance Data Obtained by Three Methods, Indiana Skid Test Car (© Dillard and Mahone, 1963. Used by permission.)

Type of Speed Measurement	Stopping Distance Coefficient														
	Site I			Site II			Site III			Site IV			Site V		
	20	30	40	20	30	40	20	30	40	20	30	40	20	30	40
Chalk-to-gun	0.32	0.28	0.22	0.44	0.36	0.30	0.54	0.48	0.39	0.78	0.68	0.61	0.87	0.80	0.71
Observed	0.31	0.29	0.21	0.44	0.38	0.32	0.54	0.46	0.38	0.75	0.68	0.63	0.75	0.92	0.75
Stopmeter	0.28	0.26	0.20	0.35	0.31	0.28	0.44	0.42	0.36	0.58	0.57	0.54	0.62	0.65	0.60

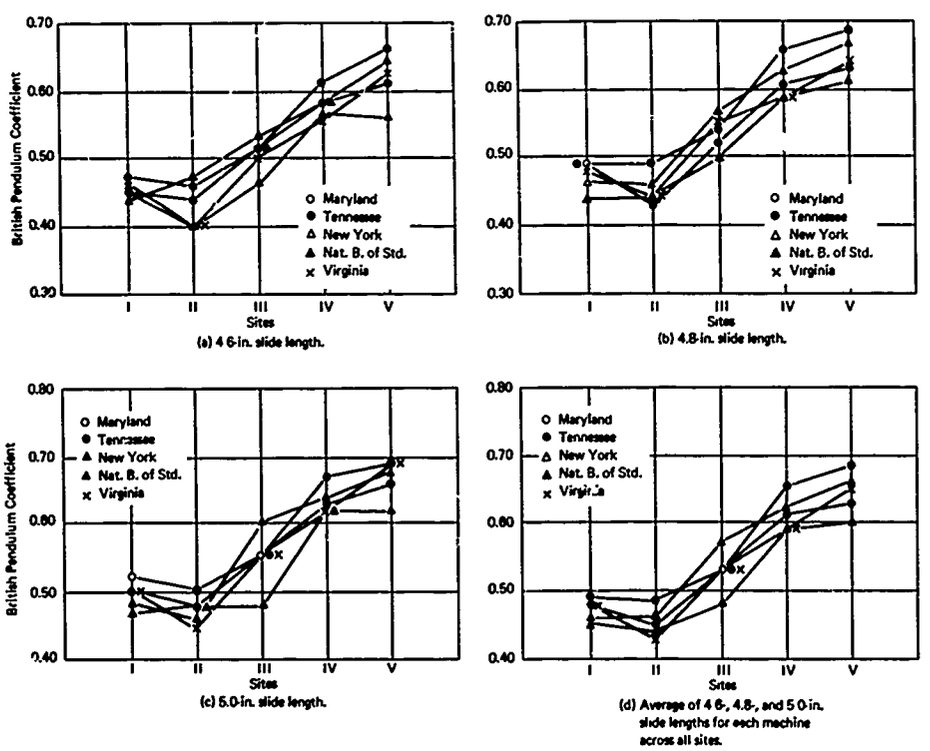

Figure 20. Mean BPC of testers using British rubber. (© Dillard and Mahone, 1963. Used by permission.)

the distance between the center of oscillation and center of gravity, and the slider load. The deviation of each instrument constant from the average instrument constant was used as a correction factor for the British pendulum coefficient (BPC).

Figure 20 shows the BPC for the five testers using the British rubber. Figure 20d is the average of the three slide lengths across all sites. The five testers do not maintain an identical relationship across all sites and slide lengths. A statistical analysis was conducted based on the least significant difference of the average for each tester on all sites. The purpose was to determine if the differences between the testers were great enough to be of consequence. There are 10 possible comparisons of the results between the five testers. The results showed that there is no significant difference in 3 of the 10 comparisons of the measured BPC, and this improved to 7 out of the 10 comparisons of the corrected BPC. The differences for the remaining comparisons are considered statistically significant. However, this does not indicate that the differences are significant from the practical standpoint. Results from similar tests and analyses for American rubber sliders showed that, based on both the average and corrected BPC, there is no significant difference in 5 out of the 10 comparisons. The lack of improvement in correlation by application of the correction factor can be explained by the low maximum difference in the average BPC. In addition, the measured averages and the corrected averages are not too different because of the degree of agreement in the correction factors.

Table 5 shows the mean values of all the British pendulum testers using British and American rubber for all three slide lengths, together with the mean values for the National Crushed Stone Association bicycle wheel apparatus and those for the Pennsylvania State drag tester. A comparison of the results of the portable testers leads to the following conclusions:

1. Good agreement exists between the results of the bicycle wheel apparatus and the drag tester on all surfaces except that of Site III.

2. The British pendulum testers using the American rubber sliders have better agreement with the other two types of portable testers than those using the British rubber sliders.

3. More realistic values are given by the bicycle apparatus and the drag tester than either group of the British testers.

4. The five testers using British rubber sliders give lower readings than the five using American rubber sliders. However, the difference is not entirely caused by the rubber, since the correction factor did not consider the relationship between the two types of rubber.

Table 5. Mean Friction Values Measured by Portable Testers

Site	British Rubber	American Rubber	Drag Tester	Bicycle Wheel*
4.6-In. Slide Length				
I	0.45	0.46	–	–
II	0.43	0.49	–	–
III	0.50	0.59	–	–
IV	0.58	0.64	–	–
V	0.62	0.71	–	–
4.8-In. Slide Length				
I	0.48	0.47	–	–
II	0.45	0.50	–	–
III	0.54	0.62	–	–
IV	0.62	0.65	–	–
V	0.65	0.74	–	–
5.0-In. Slide Length				
I	0.49	0.50	0.38	33 deg = 0.40
II	0.47	0.53	0.50	29 deg = 0.52
III	0.55	0.65	0.61	20 deg = 0.79
IV	0.64	0.67	0.73	22 deg = 0.73
V	0.67	0.78	0.75	21 deg = 0.76

* The National Crushed Stone Association bicycle wheel gives readings in degrees. For the purpose of comparing values in this study an arbitrary relationship of 1 deg = 0.03 from 20 to 33 deg has been employed.

Figure 21 shows the averages of all the various types of devices used in the investigation. The values for the trailers and stopping-distance cars are for 40 mph. There is a similarity in the shape of the curves for the trailer and cars. The difference is quite uniform on all five sites, the trailer values are slightly lower than those for the cars. However, there is a different relationship between the portable testers and the trailers or stopping-distance cars. The portable testers provide higher values, especially at Sites I, II, and III, but show a lower rate of rise with respect to the increase in test site numbers than the other devices. This lower rate of rise permits the results to be closer at Sites IV and V.

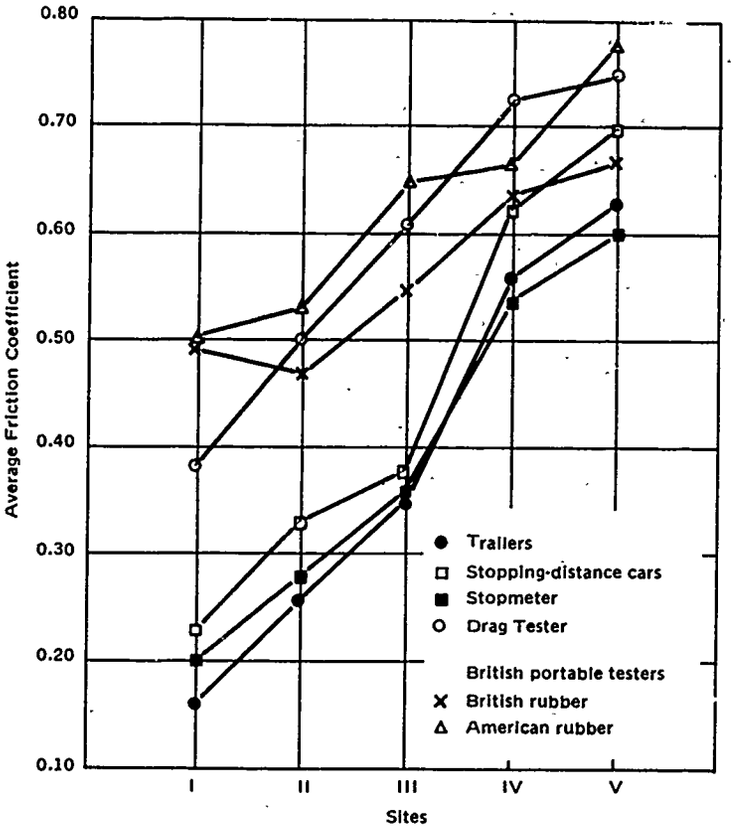

Figure 21. Comparison of average of trailers, stopping-distance vehicles (40-mph test speed), British testers (British and American rubber) and Pennsylvania State University drag tester. (© Dillard and Mahone, 1963. Used by permission.)

The secondary experiments had varied objectives. In general, the main objective was to provide an insight into some aspects of the correlation study. The following findings were obtained from the experiments:

1. Variation in water film thickness does not appreciably influence the test results of the trailers and stopping-distance cars. It should be noted that there were differences in the amount of water accumulated on the five sites used in the investigation.

2. Many of the British pendulum testers give lower values with an increase in water film thickness, while the reverse is true for a few of the other devices. The mean values of all testers, however, show a decrease as the film thickness is increased.

3. On the basis of the results from one trailer test, lowering the center of gravity has little effect on the SC.

4. Watering the pavement surface with the self-watering system of the trailers generally provides a higher SC than watering with the regular sprinkling system.

5. The addition of weights up to 410 pounds on a trailer and 900 pounds on a stopping-distance car has very little effect on the results.

6. Changing the tread design of tires (ASTM E-17 standard test tire to General Jet Air) with the same rubber composition does not appreciably vary the results of a stopping-distance car.

7. The statistical analyses made on the device-operator-site variables for the portable testers indicate that a well-designed experiment was used in the study. The analyses show that the devices and operators taking part in the experiment were alike for all practical purposes and that the sites were significantly different from each other.

8. In the experiments with experienced and inexperienced operators of the British pendulum testers, an inexperienced operator is able to provide valid results after receiving 15 minutes of instruction plus 15 minutes of practice.

Rizenbergs and Ward (1967) conducted an extensive investigation on six selected pavements using the stopping-distance method. The purpose of the investigation was fourfold: (1) to compare theoretically similar coefficients obtained from measurements of different parameters, (2) to determine the repeatability of tests, (3) to correlate dissimilar coefficients, and (4) to select a standard test. The test vehicle was a 1962 Ford sedan instrumented to record time, distance, velocity, and deceleration. Brake application, brake light energization, and wheel rotation were also recorded. All skid measurements were made using ASTM E-17 standard tires (ASTM E249-66) with an inflation pressure of 24 psi. The various measurements taken are shown in Figure 22; the SDCs derived by using the various measurements in Equations 21 and 23 and the DCs derived by using the various measurements in Equation 25 are given in Table 6. The magnitudes of the SDCs and DCs are listed in Table 7.

Table 7 reveals that the theoretically similar SDCs are generally different. For the same interval of skid, the SDCs determined from velocity and time measurements are higher than those determined from velocity and distance measurements. However, there are almost no differences in SDCs over small increments of velocity above 10 mph if the velocity, distance, and time measurements are used. These characteristics of the SDCs indicate that the equations used do not properly relate the nonlinearity of the parameters over large increments. Thus, it appears best to determine the SDC based on velocity and time, or velocity and distance, from 30-20 mph or 20-10 mph rather than from 30-0 mph.

Table 6. Coefficients Obtained From Various Measurements in the Stopping-Distance Method and Deceleration Method
(After Rizenbergs and Ward, 1967)

SDC_{O_o} = Coefficient, computed from Equation 21, obtained from measurement of observed stopping distance and meter-indicated velocity at the instant of brake application.

SDC_{O_w} = Coefficient (Equation 21) obtained from the measurement of observed stopping distance and the actual (Sanborn chart) velocity at wheel lock.

SDC_{M_o} = Coefficient (Equation 21) obtained from measurement of magnetic counter-indicated stopping distance and meter-indicated velocity at the instant of brake application.

SDC_{M_1} = Coefficient (Equation 21) obtained from measurement of magnetic counter-indicated stopping distance and actual velocity at the instant brake light was energized.

SDC_{M_w} = Coefficient (Equation 21) obtained from measurement of skid distance by counting impulses of the input to magnetic counter on the C. E. chart, in the velocity increment between wheel lock and 0 mph.

$SDC_{M(30\text{-}0)}$ = Coefficient (Equation 21) obtained from measurement of skid distance by counting impulses of the input to magnetic counter in the velocity increment between 30 mph and 0 mph.

$SDC_{M(20\text{-}0)}$ = Coefficient (Equation 21) obtained from measurement of skid distance by counting impulses of the input to magnetic counter in the velocity increment between 20 mph and 0 mph.

$SDC_{M(10\text{-}0)}$ = Coefficient (Equation 21) obtained from measurement of skid distance by counting impulses of the input to magnetic counter in the velocity increment between 10 mph and 0 mph.

$SDC_{M(V_w\text{-}30)}$ = Coefficient (Equation 21) obtained from measurement of skid distance by counting impulses of the input to magnetic counter in the velocity increment between wheel lock and 30 mph.

$SDC_{M(30\text{-}20)}$ = Coefficient (Equation 21) obtained from measurement of skid distance by counting impulses of the input to magnetic counter in the velocity increment between 30 mph and 20 mph.

$SDC_{M(20\text{-}10)}$ = Coefficient (Equation 21) obtained from measurement of skid distance by counting impulses of the input to magnetic counter in the velocity increment between 20 mph and 10 mph.

$SDC_{M(V_w\text{-}10)}$ = Coefficient (Equation 21) obtained from measurement of skid distance by counting impulses of the input to magnetic counter in the velocity increment between wheel lock and 10 mph.

SDC_{V_1} = Coefficient (Equation 23) obtained from measurement of elapsed time in the velocity increment between brake light energization and 0 mph.

SDC_{V_w} = Coefficient (Equation 23) obtained from measurement of elapsed time in the velocity increment between wheel lock and 0 mph.

$SDC_{V(30\text{-}0)}$ = Coefficient (Equation 23) obtained from measurement of elapsed time in the velocity increment between 30 mph and 0 mph.

Continued

Table 6. Continued

$SDC_{V(20\text{-}0)}$ = Coefficient (Equation 23) obtained from measurement of elapsed time in the velocity increment between 20 mph and 0 mph.

$SDC_{V(10\text{-}0)}$ = Coefficient (Equation 23) obtained from measurement of elapsed time in the velocity increment between 10 mph and 0 mph.

$SDC_{V(V_w\text{-}30)}$ = Coefficient (Equation 23) obtained from measurement of elapsed time in the velocity increment between wheel lock and 30 mph.

$SDC_{V(30\text{-}20)}$ = Coefficient (Equation 23) obtained from measurement of elapsed time in the velocity increment between 30 mph and 20 mph.

$SDC_{V(20\text{-}10)}$ = Coefficient (Equation 23) obtained from measurement of elapsed time in the velocity increment between 20 mph and 10 mph.

$SDC_{V(V_w\text{-}10)}$ = Coefficient (Equation 23) obtained from measurement of elapsed time in the velocity increment between wheel lock and 10 mph.

DC_{D_w} = Average coefficient obtained from measurement of area under the deceleration curve on the Sanborn recording between wheel lock and 0 mph divided by the corresponding chart length (Equation 25).

$DC_{D(15)}$ = Coefficient obtained from measurement of deceleration at 15 mph by interpolating the deceleration trace between 12 and 18 mph (Equation 25).

$DC_{D(25)}$ = Coefficient obtained from measurement of deceleration at 25 mph by Interpolating the deceleration trace between 22 and 28 mph (Equation 25).

$DC_{D(35)}$ = Coefficient obtained from measurement of deceleration at 35 mph by interpolating the deceleration trace between 32 and 38 mph (Equation 25).

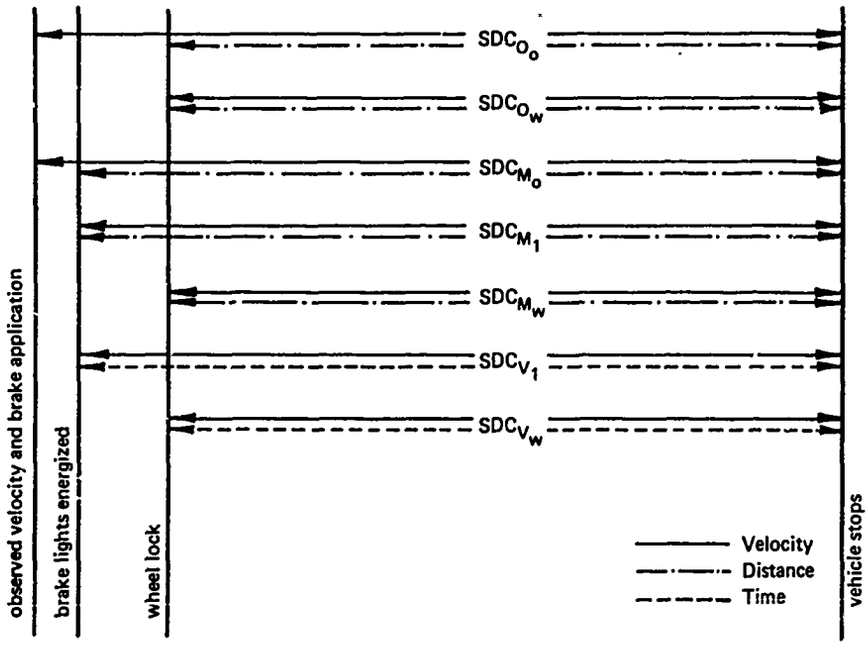

Figure 22. Measurements made for determination of several skid numbers.
(© Rizenbergs and Ward, 1967. Used by permission.)

Table 7. Correlation Study Test Data (After Rizenbergs and Ward, 1967)

Velocity (mph)	Site Ia	Site Ib	Site II	Site III	Site IV	Site V
V_o	34.9		40.0	40.1	40.0	40.1
V_b	35.4		40.4	40.5	40.1	40.4
V_1	35.3		40.3	40.5	39.9	40.1
V_w	34.3		39.4	39.6	38.5	38.9
Coefficients	Velocity and Distance					
SDC_{O_o}	0.38	0.49	0.43	0.60	0.65	0.79
SDC_{O_w}	0.37	0.46	0.41	0.58	0.61	0.74
SDC_{M_o}	0.34	0.43	0.39	0.52	0.56	0.68
SDC_{M_1}	0.35	0.43	0.40	0.52	0.55	0.68
SDC_{M_w}	0.36	0.46	0.41	0.55	0.58	0.72
$SDC_{M(30-0)}$	0.37	0.52	0.44	0.60	0.61	0.74
$SDC_{M(20-0)}$	0.45	0.60	0.50	0.66	0.68	0.79
$SDC_{M(10-0)}$	0.59	0.69	0.61	0.76	0.77	0.83
$SDC_{M(V_w-30)}$	0.35	0.39	0.37	0.50	0.54	0.71
$SDC_{M(30-20)}$	0.33	0.46	0.40	0.53	0.57	0.69
$SDC_{M(20-10)}$	0.41	0.58	0.47	0.62	0.66	0.79
$SDC_{M(V_w-10)}$	0.35	0.45	0.41	0.54	0.57	0.72
	Velocity and Time					
SDC_{V_1}	0.40	0.49	0.44	0.48	0.62	0.73
SDC_{V_w}	0.41	0.52	0.44	0.60	0.64	0.76
$SDC_{V(30-0)}$	0.42	0.57	0.47	0.64	0.67	0.78
$SDC_{V(20-0)}$	0.50	0.66	0.54	0.72	0.73	0.83
$SDC_{V(10-0)}$	0.63	0.75	0.62	0.81	0.81	0.87
$SDC_{V(V_w-30)}$	0.34	0.41	0.36	0.50	0.55	0.71
$SDC_{V(30-20)}$	0.33	0.47	0.40	0.54	0.57	0.70
$SDC_{V(20-10)}$	0.41	0.59	0.48	0.64	0.67	0.80
$SDC_{V(V_w-10)}$	0.36	0.47	0.41	0.55	0.59	0.73
	Deceleration					
DC_{D_w}	0.36	0.41	0.38	0.56	0.60	0.66
$DC_{D(15)}$	0.38	0.46	0.41	0.60	0.61	0.68
$DC_{D(25)}$	0.28	0.36	0.34	0.45	0.51	0.61
$DC_{D(35)}$		0.30	0.31	0.42	0.49	0.54

As shown in Table 7, differences are also found between SDC determined from measurements of observed stopping distance or observed velocity at brake application and those from measurements of velocity and distance from actual wheel lock. Errors in measuring observed stopping distances from wheel lock to the stopping point cause differences in SDCs when compared to those measurements determined from a magnetic counter. Differences are small between SDCs determined from observed velocity and those determined from recorded velocity at the moment of brake light energization. These differences indicate the importance of using distances and velocities recorded by instruments rather than those based on observations.

The repeatability of a particular test in the investigation was based mainly on the standard deviation of the test results obtained during one series of tests. Careful examination is required since the standard deviation is influenced by the pavement, the magnitude of the SDC, and instrumentation errors. The standard deviations indicated that the most repeatable test results are obtained by selecting the largest velocity increment for the computation of the SDC. Three reasons for this finding were given by Rizenbergs and Ward (1967):

1. The accuracy of velocity, distance, and time measurements increases with an increase in velocity increments.

2. The variability in skid resistance below 10 mph is minimized.

3. The errors are reduced in establishing the instant of rear-wheel lock and premature or delayed front-wheel lock.

In the 10-0 mph velocity increment, the cause of poor repeatability is the inability to steer the skidding vehicle in the wheel tracks. Variation in skid resistance is encountered with skids outside the wheel tracks.

The SDCs determined from measurements of velocity—time and velocity—distance for the 30-20 mph increment reveal smaller standard deviations than the deviations for the 20-10 mph increment. The reasons previously given for the most repeatable test results also apply here.

A regression analysis was made to correlate the various SDCs and DCs. The degree of correlation was based on the standard estimate of error H_s, and the correlation coefficient, C_c. As shown in Table 8 the linear regression equations permit conversion from an SDC to another SDC or to a DC. Good and fair correlations can be obtained between many results.

Table 8. Correlation Equations (After Rizenbergs and Ward, 1967)

U	R	Equation	H_s	E_s
Good Correlation				
SDC_{O_o}	SDC_{O_w}	R = 0.024 + 0.909U	1.000	0.004
SDC_{O_o}	SDC_{M_o}	R = 0.036 + 0.811U	0.999	0.004
$SDC_{V(30-20)}$	$SDC_{V(20-10)}$	R = 0.058 + 1.067U	1.000	0.006
$SDC_{V(30-20)}$	$SDC_{M(30-20)}$	R = 0.009 + 0.974U	1.000	0.006
$SDC_{V(30-20)}$	$SDC_{V(V_w-10)}$	R = -0.031 + 1.084U	0.998	0.006
SDC_{V_w}	SDC_{V_1}	R = 0.020 + 0.932U	0.997	0.006
$SDC_{V(30-20)}$	SDC_{M_w}	R = -0.023 + 1.058U	0.998	0.007
$SDC_{V(30-20)}$	SDC_{V_1}	R = 0.036 + 1.000U	1.000	0.008
SDC_{O_o}	SDC_{M_w}	R = 0.036 + 0.857U	0.999	0.008
SDC_{V_w}	SDC_{M_w}	R = -0.036 + 0.981U	1.000	0.009
$SDC_{V(30-20)}$	SDC_{V_w}	R = 0.917 + 1.073U	0.997	0.009
SDC_{V_w}	$SDC_{V(30-0)}$	R = 0.065 + 0.948U	0.996	0.009
Fair Correlation				
$SDC_{V(30-20)}$	SDC_{M_o}	R = -0.024 + 1.006U	0.994	0.011
SDC_{V_w}	$SDC_{V(20-10)}$	R = 0.071 + 0.955U	0.993	0.012
$SDC_{V(30-20)}$	$SDC_{V(30-0)}$	R = 0.082 + 1.012U	0.992	0.012
SDC_{V_w}	$SDC_{V(V_w-10)}$	R = -0.045 + 1.005U	0.996	0.013
$SDC_{V(30-20)}$	SDC_{O_o}	R = -0.074 + 1.242U	0.995	0.014
$SDC_{V(30-20)}$	$SDC_{V(V_w-30)}$	R = -0.094 + 1.120U	0.995	0.015
SDC_{V_w}	$SDC_{V(V_w-30)}$	R = -0.151 + 1.111U	0.990	0.017
$SDC_{V(30-20)}$	$SDC_{V(20-0)}$	R = 0.184 + 0.944U	0.988	0.017
SDC_{V_w}	$DC_{D(25)}$	R = -0.070 + 0.889U	0.971	0.017
$SDC_{V(30-20)}$	$DC_{D(25)}$	R = -0.062 + 0.967U	0.982	0.018
Poor Correlation				
SDC_{V_w}	$SDC_{V(20-0)}$	R = 0.187 + 0.860U	0.981	0.027
SDC_{V_w}	DC_{D_w}	R = -0.054 + 0.973U	0.981	0.029
SDC_{V_w}	$SDC_{V(10-0)}$	R = 0.336 + 0.735U	0.938	0.029
$SDC_{V(30-20)}$	DC_{D_w}	R = -0.027 + 1.024U	0.964	0.032
$SDC_{V(30-20)}$	$SDC_{V(10-0)}$	R = 0.364 + 0.754U	0.939	0.032

In selecting an interim standard test, Rizenbergs and Ward (1967) considered several criteria. These included accuracy, repeatability, rapid availability of test results, simplicity of measurement, and a minimum of instrumentation. Several ways of measuring velocity, distance, and time fulfilled most of the requirements. However, the SDC determined from Equation 23 by using the measurement of time during the 30-20 mph velocity increment was selected for the following reasons:

1. Time can be measured within an accuracy of 1%.
2. The SDC is nearly linear in the 30-20 mph velocity increment.
3. Repeatability is good, requiring five tests for an error of 5% or less.
4. Only a one-channel recorder is required.
5. The chart from the recorder can be interpreted relatively easily.

Rizenbergs and Ward (1967) included in the investigation the effects of some factors related to the stopping-distance method. These factors are velocity, air resistance, vehicle dynamics, and tire inflation pressure. Safety considerations limited the maximum test velocity to approximately 35 mph in the investigation. The test results showed that an increase in the velocity of the test vehicle decreases the SDC. This SDC–velocity relationship has been found by practically everyone engaged in skid measurements and is generally accepted.

The air resistance of an automobile can be represented by an aerodynamic equation similar to Equation 3, with the drag coefficient and frontal area of the automobile substituted for the lift coefficient and uplift area, respectively. By dividing the air resistance by the weight of the automobile and by using the proper conversion factors, constants, and other information from the automobile manufacturer, Rizenbergs and Ward (1967) provided the following equivalent friction coefficient (FC) equation for air drag:

$$FC = 7.18 \times 10^{-6} V^2 \qquad (30)$$

The velocity in terms of mph is the velocity of the automobile with respect to that of the wind velocity, which may or may not have a headwind or tailwind component. Equation 30 shows that the air resistance has little effect on FC because of the low constant, 7.18×10^{-6}, unless V is high. At the velocities used in the investigation, Rizenbergs and Ward (1967) concluded that air resistance has little effect on the measured SDC.

For the effect of vehicle dynamics, tests were conducted with the front suspension blocked, both front and rear suspensions blocked, or both unblocked. The test results were not significantly altered. Therefore, Rizenbergs and Ward (1967) concluded that vehicle dynamics has little influence on SDC.

The effect of tire inflation pressure was observed at five test sites. Inflation pressure was increased from 20 to 32 psi in 4-psi increments. The test results showed a general decrease in SDC with an increase in inflation pressure: approximately 5% (for 30-20 mph) between 20 and 32 psi. From this change, Rizenbergs and Ward (1967) concluded that the variation associated with a change in inflation pressure is significant.

Tables 7 and 8 show the various DCs determined from different incremental measurements of deceleration and the correlations associated with the SDCs. These test results indicate that, in general, the DCs are much lower than the SDCs for similar velocities. As previously mentioned, improper correction for the tilt of the automobile is cited as the error in the deceleration measurement. In addition to the DCs being low, poor repeatability and poor correlation are generally associated with DCs. Rizenbergs and Ward (1967) suggest that the method used in the investigation for holding the plate-mounted accelerometer may have been unsatisfactory and the cause of poor repeatability.

Walsh (1966) reported on a brief correlation study conducted by the New York Thruway Authority. The purpose of the study was to obtain some insight into the significance of the previously described simple Thruway skid cart. This cart, together with the British pendulum tester and the New York State Department of Public Works trailer, was tested on a broom-finished PCC surface that had not been subjected to polishing wear by traffic. On the basis of a few tests on the PCC surface the following average skid resistance values were obtained for each device:

Thruway cart at approximately 3 mph = 0.825

New York State trailer at 40 mph = 0.706

British pendulum tester at approximately 6 mph = 0.810

A ratio was obtained for each device by dividing its average value into the value obtained from any other surface and multiplying by 100. This ratio was called the Thruway skid ratio.

The results of the Thruway skid ratio method applied on four test sites are shown in Table 9. Direct readings for the skid cart and the British tester are close, but those for the British tester and the trailer show some variations. However, the Thruway skid ratios show a close relationship between all three devices. Thus, this method simplified the determination of the existence of a close correlation between the devices which otherwise might have been difficult to show.

Table 9. Relationships Between Test Readings and Thruway Skid Ratios (© Walsh, 1966. Used by permission.)

Test Site	Thruway Cart		D.P.W. Trailer		British Unit	
	D.R.	T.S.R.	D.R.	T.S.R.	D.R.	T.S.R.
I	.71	86	.60	85	.69	85
II	.46	56	.38	54	.45	55
III	.51	62	.45	64	.51	63
IV	.51	62	.42	60	.51	63

Note: D.R. = direct readings; T.S.R. = Thruway skid ratios; D.P.W. = N. Y. State Dept. of Public Works.

Kummer and Meyer (1967) reported that valid regression lines with small standard deviations showing correlation between different testing devices are difficult to maintain for all pavement surfaces and conditions. Shifts in regression lines must be expected if the affecting factors are limited or changed. These factors include pavement surfaces, range of speed, and rubber or tire characteristics. For these reasons Kummer and Meyer (1967) presented the correlation of various testing devices given in subsequent paragraphs as representing general trends only.

Figure 23 shows the correlation of the **BPN** from the British pendulum device and the **DTN** from the Pennsylvania State drag tester. The regression line is given by

$$\mathbf{DTN} = 0.68\,\mathbf{BPN}$$

Kummer and Meyer (1967) reported a correlation coefficient of 0.94 between the **BPN** and **DTN**. A correlation curve will be closer to the dotted 45-degree line if the **DTN** and **BPN** of Figure 23 are converted into **FC**. The correlation between the two testers is excellent because the frictional properties are measured with the same type of slider under the same load and at only a slight difference in velocity.

Figure 24 shows the correlation of the **BPN** from the British pendulum tester and the **SN** from the skid trailer. The results were obtained from the 1962 Tappahannock study. Kummer and Meyer (1967) reported that the correlation is not very satisfactory for two reasons: the number of sites was limited, and the British tester, as well as other low-velocity testers, is not able to appraise the drainage properties of the pavement surfaces. In addition, the regression lines are subject to change with changes in the velocity of the trailers.

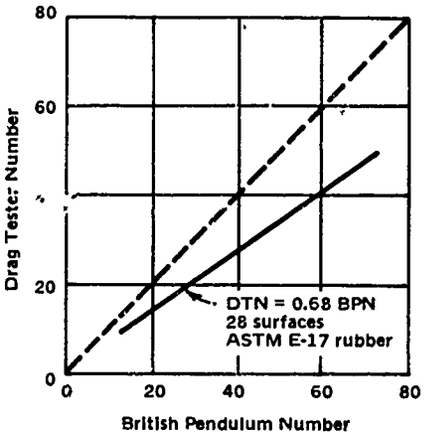

Figure 23. Correlation of British pendulum tester and drag tester. (© Kummer and Meyer, 1967. Used by permission.)

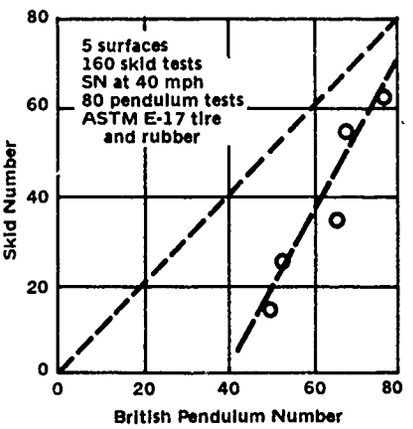

Figure 24. Correlation of British pendulum number and steady-state skid number. (© Kummer and Meyer, 1967. Used by permission.)

The correlation curve would be steeper if the trailer tests had been conducted at 50 or 60 mph. This effect of velocity change from 10 mph to 35 mph, together with the effect of tire tread design, is illustrated in Figure 25.

Some correlation curves between the Swedish "Skiddometer," a brake slip tester, and a German skid trailer are shown in Figure 26. As expected, the BSNs measured at or near the critical slip are higher than the corresponding SNs, all other factors being equal. The difference increases slightly with increasing velocity. Similar numbers are expected for both modes at velocities below 10 mph, because the relative sliding velocity of the tread elements is not very different at the lower velocities. In addition, an increase in velocity results in a decrease in SN because of additional frictional heating and hydrodynamic lift. This latter effect is more pronounced on slippery pavements, where the hydrodynamic lift is more easily developed. Thus, the SNs and BSNs are closer together on high skid resistant surfaces than on slippery pavements.

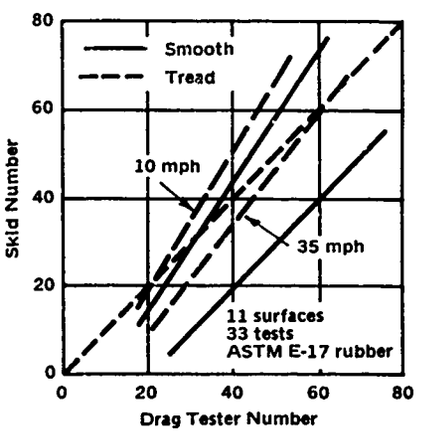

Figure 25. Effect of tire tread design and speed on correlation of drag tester and skid trailer. (© Kummer and Meyer, 1967. Used by permission.)

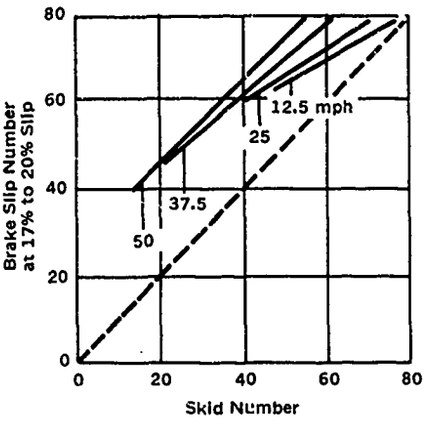

Figure 26. Correlation of stead-state skid and brake slip tests. (© Kummer and Meyer, 1967. Used by permission.)

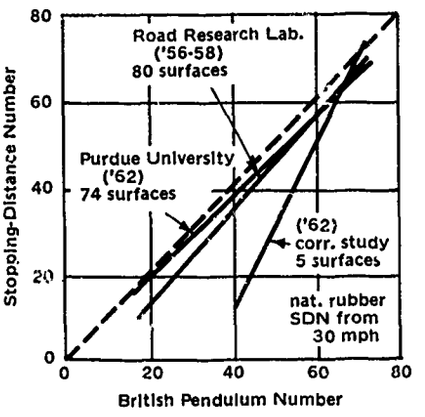

Figure 27. Correlation of British pendulum tester and stopping-distance car. (© Kummer and Meyer, 1967. Used by permission.)

The regression lines established for the SDN (100 x SDC) and the BPN by three agencies at different times and locations are shown in Figure 27. The regression lines are from the following equations, established by the different agencies:

$$SDN = -8.8 + 1.09\,BPN \text{ (British Road Research Laboratory)}$$

$$SDN = 0.96\,BPN \text{ (Purdue University)}$$

$$SDN = -66 + 1.82\,BPN \text{ (Tappahannock)}$$

Figure 27 shows that the regression line established by the Road Research Laboratory is in good agreement with that of Purdue University at the higher friction numbers. However, the 1962 Tappahannock regression line shows poor correlation with the lines of the other two agencies. Kummer and Meyer (1967) reported that the major factor involved in the poor correlation is the limited number of surfaces used in the Tappahannock study.

Figure 28 shows the regression line for SDN and SN. As previously reported, the stopping-distance car yields higher readings than the skid trailers because of the increase in sliding friction at low velocities and the possible effect of the critical slip condition.

Mahone (1962) compared the results obtained by the British pendulum tester and by the stopping-distance car on 14 test sites with various surface textures and with friction levels ranging from dangerously low to high.

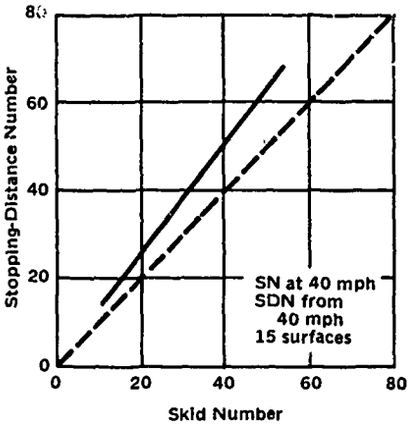

Figure 28. Correlation of steady-state skid number and stopping-distance car. (© Kummer and Meyer, 1967. Used by permission.)

Figure 29 shows the test results with the 95% confidence limits. The results show that certain combinations of slide length of the British tester and initial velocity of the stopping-distance car provide close agreement of results on some but not on all of the surfaces.

A statistical analysis was made by Mahone (1962) on the test results to determine a combination of slide length and initial velocity which will produce mean coefficients of close agreement. As shown in Table 10 there are significant differences in the mean coefficients for every slide length and test velocity combination on at least 50% of the surfaces. Thus, the two test devices do not give results which are interchangeable for all types of surfaces.

An analytical method was developed by Mahone (1962) for predicting the **SDC** when the **BPC** is known. This was done for four combinations of initial vehicle velocity and slide length. Estimating equations of the lowest order were derived which enabled the prediction of the **SDC** with 95% confidence limits. As shown in Figures 30 and 31, the derived curves with the 95% confidence limits envelop all the measured values. Thus, the **SDC** can be predicted from the measured **BPC** through the use of the estimating equations.

Table 10. Number of Sites on Which Mean Friction Coefficients From the Car and From the Pendulum Tester Were Demonstrated to be Significantly Different at the 95% Confidence Level (© Mahone, 1962. Used by permission.)

Slide Length (in.)	Test Speed (mph)			
	20	30	40	50
4.6	7/10*	7/12	7/12	1/2
4.8	5/10	10/14	6/12	2/3
5.0	6/10	11/14	9/12	3/3
5.2	–	2/2	–	1/1

* First number shows number of mean values that were significantly different; second number shows number of sites tested.

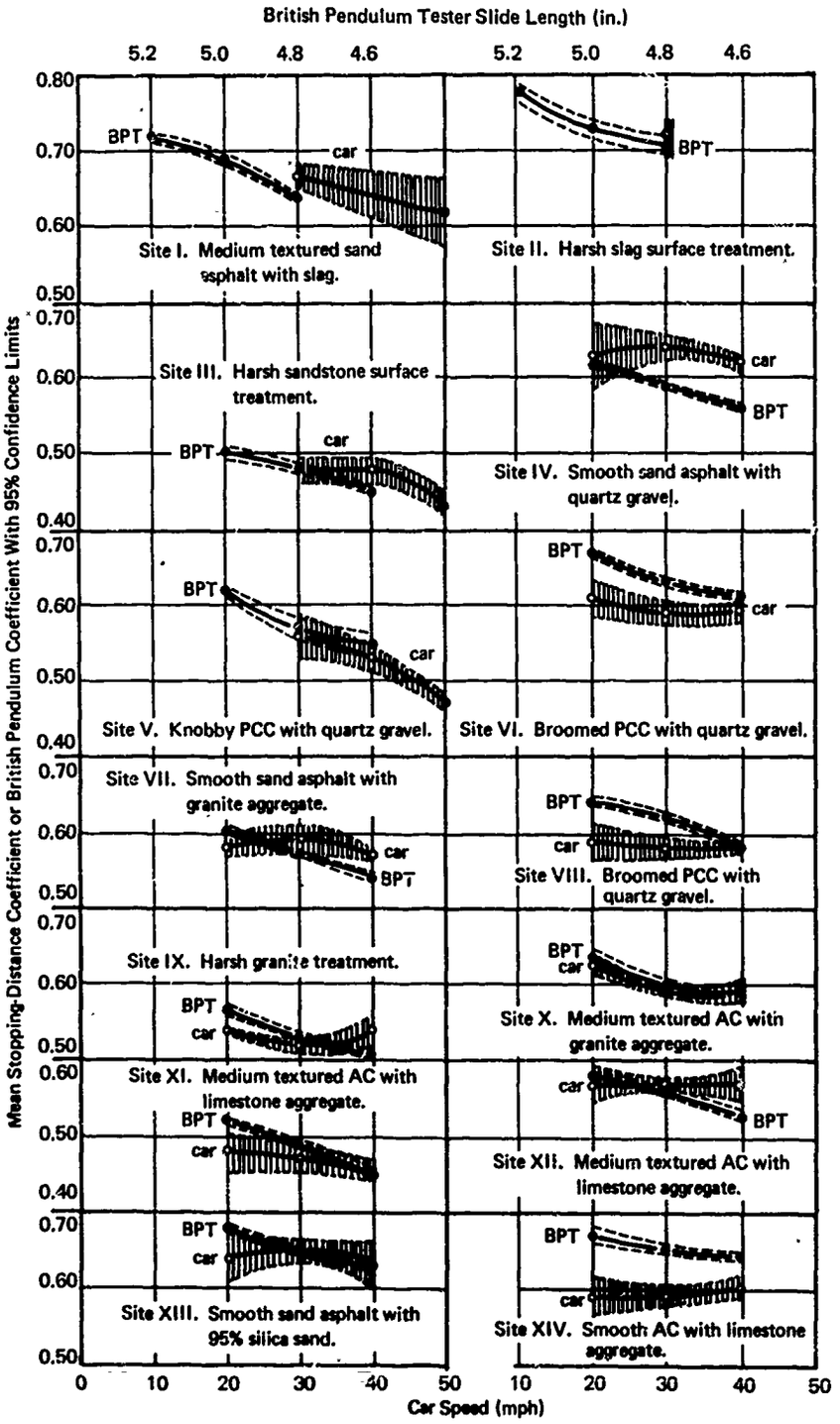

Figure 29. Relationship between the stopping-distance coefficient and test speed, and between the British pendulum coefficient and slide length.
(© Mahone, 1962. Used by permission.)

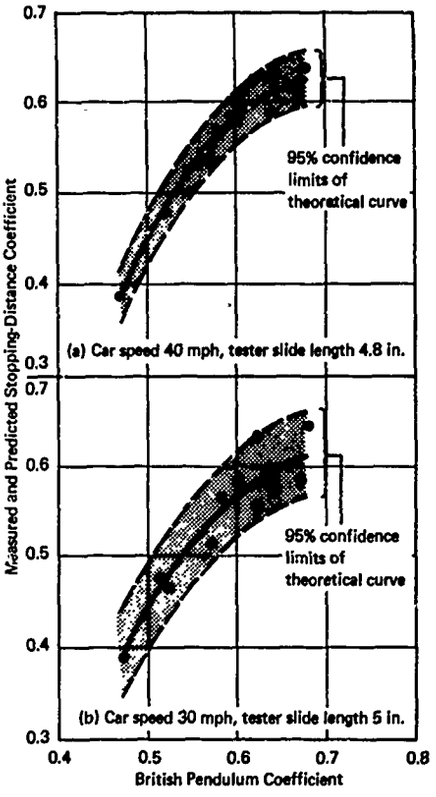

Figure 30. Prediction of mean SDC from BPC. (© Mahone, 1962. Used by permission.)

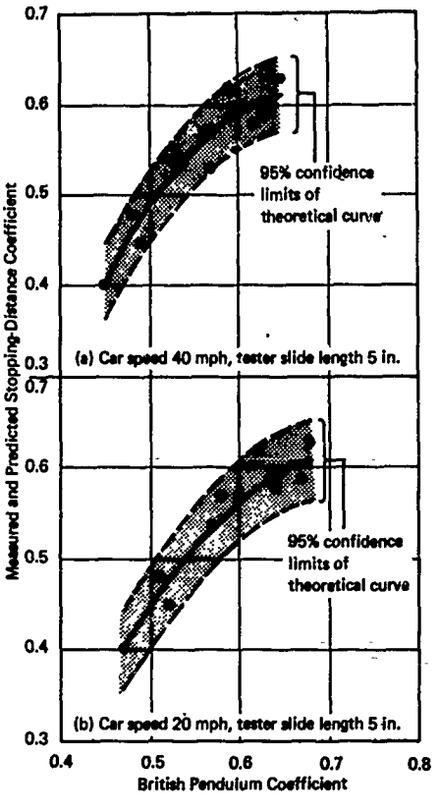

Figure 31. Prediction of mean SDC from BPC, for car speeds and test lengths different from those in Figure 30. (© Mahone, 1962. Used by permission.)

The foregoing discussions on the correlation of various friction-measuring devices indicate that generally one cannot readily convert the results obtained with one device to those obtained with another. The conversion factors can be predicted, but analysis is required which may not be simple, especially when many types of devices are involved. Thus, to avoid unnecessary difficulties, and for economic reasons, it appears best to establish a valid correlation between two or three selected devices rather than between many devices. The results from future correlation studies are expected to provide additional insight into the degree of correlation possible between various devices. An alternate solution is to correlate the skid resistance test result of a device with skidding accident frequency or risk of skidding on all types of pavement surfaces and to use the device for routine measurements. For airfield pavements, the device can be correlated with aircraft during braking. Such an effort by the FAA is discussed in the following section.

Correlation Between Devices and Aircraft

The literature search revealed that there is very little information on correlation between the friction values obtained by skid devices and by aircraft during braking. The report by Shrager (1962) is the only one uncovered during the search. Such information is vitally needed in order to appraise the various devices and to select one to measure the FC of Navy airfield pavements.

Shrager (1962) reported on the effort by the FAA to correlate the results of three friction-measuring devices with those of an aircraft during braking. The measuring devices were the Swedish Skiddometer, the British high-speed braking trailer, and a 1961 Plymouth station wagon equipped with a James braking decelerometer and a Tapley accelerometer. The test aircraft was a Convair 880 equipped with a modulating, automatic skid correction, antiskid braking system.

A PCC runway, free of visible evidence of contaminants, was used as a test site. Tests were conducted with the following five different runway surface conditions:

1. *Dry.*
2. *Damp.* This condition was obtained by spraying the runway surface with water from a fire truck and mechanically brooming the surface to remove all standing water.
3. *Wet.* This condition was characterized by standing water on the surface.
4. *Slush covered.* The concrete surface was covered with 1/2 inch to 3/4 inch of slush.
5. *Foam covered.* The concrete surface was coated with approximately 1 inch of organic foam.

In order to maintain similar conditions for purposes of comparison, the test surface was reconditioned prior to each test run.

For the initial aircraft test, the test section was entered with a velocity of approximately 140 knots and an idle power setting on the engines. Maximum braking was applied on the main landing gears throughout the test section. A similar technique was used on subsequent runs, with the entrance velocity 5 knots higher than the exit velocity of the previous run. This procedure was repeated until the aircraft stopped within the test section.

The initial run of the friction-measuring devices was made at an indicated speed of approximately 10 mph. Successive runs were made at speeds incremented by approximately 10 mph up to the maximum speed attainable by the device.

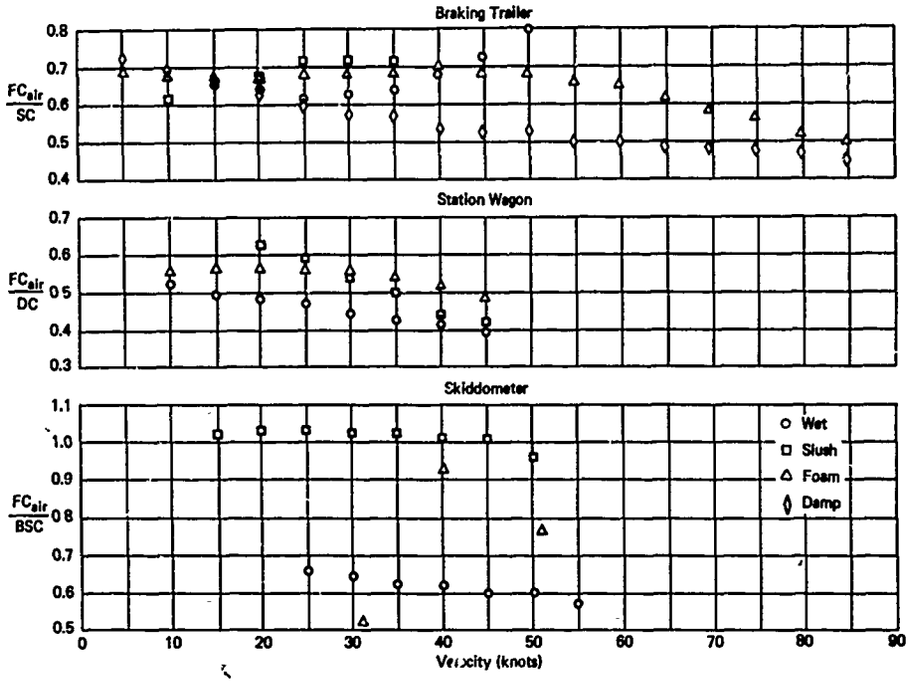

Figure 32. Ratio of aircraft to automotive vehicle friction coefficient for all test conditions. (© Shrager, 1962. Used by permission.)

Figure 32 shows the ratio of results from the aircraft braking tests to those from the measuring devices for all surface conditions. The ratio for each device does not vary significantly with velocity. A slight downward trend is noted with an increase in velocity. Low variations are indicated with respect to the various surface conditions for the braking trailer and station wagon. A higher variation is noted for the Skiddometer. Shrager (1962) indicated that the variations may have been caused by uncontrollable variations in the surface conditions.

The information from the FAA correlation study provided useful relationships between friction devices and aircraft. The results, however, are for one type of pavement and one type of aircraft and may not apply to other types of pavement surfaces and aircraft. Information received from NASA indicated that future correlation studies will provide a substantial amount of additional information on the correlation between military and civilian aircraft and skid-measuring devices.

FACTORS AFFECTING FRICTION COEFFICIENT

The factors affecting the magnitude of the friction coefficient were discussed in the previous report by Tomita (1964). All the factors were placed under three general categories: vehicle and aircraft operation factors, tire factors, and pavement factors. Speed and braking techniques were considered under the first category; tread design, tread composition, inflation, vertical load, and tire temperature under the second category; types of pavement, types of aggregates, surface textures, traffic, pavement surface contamination by foreign material, ambient temperature, weather, and climate under the third category. No new factors have been uncovered during the literature search of this investigation. However, more information has been found on the effects of the various factors and on the effects of various combinations of these factors. The additional information is presented in the subsequent paragraphs.

Velocity and Pavement Surface Wetness

The friction coefficient, though generally different for dry, damp, and wet conditions of pavement surfaces, is accepted as being independent of velocity on a dry pavement surface. However, a decreased friction level is expected at very high velocities comparable to those attained during brake application on high-speed jet fighters or attack aircraft. Horne and Leland (1962) attribute this decreased friction level to tire heating effects, which can partially be observed. At low velocities the rubber deposits on PCC pavements are observed to be in the form of small solid particles abraded during the skidding mode. Immediately after the operation the skidded area is warm to the touch. In contrast, similar skid marks resulting from locked wheels at very high velocities appear to have been deposited in a liquid state, as though they were painted on. This apparent smeared region is hot and sticky to the touch. Areas traversed after brake release show evidence of black tire imprint with each succeeding revolution of the tire. In addition, Horne and Leland (1962) reported that puffs of smoke can be seen from the tire contact region during braking at high velocities, with slip ratios ranging from 15% to 100%. Evidently the molten rubber acts as a lubricant to decrease the friction level. While this decrease is expected for landing aircraft, the real danger of braking at or near the 100% slip on a dry pavement lies in the rapid erosion of tire tread and carcass, resulting in a blowout. Horne and Leland (1962) reported that a full skid of 60 feet on a dry PCC runway can fail a high-pressure aircraft tire.

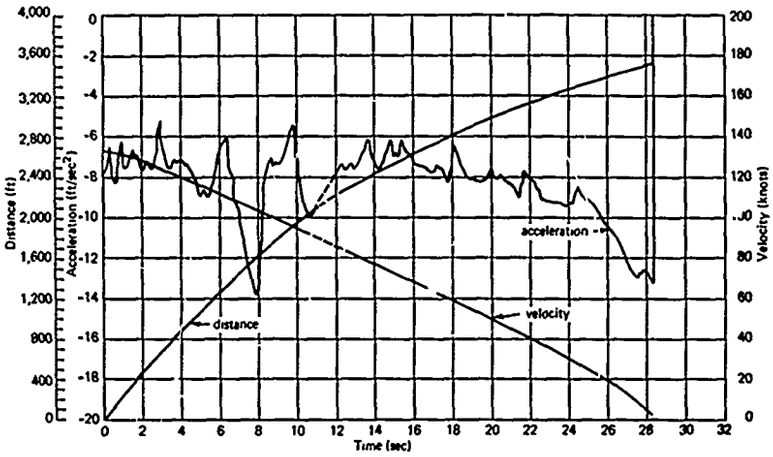

Figure 33. Test data for aircraft on a runway in a damp condition.
(©Shrager, 1962. Used by permission.)

A damp condition may reduce the friction level even more than it is reduced by a dry condition, but the friction level is still not very sensitive to a variation in velocity. This is shown by the acceleration trace in Figure 33, recorded during a jet transport braking test by the FAA. An increasing trend in deceleration is indicated by the acceleration trace at low velocities. However, this may have been caused by more water on the pavement surface than the actual damp condition. On a truly damp surface there should be no film of water to be displaced or no bulk water to be removed by the tire. This condition is somewhat difficult to achieve in practice because of the formation of puddles of water in the depressed areas of the pavement.

A wet pavement is generally considered to be covered with a visible film of water. The friction level on such a pavement is dependent on velocity, because with an increase in velocity the water film makes it progressively difficult for the tread to make contact with the pavement surface. Kummer and Meyer (1967) identified three velocity ranges in which the friction-velocity gradient differs.

Range 1: $V \leq V_w$

where $V_w = 6.4\sqrt{P_t}$ = the velocity at which a wedge of fluid begins to penetrate the tireprint area. In this velocity range the time available for displacement of bulk water is adequate, and the friction-velocity gradient is influenced only by the effective reduction of the thin, viscous film of water.

Range 2: $V_w \leq V \leq V_h$

where $V_h = 13.2\sqrt{P_t}$ = the hydroplaning velocity or the velocity at which the wedge of fluid completely penetrates the tireprint area. The friction level in this velocity range is affected by the bulk water depth as well as the thin-film effects. Thus, the friction-velocity gradient is greater in this range than in Range 1.

Range 3: $V > V_h$

The tire is not capable of removing the bulk water completely and hydroplanes in this velocity range. Tire–pavement friction is no longer significant, and the prominent factor is the hydrodynamic drag force.

Kummer and Meyer (1967) reported that the transition from Range 1 to Range 2 occurs at approximately 30 mph and that the hydroplaning velocity, V_h, occurs at 65 mph for a passenger-car tire with an inflation pressure of 24 psi. Note that a lower value of V_h results from Equation 6. This change in friction-velocity gradient at 30 mph is shown in Figure 34 for a water depth of 3/8 inch. Note that there is no such change with water depths of 3/16 and 1/16 inch. In the experiment the depth of water in a trough was carefully controlled by depth gages.

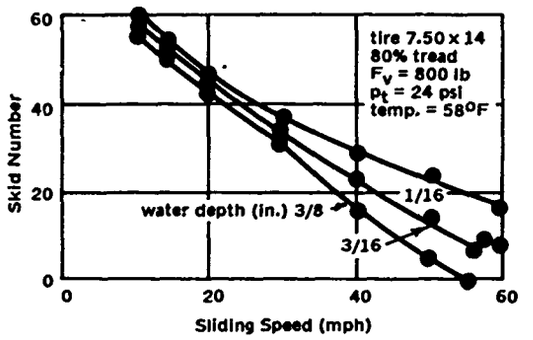

Figure 34. Demonstration of gradient increase due to penetration of fluid wedge into tire contact area. (© Kummer and Meyer, 1967. Used by permission.)

Figure 35 shows the effect of fluid depth on the effective friction coefficient, or retardation, of a jet transport braking on a concrete runway. Horne and Leland (1963) defined the shallow fluid as a wet runway surface without large puddles and the deep-fluid condition as a runway surface covered with 1/2 inch of artificially applied slush. As shown in Figure 35, there is a considerable loss in friction coefficient with an increase in water depth and velocity.

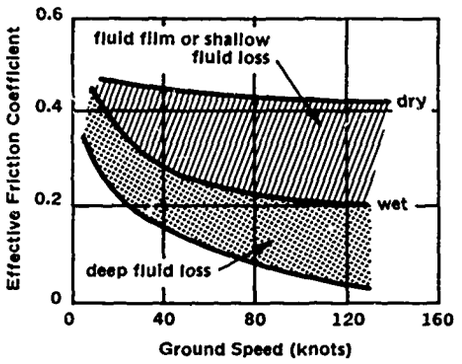

Figure 35. Jet transport braking traction on a concrete runway. New rib-tread tires and full antiskid used. (© Horne and Leland, 1963. Used by permission.)

Figure 36 shows the relationship between SDC and thickness of water film for two types of pavement surface textures. At 30 mph the SDC decreases with an increase in film thickness up to approximately 0.1 mm. Then it shows no significant change with a further increase in thickness.

Kummer and Meyer (1967) reported that large fluctuations up to 10 SN on homogeneous, smooth and fine-textured pavements indicate an insufficient amount of water used in the tests. With more water the fluctuations reduce to 2 SN. Thus, the results of some preliminary tests can be used to check the adequacy of the amount of water used in the tests.

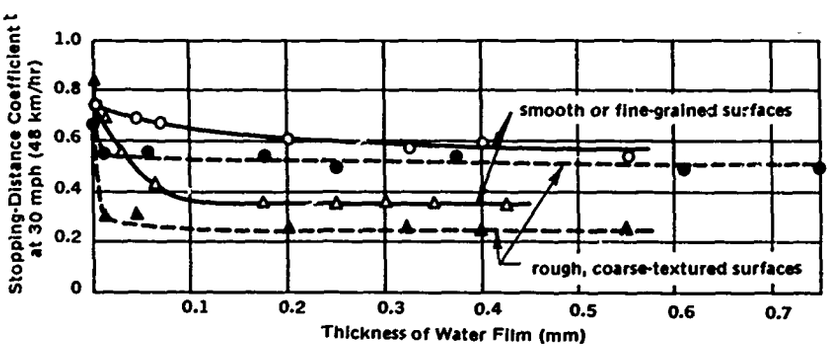

Figure 36. Water-film thickness and SDC on fine- and coarse-textured surfaces. (© Giles, 1959. Used by permission.)

Critical Slip and Skidding Modes

As previously discussed, the peak coefficient (PC) at critical slip for braking, driving, or cornering tires is higher than the corresponding skid coefficient. The exception to this condition is a smooth tire on a smooth surface such as ice. Kummer and Meyer (1967) gave the following three reasons for this condition:

1. At the critical slip point the majority of the tread elements are near the adhesion peak.

2. Tire tread temperature is lower at the critical slip point than at full skid.

3. The hydrodynamic lift is lower at the critical slip point since the relative velocity between tread elements and pavement surface is lower than at full skid.

Maycock (1965-1966) made two important statements on the ratio of PC to SC:

1. The ratios of PC to SC for most tire tread patterns and pavement surface textures are similar at a particular velocity. This statement is based on test results at 30 mph and 60 mph with ribbed or siped tires on seven different pavement surfaces. High ratios of PC to SC are obtained when the tire and pavement surface conditions provide extreme hydrodynamic lift conditions. These extreme lift conditions include smooth tires, smooth pavement surfaces, and high velocities.

2. The ratio of PC to SC increases with an increase in velocity.

Horne and Leland (1962) tested, on dry concrete, various sizes of Type VII aircraft tires (extra high pressure) with inflation pressures ranging from approximately 100 psi to 260 psi. The relationship between the ratio of SC to PC and velocity is shown in Figure 37. It should be noted that the ratio in Figure 37 is SC to PC rather than PC to SC. Thus, the SC to PC ratio, decreasing with increasing velocity, corresponds to Maycock's second statement.

Tire and Pavement Surface Effects

The principal factors involved in tires are the rubber properties and the tread design. Resilience or its complement damping, hardness of the rubber, tire inflation pressure, and contact pressure are of interest, together with various available treads ranging from smooth to grooved and slotted designs. The variations of these properties, coupled with those of pavement surface textures or the macroscopic and microscopic roughness of pavement surfaces, yield friction coefficients which are difficult to predict. However, some progress has been made through research towards understanding the effects of these factors, taken either singly or in combination.

Maycock (1965-1966) conducted a number of skid tests using the deceleration method. In these tests tires with three tread patterns and three tread compounds were used on seven pavement surfaces with varying textures.

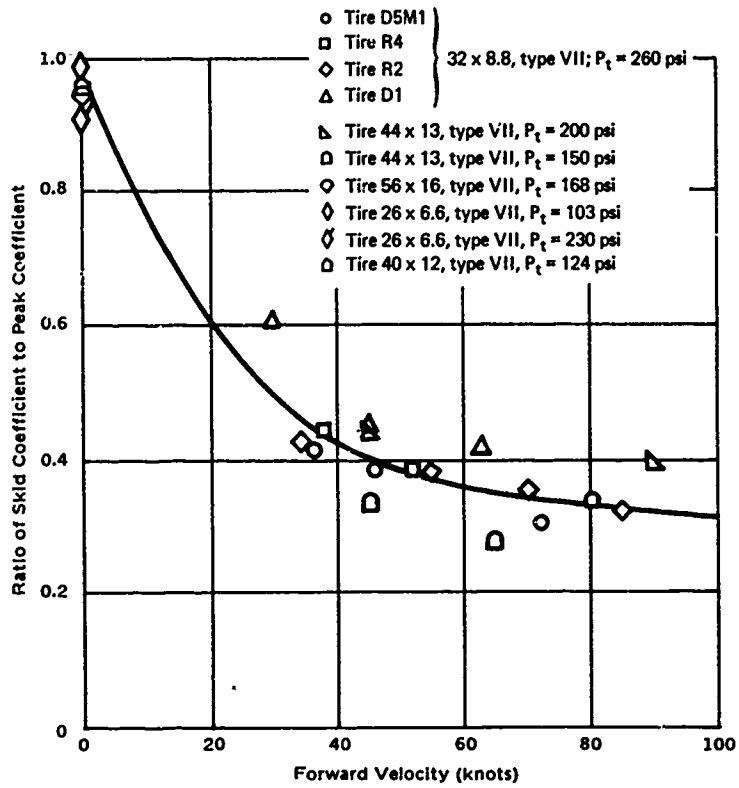

Figure 37. Effect of forward velocity on the ratio of skid coefficient to peak coefficient. Data obtained on dry concrete runways. (© Horne and Leland, 1962. Used by permission.)

The tires had (1) completely smooth tread, (2) ribbed tread with six plain circumferential grooves, and (3) fully developed modern tread patterns with multipie sipes. The specifications of the three tread compounds used are as follows:

1. *Natural rubber*: 48 parts per hundred of high abrasion furnace black.
2. *Synthetic rubber*: oil-extended styrene butadiene rubber with 55 parts per hundred of superior abrasion furnace black.
3. *High-styrene synthetic rubber*: oil-extended high-styrene butadiene rubber with 60 parts per hundred of superior abrasion furnace black.

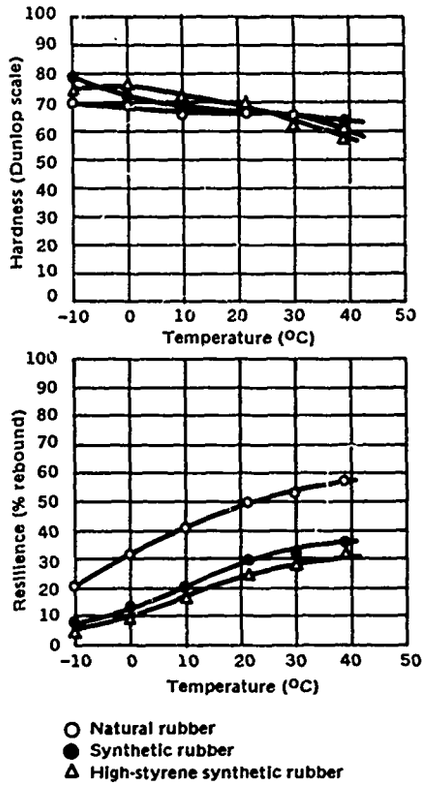

Figure 38. Hardness and resilience of tread materials as a function of temperature. (© Maycock, 1965-66. Used by permission.)

The hardness and resilience of these compounds were measured at various temperatures on sample blocks of these rubbers. As shown in Figure 38, there is only a small variation in hardness between the three compounds throughout the temperature range of -10°C to 40°C. In addition, there is only a slight decrease in hardness with an increase in temperature. This indicates the insensitivity of the rubber compounds to temperature variations within the temperature range. However, there is an increase in the resilience of all three compounds with an increase in temperature. The difference in resilience between synthetic rubber and high-styrene synthetic rubber is small and is approximately the same throughout the temperature range, the synthetic rubber being more resilient. The natural rubber exhibits almost twice as much resilience as the synthetic rubber throughout the temperature range.

The seven pavement surfaces listed below were special sections laid on the Road Research Laboratory's test track:

1. Mastic asphalt
2. Polished concrete
3. Fine cold asphalt
4. Asphalt with chippings
5. Rounded gravel carpet
6. Mixed aggregate
7. Quartzite

Surface textures of the above sections increase in coarseness as they increase numerically. Thus, the two smoothest and polished surfaces are 1 and 2, while the most harsh, coarse-textured surface is 7.

The test surfaces were sprayed with water from spray-bar facilities. As in many field experiments, a uniform water film was not obtained. It varied from 0.005 inch to 0.080 inch above the top of the aggregates and from 0.040 inch to 0.080 inch for the fine-textured surfaces.

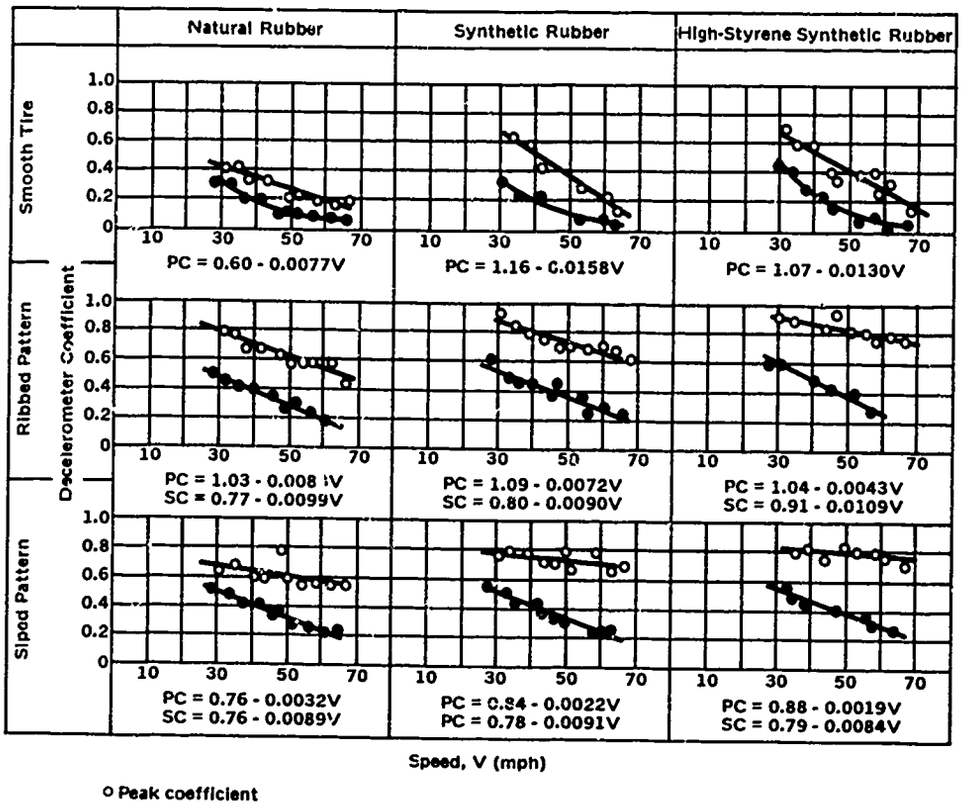

Figure 39. Test results on surface 4—asphalt with chippings. (© Maycock, 1965-66. Used by permission.)

Tire pressure for the tests was adjusted periodically to 24 psi. The measured air and water temperatures varied from 17°C to 24°C for all surfaces except surface 1, which had temperature ranges of 4°C to 7°C. The test velocity ranged from 30 mph to 65 mph.

The test results for surface 4 are shown in Figure 39, together with the equations from regression analyses. Maycock (1965-1966) presented similar results for the remaining surfaces. These are not repeated herein. Figure 39 shows the trend of the results to be typical. That is, the DC increases with an increase in velocity, and the PCs are higher than the SCs.

Table 11 shows the mean ratios of PC and the ratios of SC for the different tread designs. Table 12 shows similar ratios for the different rubber compositions. From the results given in Table 11 the following statements can be made concerning the effectiveness of tread design:

Table 11. Mean Ratios of Peak and Skid Coefficients Obtained With Different Tread Patterns on the Test Surfaces Numbered 1-7 (After Maycock, 1965-1966)

Ratio	Peak Coefficient							Skid Coefficient						
	1	2	3	4	5	6	7	1	2	3	4	5	6	7
	30 mph							30 mph						
Ribbed / Smooth	3.7	4.0	1.40	1.49	1.10	1.17	0.95*	**	**	1.43	1.44	1.04*	0.98*	0.96
Siped / Smooth	4.2	3.3	1.12	1.31	1.22	1.17	0.96*	**	**	1.31	1.40	1.26	1.10	1.01*
Siped / Ribbed	1.12	0.83	0.81	0.88	1.10	1.0*	1.0*	1.63	1.25	0.92	0.97*	1.21	1.12	1.06
	60 mph							60 mph						
Ribbed / Smooth	**	**	7	2.9	1.44	1.21	1.07	–	**	**	3.5	1.7	1.6	1.0*
Siped / Smooth	**	**	7	3.0	1.70	1.43	1.02*	–	**	**	3.6	2.0	2.0	1.13
Siped / Ribbed	1.63	1.40	1.04	1.04*	1.19	1.19	0.95	–	2.1	0.97*	1.09*	1.22	1.28	1.12

* Denotes that the ratio is not significantly different from unity at the 5% level.
** The denominator involved was very small.

Table 12. Mean Ratios of Peak and Skid Coefficients Obtained With Different Tread Compositions on the Test Surfaces Numbered 1-7 (After Maycock, 1965-1966)

(Results for smooth tires omitted.)

Ratio	Peak Coefficient							Skid Coefficient						
	1	2	3	4	5	6	7	1	2	3	4	5	6	7
	30 mph							30 mph						
S.R. / N.R.	1.27	1.32	1.21	1.14	1.16	1.32	1.33	0.81	1.03*	1.12	1.07	1.02*	1.23	1.14
H.S.S. / N.R.	1.45	1.32	1.24	1.20	1.30	1.47	1.34	1.08*	1.10*	1.19	1.16	1.10	1.27	1.30
H.S.S. / S.R.	1.13	1.02*	1.04*	1.06*	1.11	1.12	1.02*	1.35	1.10	1.07	1.08	1.07*	1.03*	1.15
	60 mph							60 mph						
S.R. / N.R.	1.48	1.37	1.20	1.24	1.25	1.32	1.23	–	–	1.02*	1.25	1.10*	1.0*	1.09
H.S.S. / N.R.	1.92	1.44	1.34	1.42	1.45	1.41	1.41	–	–	1.02*	1.36	1.29	1.15	1.19
H.S.S. / S.R.	1.27	1.06*	1.13	1.14	1.15	1.07	1.29	–	–	1.0*	1.11*	1.20	1.16	1.09

* Denotes that the ratio is not significantly different from unity at the 5% level.
Note: S.R. = synthetic rubber; N.R. = natural rubber; H.S.S. = high-styrene synthetic rubber.

1. Tread patterns provide vast improvements over smooth tires in both **PC** and **SC** on smooth surfaces. The effect is more pronounced at the higher velocities than at the lower velocities.

2. The siped tire or the tire with fully developed modern tread pattern having multiple sipes offers significant advantages over the ribbed pattern on smooth surfaces, especially at the higher velocities. This advantage diminishes on coarse open-textured surfaces.

3. The effectiveness of tread pattern decreases with an increase in the coarseness of the surface. This can be seen from both **PC** and **SC** ratios for surface 7.

The effectiveness of tread patterns on various pavement surface textures can be explained mainly on the basis of water drainage from the tire contact area. As previously discussed, the presence of water causes hydrodynamic lift and decreases the adhesion component of friction. On a smooth surface the drainage is facilitated by the grooves and sipes of the tire tread. On a coarse surface the channels combined with the grooves and sipes facilitate drainage. The channels in surface 7 appear to be sufficient to remove most of the water at 30 mph and 60 mph. Thus it appears that tire tread patterns are not very important on coarse-textured surfaces. However, their importance at velocities above 60 mph is not known.

From the ratios given in Table 12 the following statements can be made concerning the effectiveness of tread composition:

1. An increase in **PC** of 20 to 50% is obtained by using synthetic rubber rather than natural rubber. Approximately equal proportionate increases are found on all surface textures.

2. The corresponding improvements in **SC** are generally lower than those in **PC**. The increase rarely exceeds 30%. For 30 mph lower ratios are given for surfaces 1, 2, and 5 than for the others. This indicates that a large number of small, sharp asperities, such as those in surfaces 3 and 4, have better interaction with the tread materials than the larger rounded stones of surface 5.

3. The ratios reflect little difference between the two synthetic rubbers. The difference that does exist corresponds to the small difference in the resilient properties of the two rubbers shown in Figure 38. This fact indicates that there is a definite association between friction coefficient and resilience of tread rubber.

4. Both skid and peak ratios at 30 mph are, in general, similar to those at 60 mph, the latter being slightly higher.

Regarding the interaction between tread design and rubber composition, the ratios from Tables 11 and 12 indicate that the smooth tire–natural rubber combination should yield abnormally low PCs and SCs. The reason for this may be due to the peculiarity of the combination or strictly to the tread resilience. Another reason may be the cooling action of water in the grooves, providing higher values of decelerometer coefficient than expected.

Since the test results showed the importance of tire tread design, Maycock (1965-1966) conducted a second series of tests using eight different tread designs on surfaces 2, 3, and 4, with a water film thickness of approximately 0.04 inch. The tests were conducted in a manner similar to the first series. Table 13 summarizes the features of the tires and their effect on PC and SC. The following findings from this experiment can be made:

1. As found from the results of the first series, changes in tread design have greater effect on smooth and fine-textured surfaces than on coarse-textured surfaces. The effectiveness is greater at the higher velocities than at the lower velocities, where even some reduction in SC can be expected. In addition, tread design modifications affect PC to a greater extent than they do SC.

2. An increase in the number of ribs results in a considerable increase in the PC at high velocities, but only in a slight increase in SC.

3. An increase in the size of circumferential grooves improves both the PC and the SC at high velocities, especially the SC. An increase is also obtained with the introduction of diagonal drainage channels, particularly on the fine-textured surfaces. Of the two modifications, the wider circumferential grooves in general give a slightly higher PC and SC at the higher velocities. However, diagonal drainage channels provide a higher PC on the smoothest surface.

4. The radial-ply tire gives a higher PC but a lower SC at the higher velocities than the conventional tire with identical tread design. Since the results are for two test surfaces only and with test tires, this finding does not necessarily apply to other surfaces and production tires.

Horne and Leland (1963) reported on the effect of tread design on friction coefficient measured during full-scale aircraft braking tests. As shown in Figure 40 there is an increase in the average friction coefficient when circumferential grooves are cut in the aircraft tire. The process of tread wear may be considered as the reverse of cutting grooves, and the smooth tread can be assumed to represent a completely worn ribbed tread. The question as to what stage of wear the rib tread tire becomes ineffective is difficult to answer. Horne and Leland (1963) indicated that this may occur when 80 to 90% of the tread is worn.

Table 13. Summary of Results—Second Series (After Maycock, 1965-1966)

(Bold numbers indicate tread design; (2) = polished concrete; (3) = asphalt with sandpaper texture; (4) = asphalt with 3/4 in. chippings rolled into the surface.)

Tire Features				Effect of Changing From Tire *a* to Tire *b* on:			
Tire *a*		Tire *b*		Surface	Peak Coefficients	Surface	Skid Coefficients
1	5 ribs (straight circumferential grooves)	**2**	6 ribs (straight circumferential grooves)	(2)	Considerably reduced speed effect*	(2)	Slightly reduced speed effect*
				(3)	Considerably reduced speed effect	(3)	No effect
				(4)	Insufficient data	(4)	Insufficient data
3	Standard pattern (6 ribs)	**2**	6 ribs (as above)	(2)	Slightly increased speed effect	(2)	Increase in coefficient (0.05)
				(3)	No effect	(3)	No effect
				(4)	Insufficient data	(4)	Insufficient data
3	Standard pattern (radial ply)	**4**	Standard pattern (biased ply)	(2)	Decrease in coefficient (0.08)	(2)	Slightly reduced speed effect
				(3)	No effect	(3)	Slightly reduced speed effect
				(4)	Decrease in coefficient (0.08)	(4)	Slightly reduced speed effect
3	Standard pattern	**5**	Grooves straightened and widened	(2)	No effect	(2)	Reduced speed effect
				(3)	Reduced speed effect	(3)	Reduced speed effect
				(4)	No effect	(4)	Reduced speed effect
3	Standard pattern (6 ribs)	**8**	7 rib version	(2)	Increase in coefficient (0.04 and 0.12 resp.)	(2)	Slightly reduced speed effect
				(3)	Increase in coefficient (0.04 and 0.12 resp.)	(3)	No effect
3	Standard pattern	**7**	Additional diagonal grooves creating blocks (experimental block)	(2)	Considerably reduced speed effect	(2)	Reduced speed effect
				(3)	Considerably reduced speed effect	(3)	No effect
				(4)	Slightly reduced speed effect	(4)	Reduced speed effect
7	Experimental block pattern	**6**	Production block pattern	(2)	No effect	(2)	Slightly increased speed effect
				(3)	Increase in coefficient (0.05)	(3)	No effect
				(4)	No effect	(4)	No effect
5	**7** Both tires standard pattern with additional drainage channels			(2)	Reduced speed effect	(2)	No appreciable effect
				(3)	Increase in coefficient (0.05)	(3)	Slightly increased speed effect
				(4)	No effect	(4)	Slightly increased speed effect

* Speed effect is the fall of coefficient as the speed increases. Every case above, in which the speed effect is recorded as having been reduced, has resulted in increased coefficients at the higher speeds.

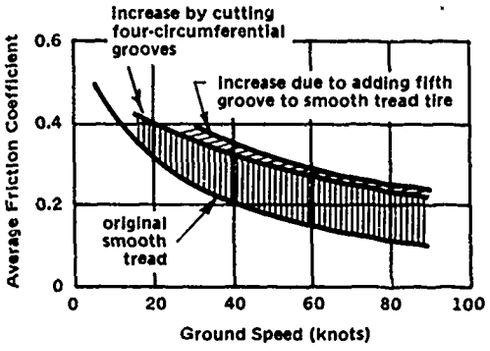

Figure 40. Effect of tire tread on friction coefficient PCC surface; water depth = 0 to 0.3 inch. (© Horne and Leland, 1963. Used by permission.)

Horne and Leland (1962) measured the variations in friction coefficient of various aircraft tires in the Langley landing-loads track. The vertical load was 10,000 pounds, with a tire inflation pressure of 260 psi. The track surface was PCC with a water film thickness of approximately 0.3 inch. Figure 41 shows the average friction coefficient for the tires with the various tread designs. It should be noted that very little difference in friction coefficient was measured between the smooth and dimple treads throughout the velocity range. Thus, a single curve is shown in Figure 41 for the two tread designs which provide the least average friction coefficient. The tire with nine circumferential grooves gives the highest values, followed by the tire with five grooves. Thus, an increase in the number of grooves generally corresponds to an increase in the friction coefficient. However, the design of tires involves a compromise between many requirements and factors, such as tread wear and the shear strength of rubber, which limit the number of grooves. For this reason, the tire in Figure 41 with nine grooves is not permitted for use on high-speed aircraft.

The curves for the two diamond tread tires in Figure 41 indicate that the small-diamond tread (more grooves) develops a higher friction coefficient than the large-diamond tread. This corresponds to the previous findings regarding the number of circumferential grooves. In addition, lateral grooves and diamond tread are shown in Figure 41 to be less effective than circumferential grooves.

Giles, Sabey, and Cardew (1962) used the British pendulum tester to find the relationship between the BPN and the resilience of rubber sliders for four different surfaces. As shown in Figure 42, the relationship depends on the type of surface. No change in BPN is seen for a glass surface. However, there is a definite decrease in BPN for the other surfaces. The rate of decrease is higher for coarse-textured surfaces than for smooth surfaces. The reasons for these characteristics appear to be that (1) resilience increases with a rise in temperature, which tends to decrease the friction coefficient and (2) with an increase in resilience more rubber is deformed, and there is a greater change in friction coefficient per unit change in resilience.

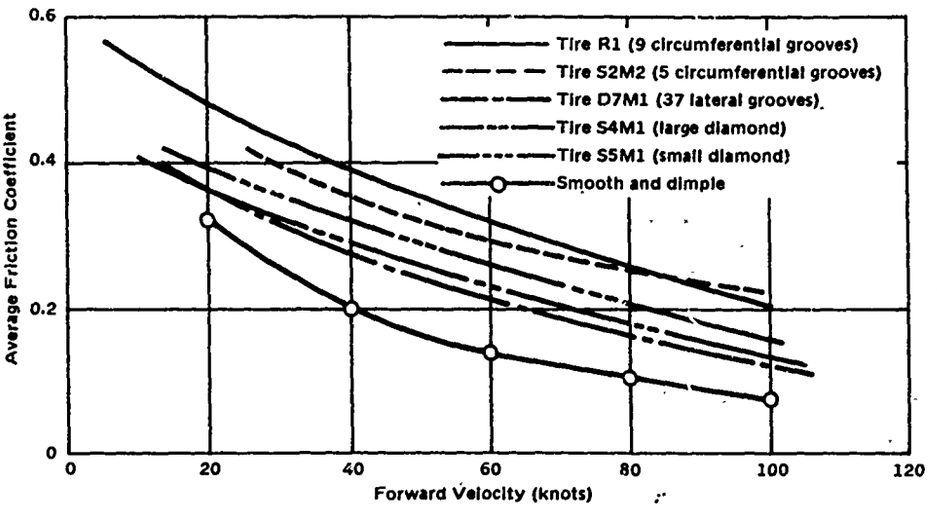

Figure 41. Wet-runway braking effectiveness of tire treads on a wet concrete runway. $F_v \approx 10{,}000$ pounds; $P_t = 260$ psi; water depth = 0 to 0.3 inch. (© Horne and Leland, 1962. Used by permission.)

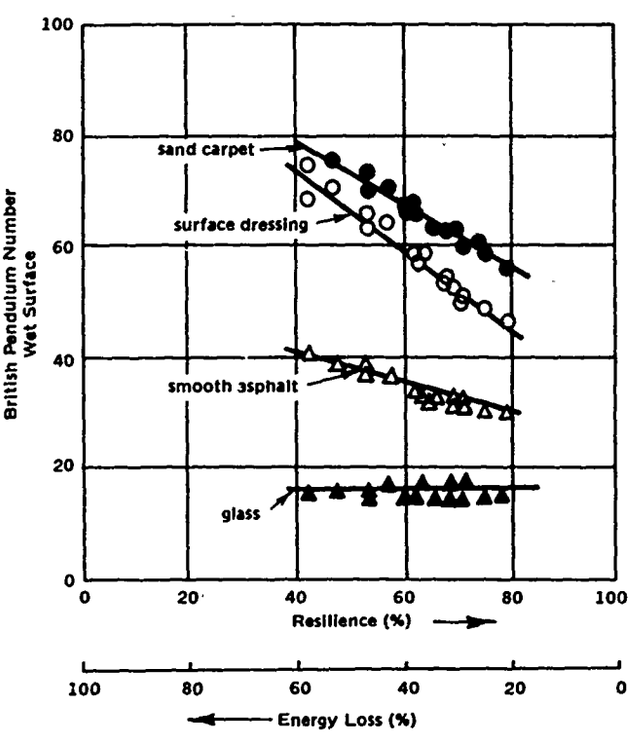

Figure 42. Dependence of BPN on rubber resilience (energy loss). (© Giles, Sabey, and Cardew, 1962. Used by permission.)

Table 14. Details of Rubber Compounds Used in the Resilience and Hardness Tests (© Sabey and Lupton, 1964. Used by permission.)

(All compounds are vulcanizates of a tire tread type, although not all are known to have been used in tires. The compounds are grouped according to the source of manufacture.)

Code No.	Basis of Compound	Remarks
1*	Natural rubber	Specially compounded to give a range of hardness
2*		
3		
4	Natural rubber	Two compounds with different amounts and types of carbon black; no. 4, 5, and 6 are three batches of one compound made to nominally the same specification.
5		
6*		
7		
8	Natural rubber	Specially compounded to give a range of resilience
9		
10		
11*		
12	Natural rubber	
13*	Natural rubber	Specially compounded to give low resilience
14	SBR**	
15	Natural rubber	Normal tread compounds in use in Great Britain; no. 16 a normal synthetic compound in use immediately prior to 1961; no. 17 a new compound introduced in 1961.
16*	SBR	
17	SBR (oil extended)	
18	SBR	Normal tread compound in use in Europe
19	SBR (oil extended)	Compounds extended to give decreasing resilience
20	SBR (oil extended)	
21	SBR (extended)	
22*	Polybutadiene	
23*	Ethylene/propylene	
24	Butyl	
25*	Butyl	

* Compounds selected for the friction tests.

** Styrene butadiene rubber.

Sabey and Lupton (1964) investigated the variations in hardness and resilience with temperature of a wide variety of rubber compounds and determined the effect of these characteristics on BPN under wet conditions. Twenty-five rubber compounds (listed in Table 14) were used in the hardness-

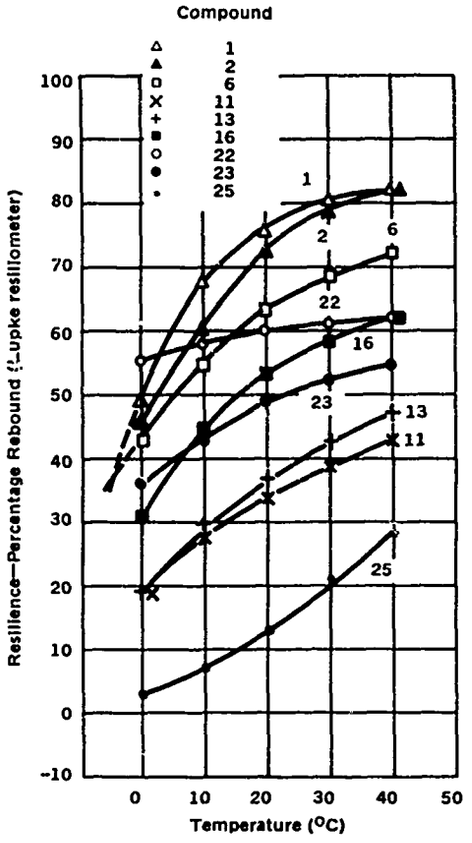

Figure 43. Variation in resilience with temperature for nine selected rubber compounds. (© Sabey and Lupton, 1964. Used by permission.)

resilience-temperature relationship study. The temperature for the hardness and resilience tests ranged from 0 to 80°C. Nine of these compounds were selected for the friction tests with the British pendulum tester on seven different surfaces (shown in Table 15), with temperature ranging from 1 to 40°C.

Figures 43, 44, and 45 show the relationship of temperature to resilience, hardness and BPN. In general, Figure 43 shows that all rubber compounds increase in resilience with an increase in temperature. However, the rate of increase varies from compound to compound. A batch-to-batch variation of up to 8% can also be expected. Natural rubber compounds have, in general, higher resilience than synthetic rubber compounds, although there is overlap in the results. The butyl compound, 25, is the least resilient over the 0 to 40°C temperature range.

Table 15. Test Surfaces Used in the Friction Tests With Nine Selected Rubber Compounds (© Sabey and Lupton, 1964. Used by permission.)

(Surfaces listed in increasing order of roughness.)

Code No.	Description	Texture Depth* (in.)
I	Very smooth, very highly polished	<0.001
II	Smooth, polished	0.002
III	Smooth looking, sandpaper texture	0.006
IV	Very harsh, projections of the order of 0.1 in. in size	0.026
V	Rough coarse, textured, mixture of harsh and polished stones	0.028
Vi	Rough coarse textured, harsh stones	0.039
VII	Rough coarse textured, polished stones	0.040

* Measured by the sand-patch method.

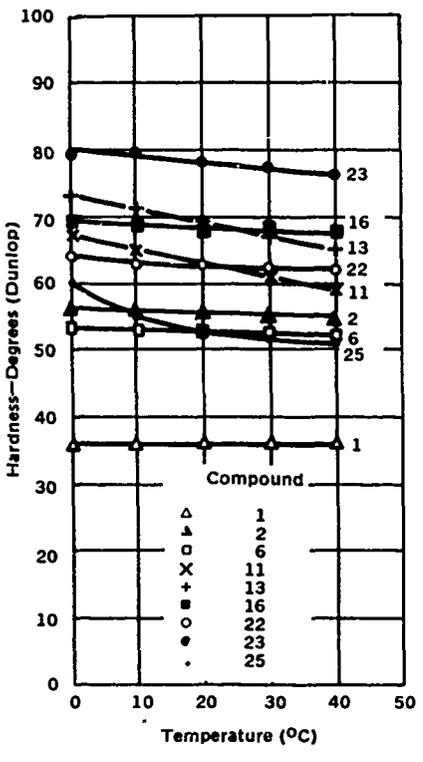

Figure 44. Variation in hardness with temperature for nine selected rubber compounds. (© Sabey and Lupton, 1964. Used by permission.)

Figure 44 shows that changes in hardness with temperature are much lower than changes in resilience. In general, there is a slight decrease in hardness with an increase in temperature. With the exception of one compound (no. 1), the hardness values range from 53 to 79 degrees on the Dunlop hardness gage at 0°C and 52 to 76 degrees at 40°C.

A comparison of Figures 44 and 45 indicates that some compounds (1, 2, 6, and 16) showing little hardness change with temperature exhibit significant changes in BPN with temperature. For other compounds with higher hardness changes the reverse is true. Thus, the results suggest that the effect of hardness is small, and that another factor has a greater influence on friction.

A comparison of Figures 43 and 45 indicates that changes in BPN with temperature are related more closely to resilience changes than to hardness changes. With the exception of compound 25, an increase in resilience with temperature is associated with a decrease in BPN. While this pattern is obvious, the order of BPN and resilience is not the same at the same temperature, as shown by the following example at 20°C, where compounds 22 and 23 particularly are out of order:

Increasing BPN (in Figure 45): 22, 23 (1 and 2), 6, 16, 13, 11, and 25.

Decreasing resilience (in Figure 43): 1, 2, 6, 22, 16, 23, 13, 11, and 25.

A direct comparison of the BPN and resilience values is complicated for two reasons: (1) the rubber is being deformed in different ways under the resilience test and the test with the British pendulum tester or other skid tests, and (2) the wide variety of surface textures influences the effective resilience.

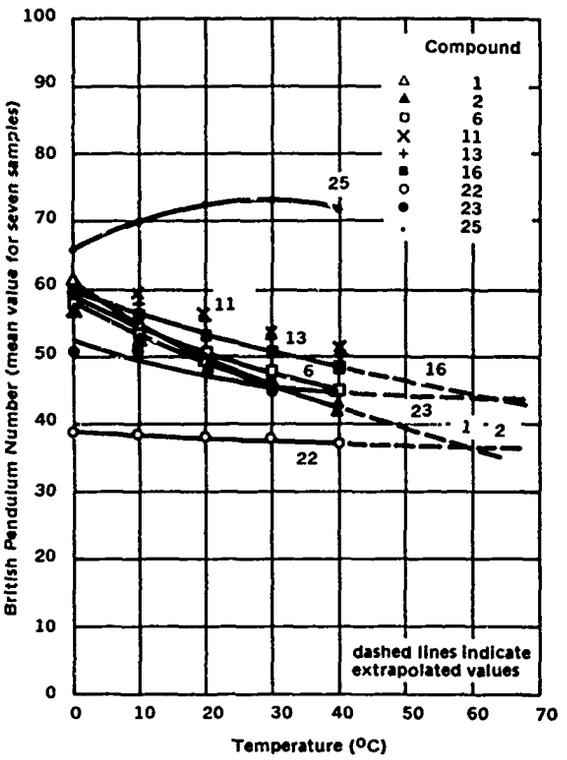

Figure 45. Variation in BPN with temperature for nine selected rubber compounds (mean value measured on seven surfaces).
(© Sabey and Lupton, 1964. Used by permission.)

Changes in tire-pavement contact pressure are brought about by variations in wheel load and tire inflation pressure, P_t. As previously discussed, the adhesion coefficient decreases with an increase in the contact pressure, but the hysteresis coefficient is not affected. Hofelt (1959) reported that the influence of tire inflation pressure is greater than that of wheel load on contact pressure. It should follow then that changes in the tire inflation pressure should have a more pronounced effect on the friction coefficient than changes in the wheel load.

Kummer and Meyer (1967) investigated the effects on SN of varying the wheel load at a constant tire inflation pressure and of varying the tire inflation pressure at a constant wheel load. As shown in Figure 46, there is a small reduction in SN associated with an increase in F_v at a P_t of 24 psi. The reduction is slightly more with the treaded tire than with the smooth tire at 10 mph. However, the curves for the treaded tire appear to converge faster with an increase in velocity.

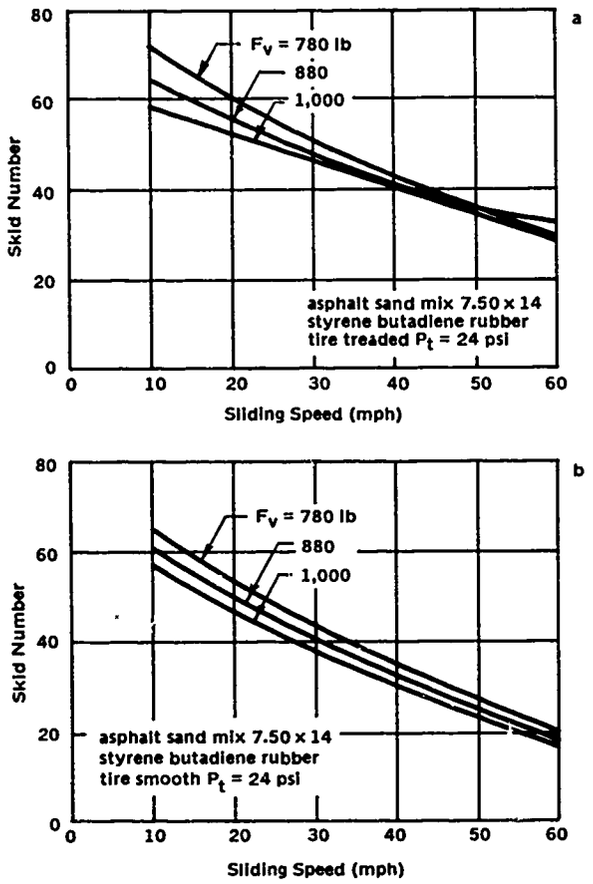

Figure 46. Influence of wheel load on skid resistance for (a) treaded and (b) smooth tires on fine-textured, rounded aggregate surface.
(© Kummer and Meyer, 1967. Used by permission.)

As shown in Figure 47, increasing the tire inflation pressure, P_t, with an F_v of 800 pounds generally results in a decreasing SN. The reduction is again small. Surface 4 appears to show the highest difference in SN with changes in the tire inflation pressure.

Horne and Leland (1963) investigated the effects on the average friction coefficient of changing the tire inflation pressure. As shown in Figure 48, the test results obtained with three different tires on PCC indicate practically no effect. Some effect is shown for one tire on an AC runway. The water depth of 0 to 0.5 inch indicates shallow fluid on the runway, with puddles, but with the higher portions of the surface projecting through the fluid surface.

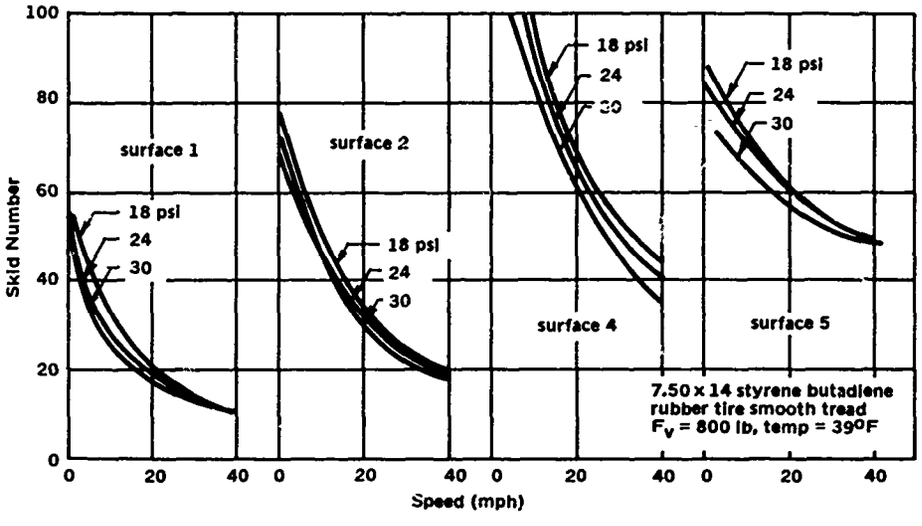

Figure 47. Effect of inflation pressure on the skid resistance of four different surface types. (© Kummer and Meyer, 1967. Used by permission.)

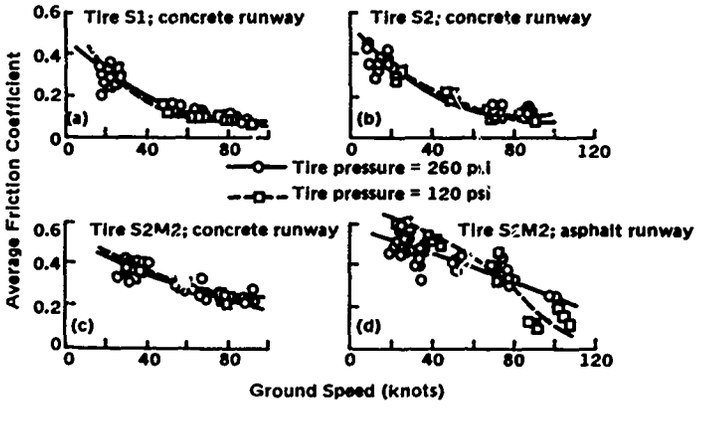

Figure 48. Effect of tire pressure and type of runway surface on friction coefficient; water depth = 0 to 0.5 inch. (© Horne and Leland, 1963. Used by permission.)

Horne and Leland (1962) investigated the effects on the friction coefficient of changing the wheel load while keeping the tire inflation pressure constant. As shown in Figure 49, an increase in wheel load of 12,000 pounds decreases the average friction coefficient by approximately 0.05 throughout the velocity range of 20 to 100 knots.

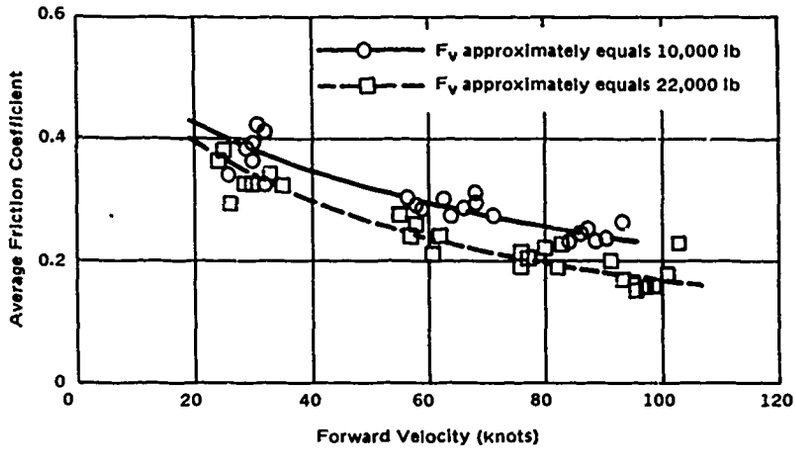

Figure 49. Average friction coefficients obtained during single-wheel braking runs with tire S2M2 at ground vertical loads of approximately 10,000 and 22,000 pounds. Wet concrete runway; water depth = 0 to 0.3 inch; P_t = 260 psi. (© Horne and Leland, 1962. Used by permission.)

As previously mentioned, the macroscopic roughness of the pavement surface and the microscopic roughness of the aggregate particles have the most effect on the friction coefficient. On any relatively clean, dry surface high skid resistance can be obtained regardless of velocity. Apparently the coupling of the adhesion and hysteresis coefficients in a complementary manner yields this characteristic. On wet pavement, however, the brake slip coefficient and, more so, the skid coefficient decrease with an increase in velocity. The rate of decrease is closely related to the macroscopic roughness of the surface and the velocity. The macroscopic roughness can be characterized by the mean width of the voids between the protruding aggregate particles or by the mean height of the aggregate particles.

Shulze and Beckmann (1962) investigated the effect of macroscopic roughness on the SC–velocity relationship; they based their conclusions on measurements made with a skid trailer on 48 wet pavement surfaces. Stereophotographs were taken to determine the macroscopic features of the surfaces, which were classified from close-textured (fine) to open-textured (coarse). These classifications were based on the mean width of the voids between the protruding aggregate particles. The difference in SC at 20 and 60 km/hr was used to characterize the steepness of the SC–velocity curves.

As shown in Figure 50, there is a significant correlation between the mean widths of surface voids and the gradient of the SC–velocity curve. The higher SC–velocity gradient is associated with the closer void width, and the lower SC–velocity gradient with the wider width. Better drainage capability

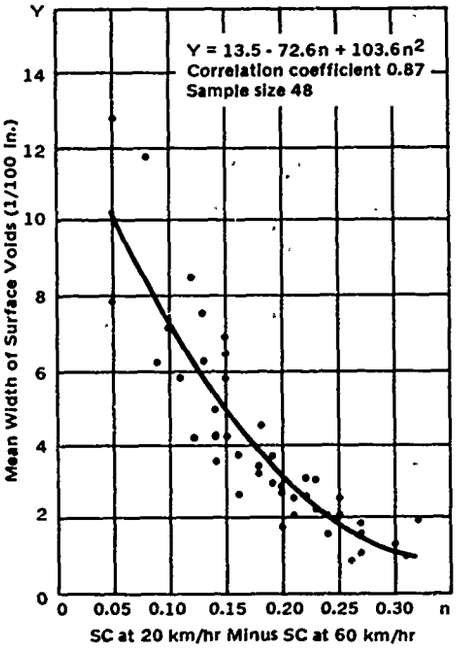

Figure 50. Correlation between surface texture and steepness of the curve relating skid coefficients to speed. (© Shulze and Beckmann, 1962. Used by permission.)

with an increase in void width is one explanation of the behavior. Thus, the advantage of the wider width occurs at higher velocities. At the lower velocities, however, the lower contact area of the open-textured surfaces may result in a lower SC than would be found on fine-textured surfaces.

Shulze and Beckmann (1962) indicated that the gradient of the SC–velocity curve is independent of the magnitude of the SC. For example, if two surfaces with the same mean void width but with different small-scale macroscopic roughness are tested at various velocities, the resulting SC–velocity curves will be similar, with a constant difference throughout the velocity range. The small-scale macroscopic roughness, or "grittiness," of the surface appears to determine the magnitude of the SC.

Sabey (1965) investigated the effect of texture depth on the percent decrease in SC from 30 to 80 mph as determined from measurements with a skid trailer. The texture depth was determined by the "sand-patch" method. In this method a known volume of fine, uniform-particle sand is poured on the pavement surface. The sand is spread to form a uniform circular patch so that the surface depressions are filled to the level of the peaks. The diameter of this patch is measured. The texture depth is the ratio of the volume of sand to the area of the patch. In general, surfaces with texture depth less than 0.010 inch are considered smooth, those with more than 0.020 inch coarse. Although the scatter is large in the results shown in Figure 51, the percentage decrease in SC decreases with an increase in texture depth, from approximately 40% at 0.010-inch texture depth to approximately 10% at 0.040 inch.

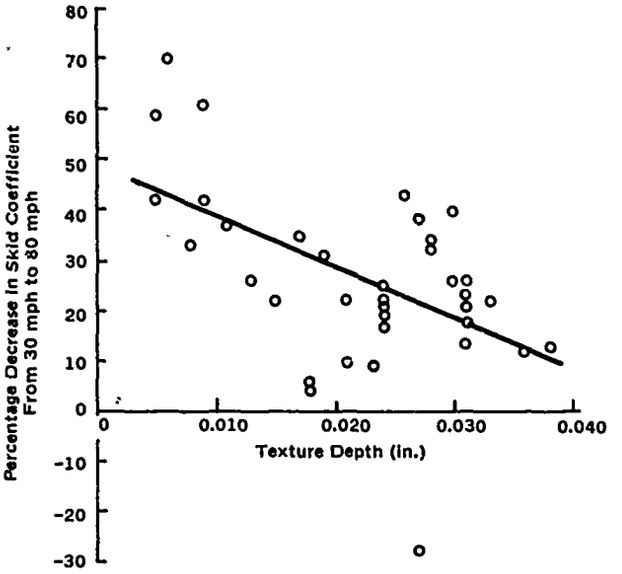

Figure 51. Relation between percentage decrease in skid coefficient resistance between 30 and 80 mph and texture depth. (© Sabey, 1965. Used by permission.)

In addition to the mean void measurement and the sand-patch method, the grease-smear method and the drainage meter have been used to determine the drainage capability of a pavement surface. The grease-smear method used by NASA yields a ratio of volume to area similar to that of the sand-patch method by relating a known volume of grease to the smeared area. The drainage meter, developed at Pennsylvania State University, is a transparent cylinder, approximately 5 inches in diameter and 12 inches high, with a rubber ring glued to one face. This cylinder is placed with the rubber ring in contact with the pavement surface. Various loads can be applied to the cylinder to obtain different contact pressures between the rubber ring and the pavement surface. The time it takes a known volume of water to escape from between the rubber ring and the pavement surface, together with the density of the aggregate particle peaks, determines the drainage potential of the surface.

As previously mentioned, the small-scale macroscopic roughness determines the magnitude of the friction coefficient. This roughness can be attributed to (1) the characteristics of the coarse aggregate particles exposed to the surface, (2) the mortar of sand and cement, or (3) a combination of the two. If a surface has a high percentage of exposed coarse aggregate, its polishing resistance mainly determines the relationship between friction coefficient and the number of vehicles. When the mortar forms a significant

part of the surface, it governs the friction coefficient–traffic number relationship. This latter surface may contain coarse aggregates with small-scale macroscopic roughness and yet yield a low friction coefficient because of the predominant influence of the mortar. Bituminous surfaces can have a low percentage of coarse aggregates at the surface as a result of excessive rolling during construction or compaction under traffic. For PCC the coarse aggregate generally is less important in determining the small-scale texture, because it is less exposed than it is on some bituminous surfaces. Thus, the magnitude of friction coefficient for these surfaces depends on the type and grading of the fine aggregate and on the proportions of the mix.

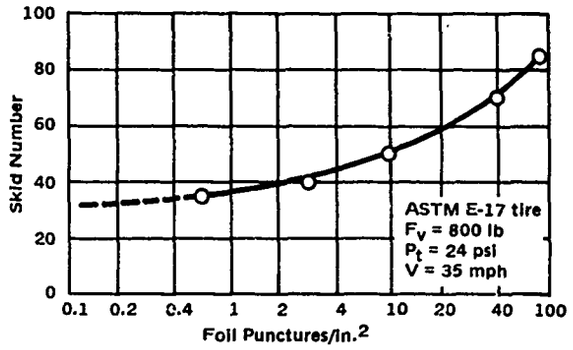

Figure 52. Characterization of friction properties of pavement surfaces by foil-piercing techniques. (© Kummer and Meyer, 1967. Used by permission.)

Kummer and Meyer (1967) reported on the relationship between the density of sand-size particles and the friction properties of pavement surfaces. The density was obtained by using a foil-piercing technique. In this technique a piece of aluminum foil placed on the pavement surface is impacted by a rubber-tipped plunger released from a predetermined height. The impact forces the foil to conform to the pavement texture, with the sharper particles piercing the foil. The number of piercings, or punctures, is counted in the foil or on a photographic negative of the foil. As shown in Figure 52, a minimum of 10 punctures/in.^{2} is needed to obtain an SN of 50.

Kummer and Meyer (1967) reported that, in addition to the large-scale and the small-scale macroscopic roughnesses of the pavement surface, the microscopic roughness of the aggregate particles must have a measurable influence on the friction coefficient. This statement is based on the variation in skid resistance before, during, and after rainy periods. Rain appears to attract the larger sizes of polishing agents on aggregate particles and also on tires. This increases the microscopic roughness rather readily on soft aggregates such as limestone, resulting in a temporary increased skid resistance. However, the polishing action is less effective on other aggregates, especially those with a high reading on Mohs' scale of hardness and a high resistance to polishing.

From the foregoing discussions it appears that the friction coefficient is dependent mainly on the large-scale and small-scale macroscopic roughnesses of pavement surfaces. Thus, the description or classification of pavement surfaces based on a single adjective appears to be insufficient. Kummer and Meyer (1967) proposed the following classification, which includes the two different roughness scales:

1. Smooth surfaces (bleeding surface; highly polished stone, asphalt, or PCC surfaces).

2. Fine-textured, rounded surfaces (worn stone or silica sand surfaces of fine gradation).

3. Fine-textured, gritty surfaces (new silica sand or metal carbide-epoxy surfaces).

4. Coarse-textured, rounded surfaces (polished slag or limestone surfaces of large gradation, or uncrushed gravel surfaces).

5. Coarse-textured, gritty surfaces (new slag pavements consisting of large particles resulting in a surface with large-scale and small-scale macroscopic roughness, or limestone surfaces which contain more than 10% sand-sized siliceous material).

The cross-sectional views and the SN—velocity relationships of the five surfaces are shown in Figure 53. Note that surfaces 2 and 3, which are fine-textured, have higher SN—velocity gradients than the coarse-textured surfaces 4 and 5. As discussed previously, the gradient is determined by the initial texture scale or the drainage ability of the surfaces. Also note that the second adjective, rounded or gritty, determines the magnitude of the SN within the texture type.

Sabey (1965) also described the types of pavement surfaces on the basis of two roughness scales. The surfaces shown in Figure 54 have the following descriptions:

A. Macadam: coarse-textured, harsh stones
B. Macadam: coarse-textured, some polished stones
C. Macadam: coarse-textured, all highly polished stones
D. Fine cold asphalt: fine-textured, sandpaper
E. Concrete: fine-textured, slightly polished
F. Mastic asphalt: fine-textured, highly polished

In these descriptions the harsh stones and sandpaper correspond to the word "gritty" used by Kummer and Meyer (1967) and the polished stones to the word "rounded." In Figure 54 the texture corresponds to the gradient, and the grittiness corresponds to the magnitude of the friction coefficient within the same texture type.

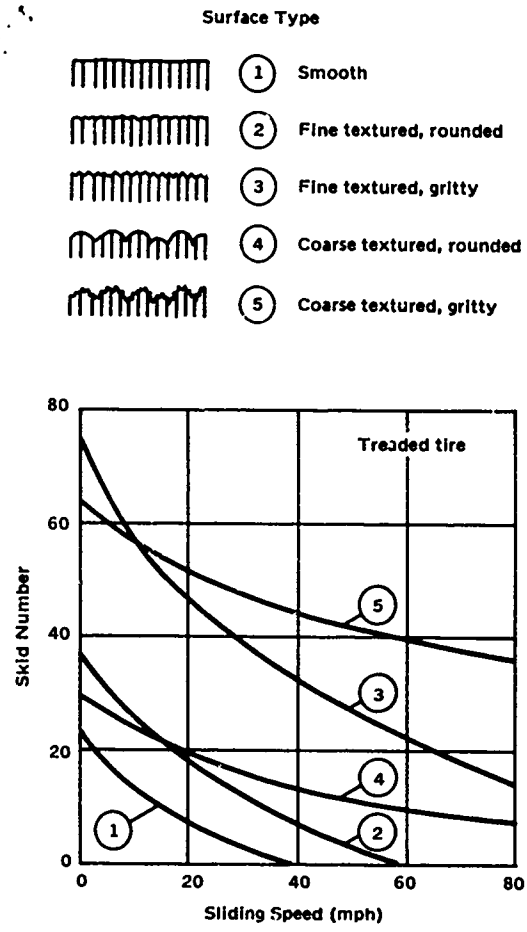

Figure 53. Classification of pavement surfaces according to their friction and drainage properties. © Kummer and Meyer, 1967. Used by permission.)

Some of the tire and pavement surface factors discussed in this section have a marked influence on slip and skid resistances. Tables 16, 17, and 18 summarize the influence of the factors in qualitative terms.

Traffic and Seasonal Changes

Some effects of traffic and seasonal changes on the friction coefficient were discussed previously by Tomita (1964). These changes included polishing wear and surface contamination caused by traffic, foreign material, and climate. The following paragraphs provide some additional results found in the literature.

Horne and Leland (1962) investigated the effects of JP-4 jet fuel spillage on AC surfaces and rubber deposits on PCC surfaces in the Langley landing-loads track. Fuel spillage on runways, though not a usual occurrence, may present a serious problem with asphaltic concrete. Evidence is numerous of rubber deposits on many of the Navy airfield runways, mostly confined to the runway ends. The test results, as shown in Figure 55, indicate that a damp asphaltic concrete surface with spilled JP-4 provides approximately 60% of the average friction number for a similar damp or wet surface without the spilled fuel. Figure 56 shows that rubber contamination of a dry PCC surface definitely lowers the friction values at slip ratios ranging from 0.1 to 1.0. These findings indicate that fuel spillage and rubber deposits can present a potential skid problem for aircraft operations.

Table 16. Influence of Pavement Surface Geometry on Skid Resistance (Treaded Tire, All Other Factors Constant) (© Kummer and Meyer, 1967. Used by permission.)

Surface Type	Surface Roughness		Surface Properties		Wet Skid Resistance	
	Scale of 1/32-1/8 in.	Scale of 1/8-1/2 in.	Friction	Drainage	at 0-35 mph	at 35-70 mph
1. Smooth	none	none	poor	none	poor	none*
2. Fine textured, rounded	yes	none	marginal	poor	marginal	poor
3. Fine textured, gritty	yes	none	excellent	poor	excellent	marginal
4. Coarse textured, rounded	none	yes	marginal	good	marginal	marginal
5. Coarse textured, gritty	yes	yes	excellent	good	very good	good

* Slipping tires with well-designed tread patterns will transmit small forces in this case.

Table 17. Change of Slip and Skid Resistance Due to Increase in Rubber Hardness and Damping and the Addition of Tread Grooves and Slots on Different Surface Types (Other Factors Constant) (© Kummer and Meyer, 1967. Used by permission.)

Surface Type	Change of Slip and Skid Resistance Due to Increase or Addition of			
	Rubber Hardness	Rubber Damping	Grooves*	Slots and Slits**
1. Smooth	increasing	not affected	increasing	increasing
2. Fine textured, rounded	increasing	not affected	increasing	increasing
3. Fine textured, gritty	not affected	increasing	increasing	not affected
4. Coarse textured, rounded	decreasing	increasing	decreasing	increasing
5. Coarse textured, gritty	decreasing	increasing	decreasing	not affected

* Grooves placed circumferentially.
** Placed transversely or obliquely to grooves (slots are molded, slits are cut after molding).

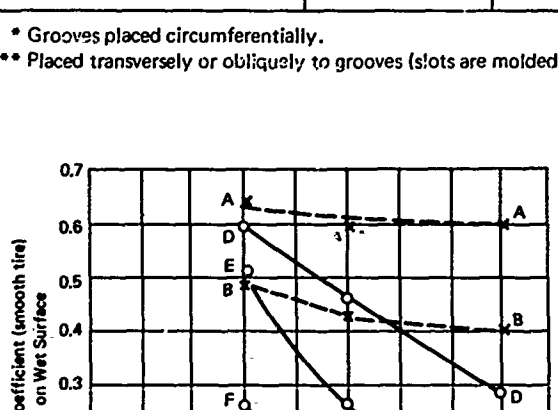

Figure 54. Change in skid coefficient with speed on six surfaces on the Road Research Laboratory test track. (© Sabey, 1965. Used by permission.)

Table 18. Influence of Surface Type and Tread Pattern Combinations on Slip and Skid Resistance (All Other Factors Constant) (© Kummer and Meyer, 1967. Used by permission.

Surface Type	Tread Pattern	Slip Resistance		Skid Resistance	
		at 0-35 mph	at 35-70 mph	at 0-35 mph	at 35-70 mph
1. Smooth	smooth	poor	none	very poor	none
	grooves only	poor	very poor	very poor	none
	slots and slits only	marginal	very poor	poor	none
	grooves, slots, and slits	marginal	poor	poor	very poor
2. Fine textured, rounded	smooth	marginal	very poor	very poor	none
	grooves only	marginal	poor	poor	very poor
	slots and slits only	marginal	poor	poor	very poor
	grooves, slots, and slits	good	marginal	marginal	poor
3. Fine textured, gritty	smooth	excellent	good	very good	marginal
	grooves only	very good	good	good	marginal
	slots and slits only	excellent	good	very good	marginal
	grooves, slots, and slits	very good	good	good	marginal
4. Coarse textured, rounded	smooth	good	marginal	marginal	poor
	grooves only	good	marginal	marginal	poor
	slots and slits only	very good	good	good	marginal
	grooves, slots, and slits	very good	good	good	marginal
5. Coarse textured, gritty	smooth	excellent	very good	excellent	good
	grooves only	excellent	very good	very good	good
	slots and slits only	excellent	very good	excellent	good
	grooves, slots, and slits	excellent	very good	very good	good

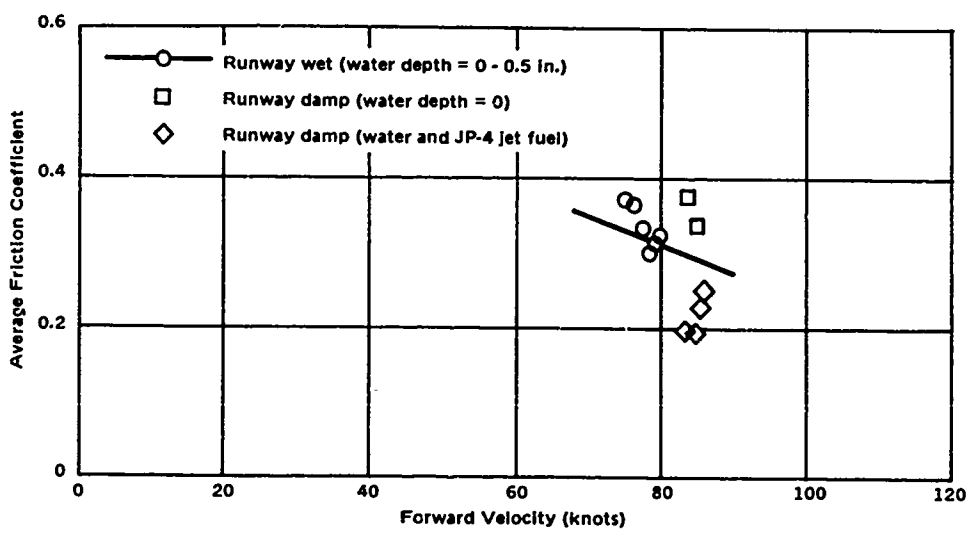

Figure 55. Comparison of average friction coefficients obtained on water-covered and damp asphaltic concrete runways. Data obtained during single-wheel braking tests. $F_v \approx 10{,}000$ pounds; $P_t = 260$ psi. (© Horne and Leland, 1962. Used by permission.)

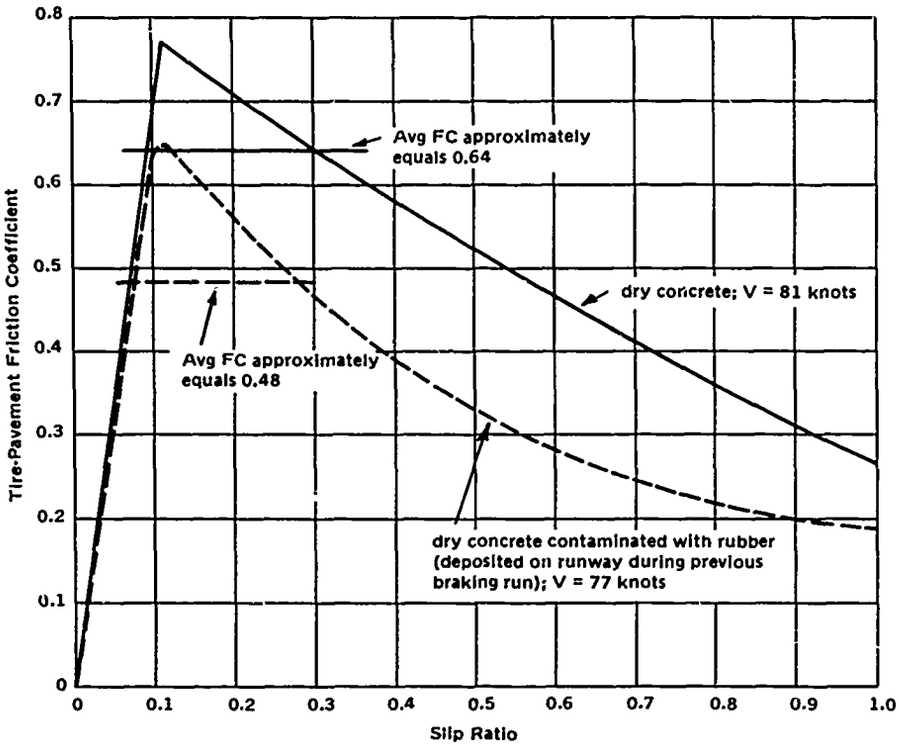

Figure 56. Effect of rubber contamination of a concrete runway surface on the braking friction developed by a 44 x 13, type VII, 26-ply-rated aircraft tire. $F_v \approx 20{,}400$ pounds; $P_t = 150$ psi. (© Horne and Leland, 1962. Used by permission.)

Giles, Sabey, and Cardew (1962) used the British pendulum tester to evaluate the suggested temperature correction on eight pavement surfaces with various surface textures. The results, shown in Figure 57, indicate that the temperature correction becomes really important for tests below 10°C, where the corrections are large. The corrections will permit a more accurate assessment of skid resistance experienced by tires, because tires in motion are generally hotter than the rubber slider of the pendulum tester. The following list, which relates the average temperatures of a rubber slider to those of tires on moving vehicles, is based on 500 comparative measurements:

Slider	Tire
5°C	15°C
20°C	25°C
30°C-40°C	30°C-40°C

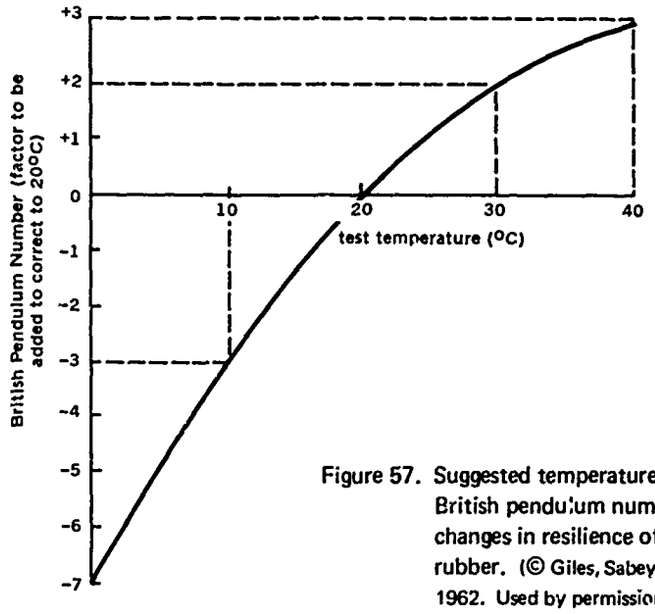

Figure 57. Suggested temperature corrections for British pendulum number to allow for changes in resilience of the slider rubber. (© Giles, Sabey, and Cardew, 1962. Used by permission.)

Since very high velocities are generally involved during the landing of aircraft, the temperature of the tires shortly after touchdown is expected to be much higher than those of highway vehicles. As previously reported by Tomita (1964), the tire surface temperature can be as high as 1,000°F under the locked-wheel condition. Under this high velocity and skid condition, the friction coefficient can be considered to be very low, because the rubber is in a molten state. Fortunately, the locked-wheel condition is not a usual operating mode of aircraft tires.

Sabey (1965) indicated that the time of year or season in Great Britain has a definite effect on the skid resistance of pavement surfaces. The seasonal variation is shown in Table 19 by the monthly index for seven years. In general, the results indicate that the minimum and maximum values of BPN are obtained during the summer and winter months, respectively. The minimum value obtained during the summer varies from year to year but generally occurs in June or July. Low values, however, can occur any time between May and September.

Sabey (1965) also reported that seasonal changes in BPN are related to the frequency of skidding accidents. As shown in Figure 58, the summer months, which are related to low BPN, show a higher percentage of wet skidding accidents than the winter months. Extrapolation of the straight

Table 19. Monthly Index of Seasonal Changes in British Pendulum Number (© Sabey, 1965. Used by permission.)

Month	1958	1959	1960	1961	1962	1963	1964
Jan.	114	117	112	105	119	130	114
Feb.	112	112	114	103	112	121	114
Mar.	114	107	107	93	110	115	107
Apr.	102	95	95	97	99	109	104
May	90	83	91	90	99	105	96
June	98	83	86	86	89	97	93
July	91	79	97	89	92	99	83
Aug.	97	81	98	88	90	97	92
Sept.	97	83	103	87	94	102	96
Oct.	100	95	103	103	97	103	102
Nov.	103	103	109	109	110	110	105
Dec.	114	112	117	112	114	113	112
Avg.	103	95	102	98	101	109	102

Note: An index of 100 is equivalent to the mean British pendulum number recorded over the years 1958-1960.

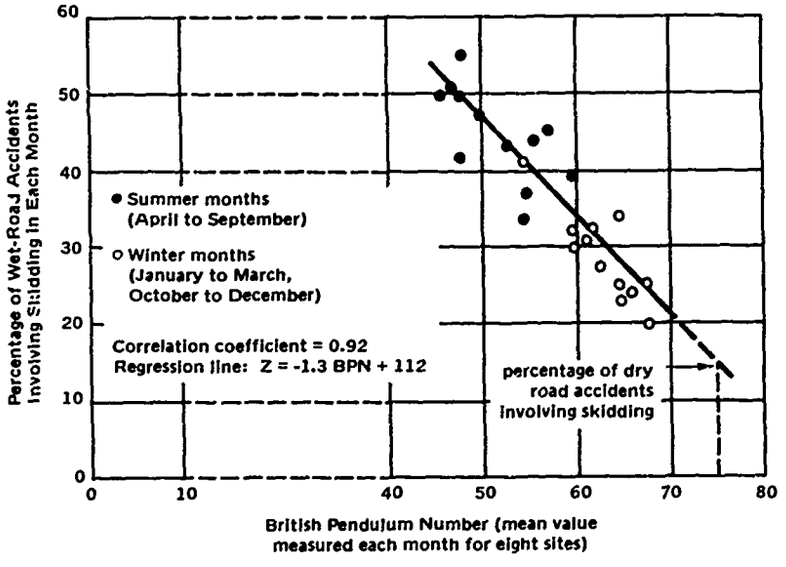

Figure 58. Monthly variations in the frequency of skidding in accidents on wet roads, and the measured skid resistance. (© Sabey, 1965. Used by permission.)

line to the percentage of skidding accidents on dry pavement corresponds to a BPN of 75. This correlation of seasonal change with accident data indicates that the British pendulum tester is able to measure effectively some of the frictional properties sensed by vehicles on wet pavement surfaces.

Kummer and Meyer (1967) found a correlation between the percentage of skidding accidents in five states and three of the four seasons. As shown in Table 20, the average percentage of skidding accidents for five years is highest during the summer and lowest during the winter, with the average for fall in between. The reduced accident rate during winter is caused by low wet-pavement temperatures (high damping of rubber) and high microscopic roughness of the surfaces. High temperatures and low microscopic roughnesses cause the high accident rates during the summer. Fall temperatures are lower, but the surface of the pavement usually has a higher polish during fall than it has during summer.

Table 20. Seasonal Distribution of Skidding Accidents in Five States, Expressed as Percentage of All Wet Pavement Accidents

Year	Skidding Accidents (%)		
	Spring	Summer	Fall
1960	NA	54.7	41.3
1961	20.0	45.6	20.0
1962	14.5	8.6	33.2
1963	19.2	36.2	28.9
1964	15.8	22.3	19.0
Avg.	17.4	33.4	28.4

MINIMUM SKID-RESISTANCE REQUIREMENTS

It was reported by Tomita (1964) that very little information was available on skid-resistance standards or on acceptable minimum friction coefficients for highway pavements and that no such information was found for airfield pavements. The present literature search indicates that more effort is being made in determining the much-needed minimum requirements for highway pavements. However, again the literature reveals no such information for airfield pavements.

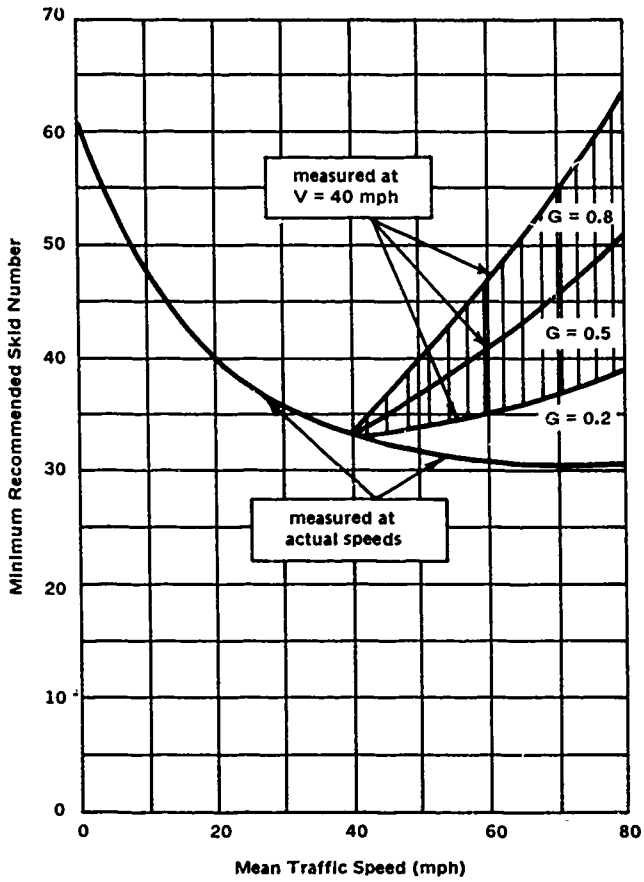

Figure 59. Minimum recommended skid numbers which satisfy normal frictional needs of traffic. (© Kummer and Meyer, 1967. Used by permission.)

Kummer and Meyer (1967) conducted a thorough investigation to provide minimum skid-resistance requirements for rural highway pavements. Many important factors were considered in this investigation which led to the selection of criteria for deriving the minimum requirements. These factors are listed below without the detailed information that can be obtained from the reference:

1. Technical and economic considerations.
2. Pavement friction and skidding accidents.
3. Frictional needs of traffic related to driver behavior.
4. Frictional needs of traffic related to vehicle and highway design factors.
5. Variable need of skid resistance by traffic.

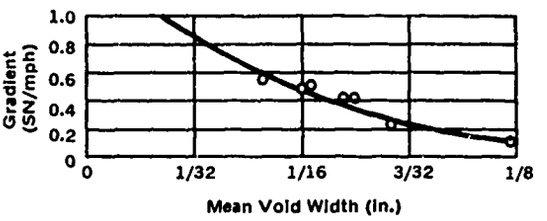

Figure 60. Characterization of drainage properties of pavement surfaces by aggregate spacing. (© Kummer and Meyer, 1967. Used by permission.)

The recommended tentative skid-resistance requirements for rural highways based on a study of driver behavior are shown in Figure 59. The gradient, G, in Figure 59 is $-\Delta(SN)/\Delta V$, which can be obtained from Figure 60. The skid numbers are minimum values measured with skid trailers in late summer or during fall, in accordance with ASTM E274-65T. The corresponding numbers measured with three other devices are given in Table 21. These values will reasonably ensure that rural highway surfaces meeting these requirements will satisfy the frictional needs of normal vehicle maneuvers. It is assumed that the vehicle is in good mechanical condition and equipped with recently designed treaded tires having a tread depth of 1/10 inch or more.

It should be noted that the recommended skid numbers in Figure 59 are minimum values and are tentative. These conditions indicate that the skid numbers for pavements should be higher if possible and that further research is needed to confirm or modify the recommended numbers. It should also be noted that the recommended values do not guarantee that the pavement surface will provide these levels under every possible surface and environmental condition or combination of these factors.

Table 21. Recommended Minimum Interim Skid-Resistance Requirements for Stopping-Distance Cars and Portable Testers* (© Kummer and Meyer, 1967. Used by permission.)

Mean Traffic Speed, (mph)	Skid Number† SN_{40}	Stopping-Distance Number,‡ SDN_{40}	British Pendulum Number§	Drag Tester Number¶
30	31	39	50	35
40	33	41	55	40
50	37	46	60	45
60	41	51	65	50
70	46	57	—	—
80	51	64	—	—

* All values based on use of ASTM E-249 rubber.
† Measured at 40 mph in accordance with ASTM E-274.
‡ Measured in accordance with current practice (ASTM method of test in preparation).
§ Measured in accordance with ASTM E-303.
¶ Measured in accordance with manufacturer's recommended test procedure.

When any highway pavement section is appraised, the skid tests should be carried out in the center of the most polished area in the direction of traffic and at the mean traffic velocity. When the maximum test velocity is lower than the mean traffic velocity, a minimum test velocity of 40 mph is recommended by Kummer and Meyer (1967). The required skid numbers at 40 mph to ensure minimum skid numbers at higher velocities can be determined from Figure 59 as a function of G. Kummer and Meyer (1967) propose use of G = 0.5 for calculating skid numbers at 50 mph from measurements at 40 mph. But for projection from 40 mph to 60 mph or higher velocities a representative gradient can be obtained from Figure 60 after estimating the mean void width of the pavement surface.

METHODS TO IMPROVE SKID RESISTANCE

Some methods employed to improve skid resistance were reported by Tomita (1964). All these methods involved the treatment of pavement surfaces. The following paragraphs present additional information found during the present investigation.

As previously mentioned, pavement grooving is a relatively recent technique used to improve skid resistance. Horne and Brooks (1967) investigated the effect of transverse grooving on braking performance. Their study was conducted with a smooth tread jet transport tire on the Langley landing-loads track. As shown in Figure 61, the skid coefficient is considerably higher for all three grooved concrete surfaces than for the conventional longitudinal burlap-dragged, ungrooved surface under damp or flooded conditions. Other test results from NASA's forthcoming experiments are expected to provide additional information on grooving.

At a Navy air station a newly fog-sealed AC runway was wire-brushed in an effort to improve its skid resistance.* Stiff wire brushes were mounted on a framework; the framework was weighted with sandbags and dragged in a circular pattern with a vehicle. It was determined, by weighing the sweeping from a given area, that this method is able to remove only a small amount of material from the pavement surface. A few before-and-after wire-brushing decelerometer readings indicated an average increase to 16 ft/sec^2 from 9 ft/sec^2. Though pilot complaints of slick pavement decreased after the wire-brushing operation, the effectiveness of this technique is questionable because the number of wet-runway landing operations before and after wire-brushing have not been compared.

* Information derived from author's experience as a consultant for the air station.

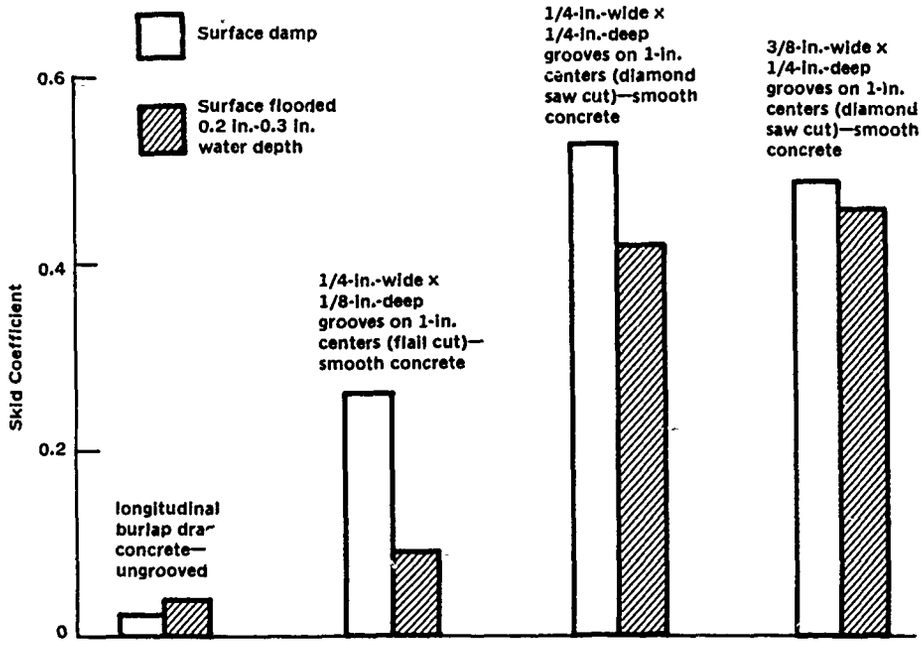

Figure 61. Effect of pavement grooving on skid coefficient of smooth-tread jet transport aircraft tire. (P_t = 170 psi; F_v = 30,000 pounds; V = 100 knots). (© Horne and Brooks, 1967. Used by permission.)

A section of a new AC runway in South Vietnam was chipped on an experimental basis to improve skid resistance.* The AC runway had a relatively smooth, tight surface. A rotating drum with many small, sharp projections was used in the operation. Average decelerometer readings increased to 19 ft/sec^2 from 16 ft/sec^2 under a wet condition. The initial test vehicle velocity was 40 mph. A coarse-grain slurry seal incorporating a maximum size aggregate of 1/4 inch was also tried on a section of the same runway in Vietnam. This type of slurry seal was used to provide a large-scale macroscopic roughness surface for better water drainage from the tireprint area, thereby increasing the friction value at the higher velocities of landing aircraft. The average decelerometer readings improved to 22 ft/sec^2 from 16 ft/sec^2 under a wet condition and in initial test velocity of 40 mph. Based on the results of these experiments, the slurry seal method was recommended for the entire runway. No report has been received on when the skid resistance work will be done.

* Personal communication to NCEL representative.

For several years, the Navy has been using skid-resistant epoxy compounds on aircraft carrier decks and more recently on landing mats. These compounds, conforming to the requirements of Military Specifications MIL-D-23003 (SHIPS) and MIL-C-81346 (WP), apparently are very successful and satisfactory for the intended purpose. The manufacturers of these compounds have recently introduced a modified epoxy compound for PCC surfaces. Information from the manufacturers indicate that trial sections of such nonskid compounds have been placed on a runway surface at John F. Kennedy Airport and at NASA's Wallops Station to determine their long-term performance. No results have been received to date.

SUMMARY

An investigation was conducted to determine the research and development efforts needed to provide safe, skid-resistant surfaces on Navy and Marine Corps airfield pavements. The investigation consisted mainly of a review of the literature published since the previous study conducted in 1963 and 1964 and a review of work being conducted outside NCEL. Much of the information reported supplements that found in the previous report by Tomita (1964) and serves to provide the reader with the latest available results and findings. Hydroplaning, a subject only briefly discussed in the previous report by Tomita (1964), is dealt with in detail, as is the subject of friction coefficient.

The investigation revealed that aircraft tires do hydroplane on runway surfaces. The velocity at which a tire reaches complete hydroplaning can be determined with a satisfactory degree of accuracy by an equation. Various factors contributing to hydroplaning have been identified, and ways to combat the phenomenon are being investigated. Thus far, the grooving of pavements has received the most attention and appears to be the best remedial measure. However, it has disadvantages, especially with asphaltic concrete pavements in hot climates, where aircraft tire loadings can close the grooves. Additional work is needed to determine the degree of pavement surface roughness or texture necessary to successfully eliminate hydroplaning on airfield runways. A review of the current requirements for transverse and longitudinal slopes of runways is also needed to provide the best aircraft-runway surface system for ground operation.

The vast number of recently published references indicates a continuing interest in the skid resistance of pavements. Most of the work has been done in the interests of highway safety. However, some work has been oriented toward improving the skid resistance of aircraft on airfields.

Work on the mechanism of rubber friction helps to explain to a great extent the friction coefficient between tires and pavements. In general, the factors influencing the adhesion and hysteresis components in rubber friction are applicable to the tire–pavement frictional phenomena. These factors are the contact area, the shear strength between the tire and the pavement, the energy dissipated by the damping of the rubber, the volume of the rubber, and to a lesser extent, the contact pressure. The effects of these factors have been verified by experimental results.

The operating modes of aircraft tires consist of the free-rolling, slipping (drive, brake, and cornering), and skidding modes. Since the free-rolling mode is of little concern and the skidding mode is not usually permitted during aircraft deceleration, the friction coefficients associated with the cornering slip and brake slip modes are most important. Thus, the friction requirements of airfield pavements should logically be based mainly on the brake slip coefficient as well as on the cornering slip coefficient and, to a lesser extent, on the skid coefficient.

The investigation revealed that the skid trailer method is being used more and more and is becoming the standard field measuring device for highway pavements. The recent additional capability of this method for testing the slip mode gives this method versatility. Three basic designs of the skid trailer are available. Of the three, the parallelogram design appears to be the simplest. The stopping-distance and deceleration methods are also in use, but to a lesser extent. There appears to be a continued use of portable testers, generally in the laboratory and as supplement devices for the trailer, to check quickly the skid resistance of pavement surfaces.

Results of correlation studies indicate that good correlation can be obtained between some friction-measuring devices, but that poor correlation exists between others. Variations in test conditions, the design of the devices, the lack of a sufficient number of tests, and other factors can influence the degree of correlation. Forthcoming results from future correlation studies are expected to provide additional information on this subject. While much work has been done to correlate various friction-measuring devices, only a token effort has been made to find a correlation between devices and aircraft during braking. Such correlation information is needed, especially if realistic skid-resistance standards based on measurements with the devices are desired for airfield pavements. Additional aircraft-device correlation information is expected from NASA.

The investigation indicated continuing research to determine the effects on the friction coefficient of the numerous factors involved in the tire–pavement interaction. There is an increase in the friction–velocity gradient with an increase in the thickness of water film. The ratio of peak coefficient to skid coefficient increases with an increase in velocity. These

factors point to the danger of the locked-wheel condition at high velocities on flooded pavement surfaces. The resilience of rubber appears to have a more significant influence on the friction coefficient than does the hardness of rubber. High resilience corresponds to a low friction coefficient. Appropriate tread patterns significantly improve skid resistance on smooth wet surfaces, especially at the higher velocities. This improvement decreases on coarse open-textured pavement surfaces. An increase in the wheel load and the inflation pressure decreases the friction coefficient, but the effect is not as significant as those of some other factors. The large-scale and small-scale macroscopic roughnesses of pavement surfaces are important factors. The microscopic roughness varies with the seasons and is less important. The large-scale macroscopic roughness related to the rate of water drainage from the tire contact area governs the friction-velocity gradient; the small-scale macroscopic roughness determines the magnitude of the friction coefficient. Other factors, such as fuel spillage, rubber deposits, and temperature and seasonal changes, can change the friction coefficient.

Some effort has been made toward establishing minimum skid-resistance requirements for rural highway pavements but not for airfield pavements. It is emphasized that the highway requirements are tentative and are based on minimum values. Further detailed research is needed to firmly establish skid-resistance requirements for highway and airfield pavements. Whenever possible, pavements should be built with skid-resistant qualities greater than established minimum requirements.

Various methods to improve the skid resistance of slick surfaces have been tried. These methods, which include grooving, wire brushing, chipping, and using carrier-deck-type nonskid coatings, supplement those discussed in the previous report by Tomita (1964). Only preliminary results on some methods are available from limited trials or investigations. Thus, no definite conclusions can be made at present on the performance of these skid-improvement methods.

RECOMMENDATIONS

1. Laboratory and field studies should be conducted to establish skid-resistance requirements for Navy and Marine Corps airfield pavements. The laboratory study should determine: (1) the required surface texture or roughness of both PCC and AC runways which will be effective against hydroplaning and (2) the friction coefficient and abrasion resistance of the required surface texture. Various surfaces found promising under the laboratory study should be duplicated in the field with conventional or specially developed construction methods. The friction coefficient–velocity

relationship of the surfaces should be established with a field-measuring device. The results should be used to determine the stopping distances and lateral stability of aircraft on these surfaces.

2. A skid trailer utilizing the simple parallelogram design and incorporating the slip mode should be developed and used as the field-measuring device. If possible, the device should be capable of measuring the cornering slip coefficient and have instrumentation sensitive enough to measure and record slush drag or hydrodynamic drag forces as well as the friction coefficient. This skid trailer should be used in the recommended field study; in any future evaluation of a promising skid-resistant surfacing material; and in combination with other subsequently developed, economical field test methods for periodically making skid measurements on Navy and Marine Corps air station pavements.

REFERENCES

Csathy, T. I., Burnett, W. C., and Armstrong, M. D. (1968) "State of the art of skid resistance research," in State of the art: Rigid pavement design, Research on skid resistance, Pavement condition evaluation, Highway Research Board, Special Report 95, Washington, D. C., 1968, pp. 34-48.

Department of the Navy. Bureau of Aeronautics. NAVAER 00-100-505: United States Naval aeronautical shore activities planning standards. Washington, D. C., 1959.

Department of the Air Force (1967) Technical Order T.O. 1T-38A-1: T-38A aircraft flight manual. Washington, D. C., Mar. 1967, p. A7-3.

Dillard, J. H. and Mahone, D. C. (1963) Measuring road surface slipperiness; presented at 66th Annual Meeting, American Society for Testing and Materials, Atlantic City, N. J., June 26, 1963. Philadelphia, Pa., American Society for Testing and Materials, 1964. (Special Technical Publication 366)

Domandl, H. and Meyer, W. E. (1968) "Measuring tire friction under slip with the Penn State road friction tester," in Surface properties of pavements and vehicle interaction, Highway Research Board, Record no. 214, Washington, D. C., 1968, pp. 34-41.

Giles, C. G. (1959) "Some European methods for the measurement of skidding resistance," in First International Skid Prevention Conference, Proceedings, pt. 1. Charlottesville, Va., Virginia Council of Highway Investigation and Research, Aug. 1959, pp. 267-296.

Giles, C. G., Sabey, B. E., and Cardew, K. H. F. (1962) "Development and performance of the portable skid-resistance tester," in Symposium on skid resistance; presented at 65th Annual Meeting, American Society for Testing and Materials; New York, N. Y., June 29, 1962. Philadelphia, Pa., American Society for Testing and Materials, Dec. 1962, pp. 50-74. (Special Technical Publication 326)

Goodenow, G. L., Kolhoff, T. R., and Smithson, F. D. (1968) "Tire-road friction measuring system—A second generation," paper presented at Society of Automotive Engineers Automotive Engineering Congress, Detroit, Mich., Jan. 8-12, 1968. (SAE paper 680137)

Harrin, E. N. (1958) Low tire friction and cornering forces on a wet surface. National Advisory Commission for Aeronautics, Technical Note, NACA TN-4406, Washington, D. C., Sept. 1958.

Hofelt, C. (1959) "Factors in tires that influence skid resistance, Part V: Effect of speed, load distribution and inflation," in First International Skid Prevention Conference, Proceedings, pt. 1. Charlottesville, Va., Virginia Council of Highway Investigation and Research, Aug. 1959, pp. 173-187.

Horne, W. B. (1967) Status report on runway grooving programs in the United States. National Aeronautics and Space Administration, Langley Research Center, Langley Working Paper LWP-489, Langley Station, Hampton, Va., Oct. 1967.

Horne, W. B. and Brooks, G. W. (1967) Runway grooving for increasing tire traction: The current program and an assessment of available results. National Aeronautics and Space Administration, Technical Memorandum, NASA TM-X-61061, Washington, D. C., Dec 1967.

Horne, W. B. and Dreher, R. C. (1963) Phenomena of pneumatic tire hydroplaning. National Aeronautics and Space Administration, Technical Note, NASA TN D-2056, Washington, D. C., Nov. 1963.

Horne, W. B. and Leland, T. J. W. (1962) Influence of tire tread pattern and runway surface condition on braking friction and rolling resistance of a modern aircraft tire. National Aeronautics and Space Administration, Technical Note, NASA TN D-1376, Washington, D. C., Sept. 1962.

———. (1963) "Runway slipperiness and slush," Royal Aeronautical Society, Journal, vol. 67, no. 633, Sept. 1963, pp. 559-571.

Hurt, H. H. (1960) Aerodynamics for naval aviators, NAVWEPS 00-80T-80, Office of the Chief of Naval Operations, Aviation Training Division, Washington, D. C., 1960.

Kummer, H. W. and Meyer, W. E. (1962) "Measurement of skid resistance," in Symposium of skid resistance; presented at the 65th Annual Meeting, American Society for Testing and Materials, New York, N. Y., June 29, 1962. Philadelphia, Pa., American Society for Testing and Materials, Dec. 1962, pp. 3-28. (Special Technical Publication 326)

———. (1967) Tentative skid-resistance requirements for main rural highways, Highway Research Board, National Cooperative Highway Research Program Report 37, Washington, D. C., 1967.

Mahone, D. C. (1962) "Pavement friction as measured by the British portable tester and by the stopping-distance method," Materials Research and Standards, vol. 2, no. 3, Mar. 1962, pp. 187-192.

Maycock, G. (1965-1966) "Studies on the skidding resistance of passenger-car tires on wet surfaces," Institution of Mechanical Engineers, Automobile Division, Proceedings, vol. 180, pt. 2A, no. 4, 1965-1966, pp. 121-141.

Moore, D. F. (1966) "Prediction of skid-resistance gradient and drainage characteristics for pavements," in Design, performance and surface properties of pavements, Highway Research Board, Record no. 131, Washington, D. C., 1966, pp. 181-203.

Rizenbergs, R. L. and Ward, H. A. (1967) "Skid testing with an automobile," in Design, performance and surface properties of pavement, Highway Research Board, Record no. 189, Washington, D. C., 1967, pp. 115-136.

Sabey, B. E. (1965) "Roadsurface characteristics and skidding resistance," British Granite and Whinstone Federation, Journal. vol. 5, no. 2, Autumn 1965, pp. 7-20.

Sabey, B. E. and Lupton, G. N. (1964) "Friction on wet surface of tire-tread-type vulcanisates," Rubber Chemistry and Technology, vol. 37, no. 4, Oct. 1964, pp. 878-893.

Shrager, J. J. (1962) Vehicular measurements of effective runway friction. Federal Aviation Agency, Systems Research and Development Service, Final Report on Project no. 308-3X (Amendment no. 1), Atlantic City, N. J., May 1962.

Shulze, K. H. and Beckmann, L. (1962) "Friction properties of pavements at different speeds," in Symposium on skid resistance; presented at 65th Annual Meeting, American Society for Testing and Materials, New York, N. Y., June 29, 1962. Philadelphia, Pa., American Society for Testing and Materials, Dec. 1962, pp. 42-49. (Special Technical Publication 326)

Snowdon, J. C. (1963) "Representation of the mechanical damping possessed by rubber-like materials and structures," Acoustical Society of America, Journal, vol. 35, no. 6, June 1963, pp. 821-829.

Tabor, D. (1959) "The importance of hysteresis losses in the friction of lubricated rubber," in First International Skid Prevention Conference, Proceedings, pt. 1. Charlottesville, Va., Virginia Council of Highway Investigation and Research, Aug. 1959, pp. 211-218.

Tomita, H. (1964) Friction coefficients between tires and pavement surfaces. Naval Civil Engineering Laboratory, Technical Report R-303, Port Hueneme, Calif., June 1964. (AD 602930)

Trant, J. P. (1959) "NACA research on friction measurements," in First International Skid Prevention Conference, Proceedings, pt. 1. Charlottesville, Va., Virginia Council of Highway Investigation and Research, Aug. 1959, pp. 297-308.

Walsh, R. J. (1966) "Skid testing on the New York Thruway," Public Works, vol. 97, no. 1, Jan. 1966, pp. 89-90.

Yoder, E. J. (1959) Principles of pavement design. New York, Wiley, 1959, pp. 18-19.

NOMENCLATURE

Symbols

A	Total area of contact for N number of aggregate particles (in.^{2})
A_a	Uplift area of the aircraft (ft^2)
A_i	Particle-rubber contact area (in.^{2})
A_n	Gross geometric area of the block (in.^{2})
A_t	Tire contact area (ft^2 or in.^{2})
a	Distance from hitch to axle of skid trailer (in. or ft)
B	Interface shear strength (psi)
b	Unit sliding length (in.)
C_a	Lift coefficient of the aircraft (nondimensional)
C_c	Correlation coefficient
C_t	Lift coefficient of the tire (nondimensional)
c	Vertical distance from axle to point of force measurement (in. or ft)
D	Energy dissipated by damping (in.-lb/in.^{3})
D_a	Aerodynamic drag (lb)
d	Deceleration (ft/sec^2)
E	Total energy dissipated within the rubber for N number of aggregate particles (in.-lb)
E_{hi}	Energy for each mineral particle dissipated per unit sliding length (in.-lb)
E_i	Unit energy (in.-lb)
e	Pneumatic trail (in.)
F	Friction force (lb)
F_a	Adhesion force (lb)
F_{ai}	Adhesion force for a protruding mineral particle (lb)
F_b	Friction force under the brake slip mode (lb)
F_c	Cornering force (lb)
F_h	Hysteresis force (lb)
F_{hi}	Hysteresis force for a protruding mineral particle (lb)
F_{sk}	Friction force under the skidding mode (lb)
F_t	True friction force (lb)
F_v	Vertical wheel load (lb)
F_{vo}	Static vertical wheel load (lb)
F_1	Force measured on Cornell Aeronautical Laboratory skid trailer (lb)
F_2	Force measured on Pennsylvania State University skid trailer (lb)
f	Horizontal distance from wheel axle to center of gravity of skid trailer (in. or ft)
G	Gradient of friction coefficient–velocity curve (SN per mph)
g	Gravitational acceleration (ft/sec^2)
H	Percent error
H_s	Standard estimate of error
h	Vertical distance from pavement surface to center of gravity of skid trailer (in. or ft)
i	Any protruding mineral particle

F_a	Adhesion force (lb)
F_{ai}	Adhesion force for a protruding mineral particle (lb)
F_b	Friction force under the brake slip mode (lb)
F_c	Cornering force (lb)
F_h	Hysteresis force (lb)
F_{hi}	Hysteresis force for a protruding mineral particle (lb)
F_{sk}	Friction force under the skidding mode (lb)
F_t	True friction force (lb)
F_v	Vertical wheel load (lb)
F_{vo}	Static vertical wheel load (lb)
F_1	Force measured on Cornell Aeronautical Laboratory skid trailer (lb)
F_2	Force measured on Pennsylvania State University skid trailer (lb)
f	Horizontal distance from wheel axle to center of gravity of skid trailer (in. or ft)
G	Gradient of friction coefficient–velocity curve (SN per mph)
g	Gravitational acceleration (ft/sec^2)
H	Percent error
H_s	Standard estimate of error
h	Vertical distance from pavement surface to center of gravity of skid trailer (in. or ft)
i	Any protruding mineral particle
j	Hitch height for skid trailer (in. or ft)
k	Horizontal distance from wheel axle to point of measuring bending moment M on skid trailer (in. or ft)
L_a	Aerodynamic lift (lb)
L_g	Sum of the vertical ground forces through all gears (lb)
M	Bending moment (in.-lb)
M_o	Moment at wheel axle (in.-lb)
m	Mass (slugs)
n	Difference between skid coefficient measured at 20 km/hr and at 60 km/hr
P_t	Tire inflation pressure (psi)
p	Contact pressure (psi)
Q	Volume of rubber involved in deformation ($in.^3$)
r	Tire radius (in. or ft)
S_b	Brake slip (nondimensional)
S_c	Cornering slip (nondimensional)
S_d	Drive slip (nondimensional)
T	Residual thrust (lb)
T_m	Measured torque (in.-lb)
t	Time (sec)
t_1	Time at the start of the measurement (sec)
t_2	Time at the end of the measurement (sec)

B

V	Velocity of vehicle or aircraft on the ground (ft/sec, mph, or knots)
V_h	Hydroplaning velocity (ft/sec, mph, or knots)
V_w	The velocity at which a wedge of fluid begins to penetrate the tireprint area (ft/sec, mph, or knots)
V_1	Initial velocity (ft/sec or mph)
V_2	Final velocity (ft/sec or mph)
W	Static weight of the aircraft or vehicle (lb)
X	Skidding distance (ft)
X_c	Distance from wheel axle to center of pressure (ft)
Y	Mean width of surface voids (in.)
Z	Percent of wet skidding accident per month
α	Slip angle (degree)
ρ	Mass density of water (slugs/ft^3)
ρ_a	Mass density of air (slugs/ft^3)
ω	Angular wheel velocity of the freely rolling tire corresponding to the velocity of the vehicle (radians/sec)
ω_t	Angular velocity of the slipping tire or torqued wheel (radians/sec)

Abbreviations

AC	Asphaltic concrete
BPC	British pendulum coefficient
BPN	British pendulum number
BSC	Brake slip coefficient
BSN	Brake slip number
CSC	Cornering slip coefficient
CSN	Cornering slip number
DC	Deceleration coefficient
DTN	Drag test number
FC	Friction coefficient
FC_a	Adhesion coefficient
FC_{air}	Friction coefficient measured with aircraft
FC_h	Hysteresis coefficient
PC	Peak coefficient
PCC	Portland cement concrete
RCR	Runway condition readings
SC	Skid coefficient
SDC	Stopping-distance coefficient
SDN	Stopping-distance number
SN	Skid number

Unclassified

Security Classification

DOCUMENT CONTROL DATA - R & D

(Security classification of title, body of abstract and indexing annotation must be entered when the overall report is classified)

1. ORIGINATING ACTIVITY (Corporate author)	2a. REPORT SECURITY CLASSIFICATION
Naval Civil Engineering Laboratory Port Hueneme, California 93041	Unclassified 2b. GROUP

3. REPORT TITLE

TIRE–PAVEMENT FRICTION COEFFICIENTS

4. DESCRIPTIVE NOTES (Type of report and inclusive dates)

Not final; July 1967 – November 1968

5. AUTHOR(S) (First name, middle initial, last name)

Hisao Tomita

6. REPORT DATE	7a. TOTAL NO. OF PAGES	7b. NO. OF REFS
April 1970	111	33

8a. CONTRACT OR GRANT NO.	9a. ORIGINATOR'S REPORT NUMBER(S)
b. PROJECT NO. Y-F015-20-01-012	R-672
c.	9b. OTHER REPORT NO(S) (Any other numbers that may be assigned this report)
d.	

10. DISTRIBUTION STATEMENT

This document has been approved for public release and sale; its distribution is unlimited.

11. SUPPLEMENTARY NOTES	12. SPONSORING MILITARY ACTIVITY
	Naval Facilities Engineering Command Washington, D. C.

13. ABSTRACT

AD602930

An investigation consisting mainly of a literature review and a review of current research done outside NCEL was conducted to determine the methods needed to provide safe, skid-resistant surfaces on Navy and Marine Corps airfield pavements. Much of the information reported herein serves to update the information contained in NCEL Technical Report R-303. For example, new information is included on friction-measuring methods, correlation of the measuring methods, factors affecting friction coefficients, minimum requirements for skid resistance, and methods of improving the skid resistance of slippery pavements. However, some new topics which are of recent interest are also discussed in detail. These topics include hydroplaning, the mechanism of rubber friction, the friction associated with various operating modes of aircraft tires, the relationship of friction coefficients to pavement surface texture and to surface drainage of water, and the effects of pavement grooving on hydroplaning and on friction coefficients.

All the information from the investigation is summarized, and recommendations are given for research and development efforts needed to provide safe, skid-resistant surfaces for airfield pavements.

DD FORM 1 NOV 65 1473 (PAGE 1)

S/N 0101-807-6801

Unclassified

Security Classification

14 KEY WORDS	LINK A		LINK B		LINK C	
	ROLE	WT	ROLE	WT	ROLE	WT
Friction coefficients						
Hydroplaning						
Skid resistance						
Rubber friction						
Skid device						
Asphaltic concrete pavements						
Portland cement concrete pavements						
Highways						
Airfields						
Pavement surface characteristics						
Highway safety						